Lyotropic liquid crystals as templates for advanced materials

Younes Saadat [1], Omar Q. Imran [2,3], Chinedum O. Osuji [3*], Reza Foudazi [1†]

[1] *Department of Chemical and Materials Engineering, New Mexico State University, Las Cruces, NM 88003, USA*

[2] *Department of Chemical and Environmental Engineering, Yale University, New Haven CT 06520*

[3] *Department of Chemical and Biomolecular Engineering, University of Pennsylvania, Philadelphia, Pennsylvania 19104, USA*

Abstract

Lyotropic liquid crystals (LLCs) have drawn attention in numerous technical fields as they feature a variety of nanometer-scale structures, processability, and diverse chemical functionality. However, they suffer from poor mechanical properties and thermal stability. Polymerization in LLCs, referred to as LLC templating, is an effective approach to overcome this issue. While the templating approach results in robust mechanical, physical, and thermal properties, retention of the parent LLC structure after polymerization has been a major concern in the field. Therefore, there have been several efforts to introduce new materials and techniques to preserve the native LLC nanostructure after polymerization. In this review, we survey the efforts put in this area along with the applications of the obtained materials from LLC templating, after providing a brief introduction of LLC structures. Moreover, polymerization kinetics in different LLC structures, as a key player in the structure retention, are analyzed. Furthermore, we discuss the outlook of the field and available opportunities.

Keywords: *Lyotropic liquid crystals, Self-assembly, Templating, Membrane, Mesophases*

1. Introduction

Nanostructured materials have attracted the attention of scientific communities as well as industries world-wide because of their unique properties which make them applicable in a variety of technical fields including biomedical devices,[1,2] light scattering,[3] membranes,[4,5] energy storage devices,[6] and so forth. Precise control of the structure in the nanometer scale is the key to improve the functionality of such materials and thus to guarantee their applicability in each field. Process-ability and chemical functionality of the components are other important factors when it comes to the large scale production of nanostructured substances.[7] As an example, inorganic materials such as zeolites that are widely used for separation in molecular scale suffer from challenging process-ability as well as limited range of chemistry (e.g., chemical functionality), resulting in restricted application as highly selective membranes.[7]

[*] Corresponding author. Email: cosuji@seas.upenn.edu.
[†] Corresponding author. Email: rfoudazi@nmsu.edu.

The “bottom-up” approach, which works based on self-arrangement in the atomic, molecular or colloidal scales, is the common method used in nanotechnology for the fabrication of precisely designed nanostructures.[8] Amongst the huge diversity of materials employed in this technique, the components that form liquid crystalline structures (LCs) through a molecular self-assembly process (supramolecular chemistry) have received a great deal of attention.[8] LCs have both ordered and disordered regions in their structures. These structures, also called mesophases, offer some of the properties of liquids and solid simultaneously (e.g., fluidity coupled with optical anisotropy). Many organic compounds show LC behavior under certain conditions. LC behavior can be observed in the molten state (thermotropic LCs), or in the presence of a solvent as in lyotropic LCs (LLCs).[9] In both cases, molecular self-assembly, liquidity and diverse chemistry not only provide an opportunity to precisely control the nanostructure, but also result in the ease of processing as well as a wide range of chemical functionality.[7]

Amphiphilic molecules, which have lipophilic tail(s) and hydrophilic head(s), are used to form LLCs in the presence of water, as the commonly used solvent. Assembly in non-aqueous phases has also been studied[10–12] but our primary concern here is for aqueous LLCs. Molecular self-assembly of these substances results in several LLC nanostructures such as normal (oil-in-water) micelles (L_1), normal discontinuous cubic (I_1), normal hexagonal (H_1), lamellar (L_α), normal bicontinuous cubic (Q_1), reverse (water-in-oil) bicontinuous cubic (Q_2), reverse hexagonal (H_2), reverse discontinuous cubic (I_2), and reverse micelles (L_2), which all are shown schematically in Fig. 1. In this review, we have assigned I_α, H_α, and Q_α as the general signs for discontinuous cubic, hexagonal and bicontinuous cubic phases regardless of the type of each structure. Temperature, pressure, light, and magnetic field are some of the external factors which can affect the phase structure of LLCs. In addition, there are other factors including concentration, chemistry and shape of the amphiphilic molecules, water content, and additives (e.g., in the oil phase) that can influence the formation of a particular nanostructure. The LLC structural transitions, which are controlled by aforementioned parameters, are explained via the critical packing parameter (CPP). CPP is defined as:

$$CPP = \frac{V}{al} \tag{1}$$

Where V, a, and l represent the lipophilic tail volume, ‘effective’ cross-sectional area of the hydrophilic head group, and extended lipophilic chain length, respectively. Although the parameter a is sometimes interpreted in LLC literature as a measure of the physical/geometric cross-sectional area of the surfactant headgroup, it is in fact an effective thermodynamic quantity,[13] which encapsulates various conditions, such as charge, solvent ionic strength, temperature, and additives.[14] Free energy minimum models for calculating a have been developed at various levels of complexity. However, examples exist in literature where simply estimating a_e as the geometrical cross-sectional area[15] of the charged headgroup still leads to excellent matching between theory and experiment.

As shown in Fig. 1, when the cross-sectional area of hydrophilic group is larger than that of lipophilic tails (CPP < 1), mean curvature is positive, resulting in the formation of normal phases. When CPP > 1, negative mean curvature is present, resulting in inverted nanostructures (inverse

phase). Lamellar structures are obtained when the mean curvature is zero (CPP = 1), meaning that the cross-sectional area of the polar head group and the tail are almost equal. Therefore, the CPP concept is a powerful semi-quantitative lens for understanding type and stability of LLC phases of amphiphiles. The solvent(s) content is the leading factor which can induce a transition in the structure as schematically shown in Fig. 1. Common techniques used for the characterization of LLC structures include Cross Polarized Light Microscopy (CPLM), Small-Angle X-ray Scattering (SAXS), X-ray Diffraction (XRD), and Nuclear Magnetic Resonance (NMR). Among commonly encountered LLC structures, only the lamellar and hexagonal phases are optically birefringent. H_α mesophases typically show a fan-like texture in CPLM, while L_α typically exhibit streaky-oil textures. Fig. 2a shows examples of these typical textures. Cubic systems lack birefringence due to the isometric nature of the system, and therefore appear dark in CPLM. This includes I_α and Q_α, e.g. body-centered cubic (*BCC*) or face-centered cubic (*FCC*) packings of micelles, and the gyroid, double diamond, and primitive bicontinuous cubic mesophases. Likewise, disordered micellar systems (L_1 and L_2) are also optically isotropic and appear dark in CPLM. In conjunction with CPLM, the relative position of Bragg peaks obtained from XRD or SAXS measurements is the most common method to identify the phase of LLCs.[16] The typically observed X-ray crystallographic features of each structure, presented in Fig. 2, will be discussed in section 2.

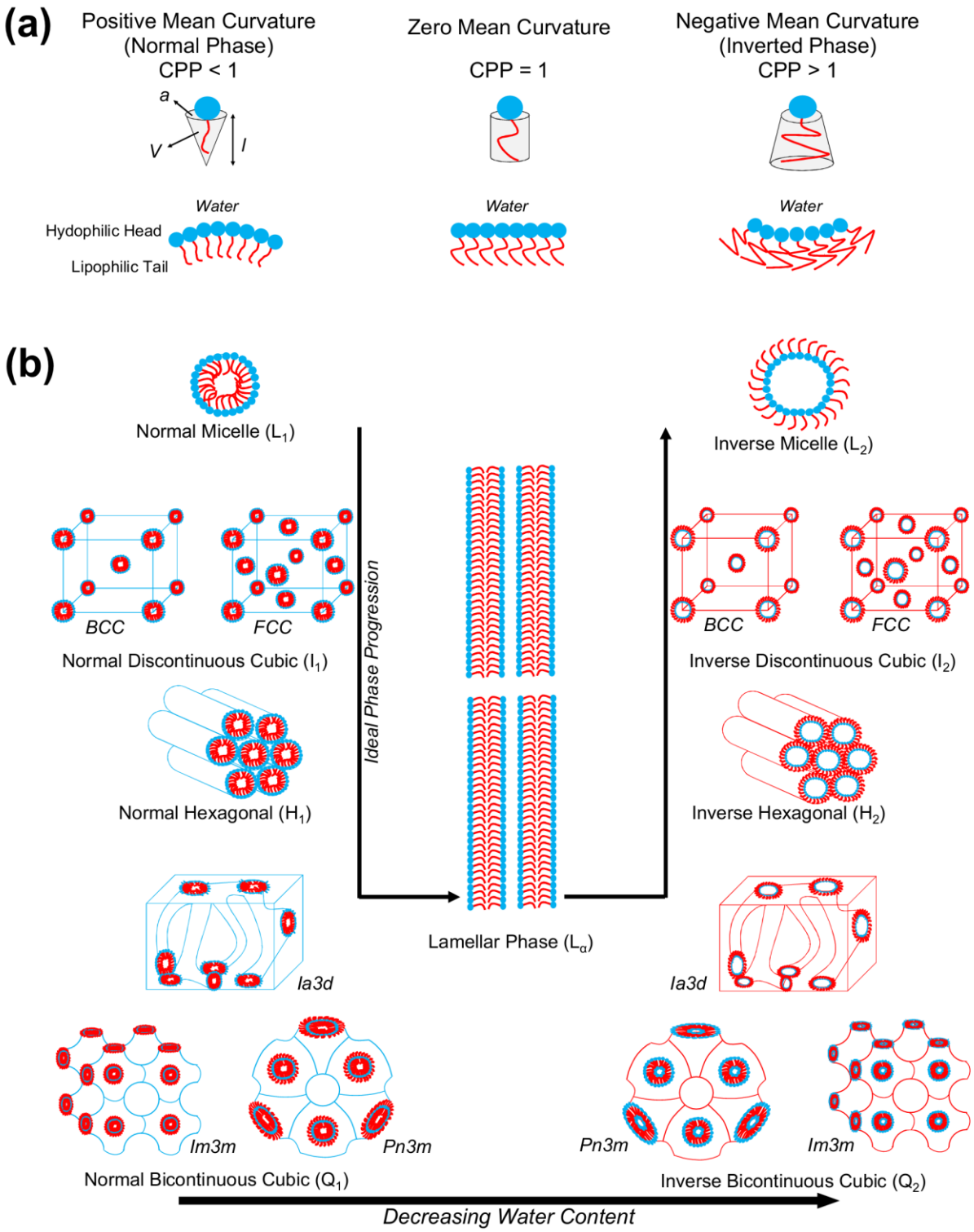

Fig. 1. (a) The schematic representation of CPP and its corresponding favorable structure. (b) Schematic diagram of common LLC structures.[9,16–18] Addition/removal of solvents, such as decreasing water content can drive the phase transition.

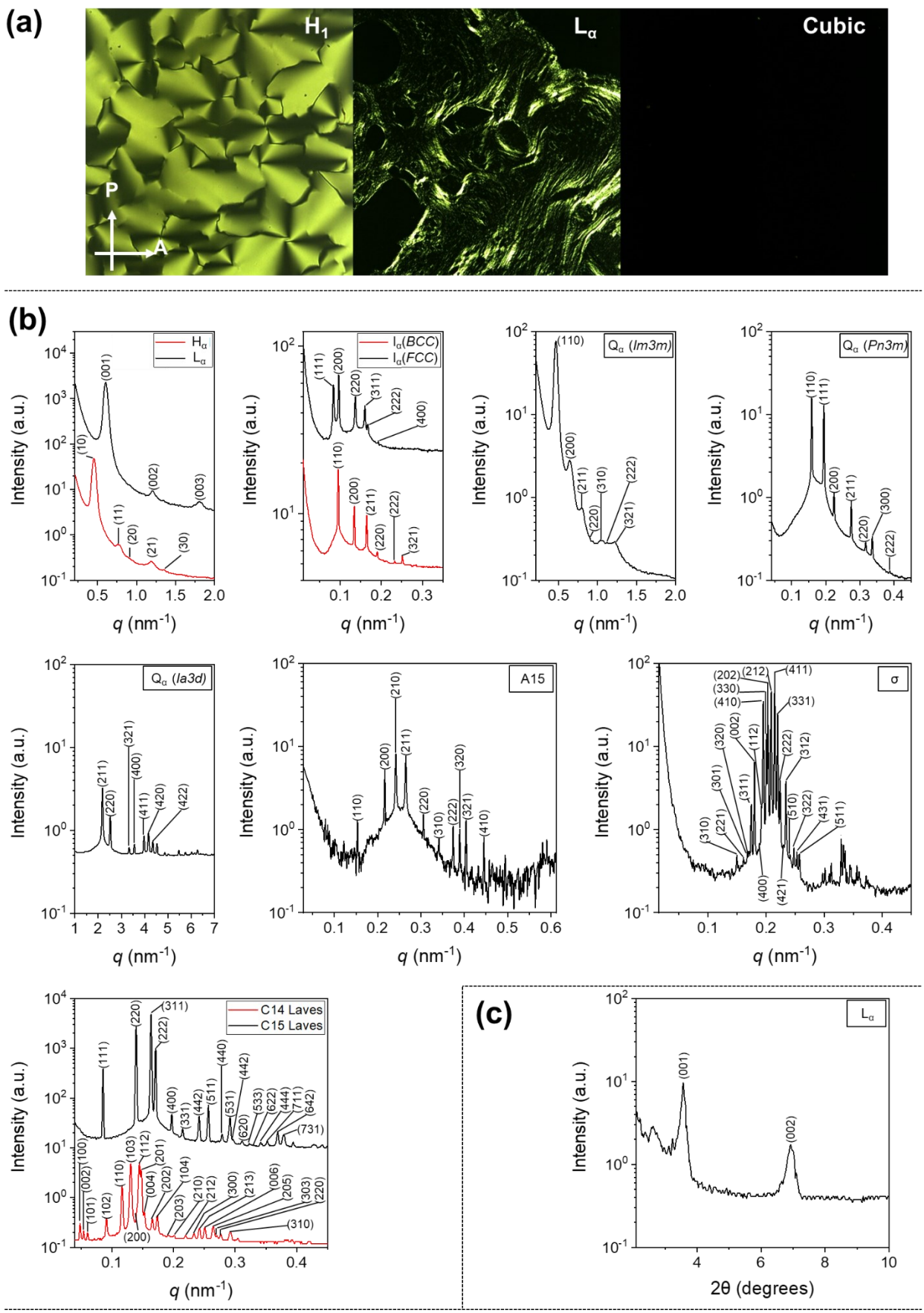

Fig. 2. (a) Typical CPLM Textures for LLC Mesophases – Representative micrographs for various LLC mesophases when samples are observed in a light microscope with a 90º difference in the Polarizer (P) and

Analyzer (A) directions. Birefringent 'fan-like' and 'oily-streak' textures are observed for the normal cylinder (H_1) and lamellar sheet L_α) mesophases. No birefringence is observed for any of the cubic phases i.e. *Im3m*, *Pn3m*, *Ia3d*, *BCC*, and *FCC*. (b) Typical 1D SAXS profiles and corresponding assigned diffraction planes observed for L_α,[19] H_α,[19] I_α (*FCC*[20] and *BCC*[20]), Q_α (*Im3m,*[19], *Pn3m,*[21] and *Ia3d*[22]) and Frank-Kasper phases (A15,[23] σ,[23] C14 Laves,[21] and C15 Laves[21]). (c) Representative example of results acquired from XRD for an L_α LLCs.[24]

Even though LLC phases offer several advantages as previously mentioned, they still suffer from poor mechanical and thermal properties which reduce their suitability in many applications. The predominant method to circumvent these limitations is to use LLCs as a template to synthesize polymers known as polyLLCs, with the desired nanostructure and chemical properties. Such templating is approached via two common routes: synergistic and transcriptive templating. In the former method, the organic component forming the LLC is polymerized, resulting in a cured template. In the transcriptive approach, the desired material is formed (e.g., via polymerization) in the nano-confinement of the LLC template, resulting in the formation of a one-to-one replica. The main challenge in the transcriptive method is to preserve the parental template nanostructure. If the structure is not retained, the method is instead referred to as reconstructive templating and the final product may have a higher or lower order compared to the parent LLC, as shown schematically for the H_2 phase in Fig. 3. Having a precisely controlled structure has led almost all of the studies to focus on high-fidelity retention of the parental nanostructure, which is considered successful LLC templating.[25] There are several reports on using LLC templating for fabrication of organic (e.g., polymers),[26] inorganic (e.g., silica and mesoporous metal and alloys),[27] and organic/inorganic hybrid[28,29] nanostructures. However, LLC templating through the polymerization of organic compounds is the focus of this review since the templating of inorganic species is usually carried out to fabricate nanostructured inorganic materials[27] rather than improving the properties of LLC templated materials.

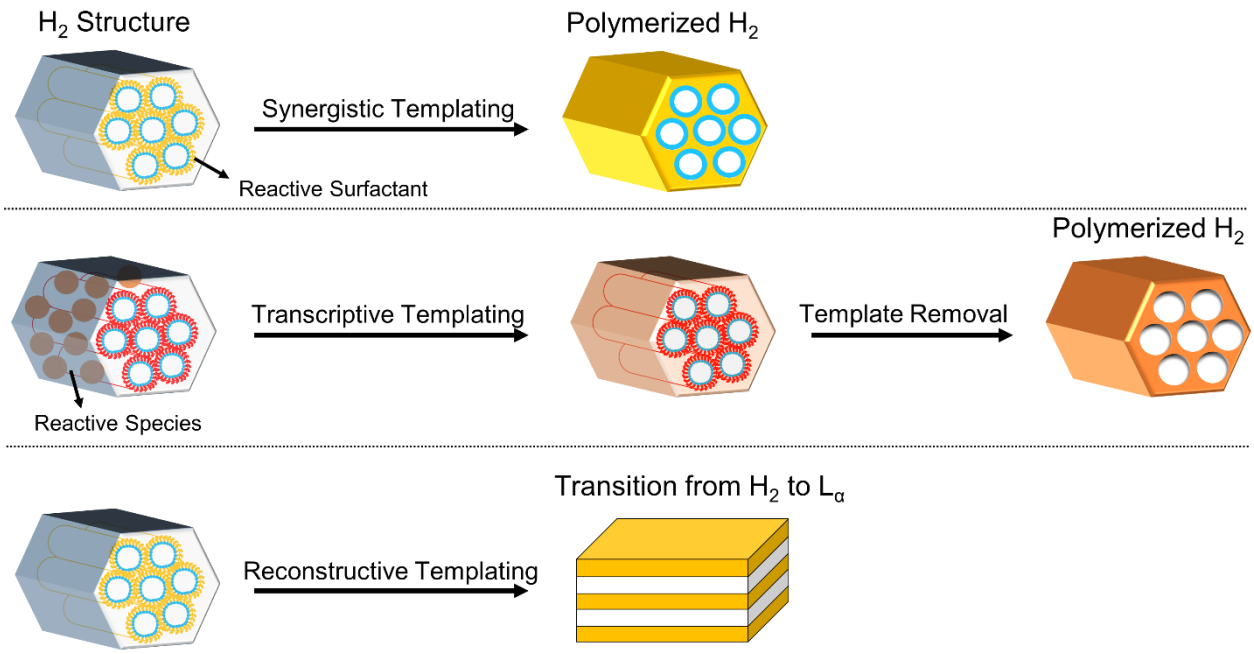

Fig. 3. Schematic illustration of typical synergistic, transcriptive, and reconstructive LLC templating using H_2 structure. The reconstructive templating may lead to various structures and the lamellar structure shown here is just one example of the phase transition possible in this method.

Thanks to the diversity in nanostructures with 1-10 nm length scale, the fabricated polyLLCs not only are applicable in a wide variety of technical applications, but also can provide enhanced properties compared to common materials. For instance, the membranes obtained from polyLLC technology show an enhanced permeability, selectivity, and fouling resistance compared to the current industry standard.[30–34] Furthermore, the LLC-templated hydrogels offer an excellent balance of water uptake, swelling/de-swelling rate, and mechanical properties while preserving key characteristics including biocompatibility, biodegradability, and stimuli-responsiveness.[35–45] For body motion sensors, LLC templating has provided an opportunity to fabricate conductive materials with improved mechanical properties over non-LLC counterparts.[46–48] Additionally, distinctive catalytic activity/selectivity compared to commercially used catalysts has been reported for the catalytic systems fabricated through LLC templating approach.[28,49] Unique light emitting properties are another advantage of LLC-templated products over non-LLC materials.[50,51] There are many other potential applications (e.g., energy storage devices[52]) for polyLLCs which will be further discussed in section 7.

The interesting properties of polyLLCs have promoted the LLC templating approach for a variety of organic compounds since the first trials of synergistic templating by Luzzati and coworkers in the 1960s.[53] In-lab synthesized reactive surfactants have been used in almost all of the synergistic templating studies. For the case of transcriptive templating, there have been several reports concerning the polymerization of widely available (co)monomers and/or cross-linkers in LLC structures created by the solution self-assembly of commercially produced non-reactive surfactant molecules. In the latter case, the cross-linker is used to prevent structure loss during polymerization by kinetically trapping the formed polymer chains and therefore avoiding phase separation/inversion.[54,55] The chemistry, polarity, shape, and concentration of LLC components

are not only key factors for preserving the structure, but also determine the reaction kinetics as well as the properties of the final nano-structure.[26] Hence, a wide variety of reactive amphiphiles and different combinations of non-reactive surfactants/(co)monomers have been used to perform successful synergistic and transcriptive LLC templating as listed in Fig. 4 and Fig. 5, respectively.

Formation of polymer and thus increasing the molecular weight of the monomer phase results in an increase in the thermodynamic penalty of mixing. Additionally, surface energy of the polymerizing phase changes upon the synthesis of polymer chains. Furthermore, the density increases (shrinkage of polymerizing phase takes place) due to the formation of polymer network. The combination of these phenomena can result in a change in the domain size and even phase separation/inversion, and thus loss of the structure.[31] Therefore, in addition to the surfactant,(co)monomer and cross-linker, the polymerization initiation system has an important role on retention of the structure since it affects the polymerization kinetics and therefore controls the formation rate of cross-linked network. According to literature reports, fast polymerization rate increases the chance of structure retention due to the rapid cross-linking of polymer network. As a rule of thumb, when the reaction rate is faster than the time scale required for demixing of growing polymer chains, the structure will most probably be preserved.[26] In addition, polymerization near room temperature decreases the risk of structure disturbance.[26,56] Therefore, photoinitiated polymerization, which typically delivers a fast polymerization rate at room temperature, has been the top choice in most of the studies.[26] A variety of photoinitiators have been employed for LLC templating, as listed in Fig. 6. Nevertheless, there are some studies which have successfully carried out templating by using other initiation systems (e.g., thermal[57] and redox[58]), as presented in Fig. 6. For enhancing readability and simplifying chemical references throughout the paper for readers, we have coded the large variety of key components used in LLC templating (as seen in Fig. 4-6), with the names or chemical formulae of the component tabulated in Table S1.

Following the above introduction on the basic concepts of LLC templating, the remainder of this article is outlined as follows. First, characteristics of common LLC structures used in LLC templating will be presented. Then, the available literature on synergistic templating will be reviewed based on the structure of the LLC template. A similar survey will be presented for transcriptive templating afterward. In each section, the efficiency of the templated products will be analyzed in the application(s) they are designed for (e.g., membranes, hydrogels, energy storage devices, light emitting components, catalyst support, tissue engineering scaffolds, and compatibilizers of immiscible monomers). These sections will be followed by a summary of polymerization kinetics in nanostructured LLCs as well as a concise comparison between synergistic and transcriptive templating techniques. The outlook of the field and available opportunities will be summarized at the end of the review.

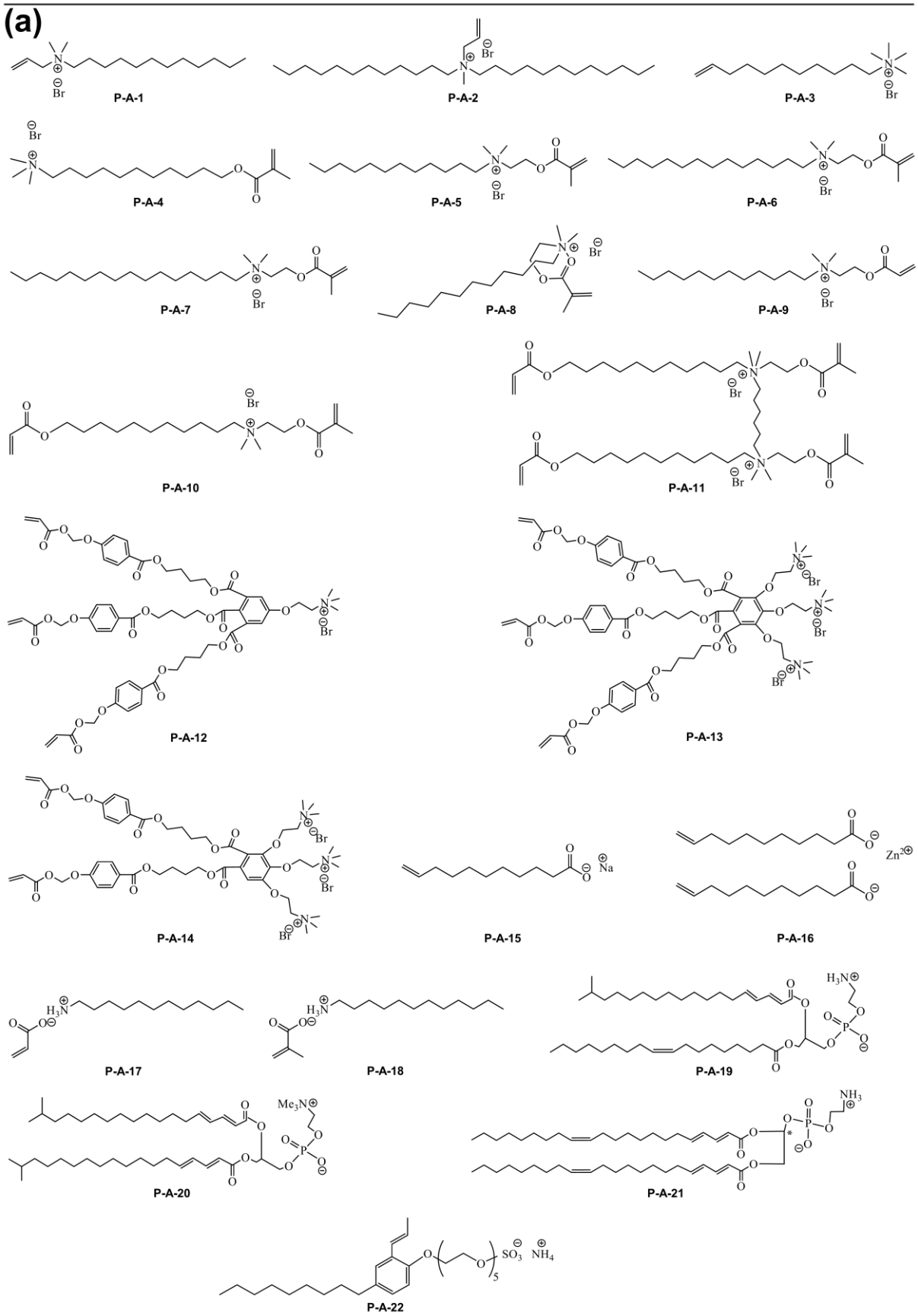

Fig. 4. Chemical structure of (a) polymerizable ionic, (b) polymerizable non-ionic and (c) non-polymerizable amphiphiles used for LLC templating.

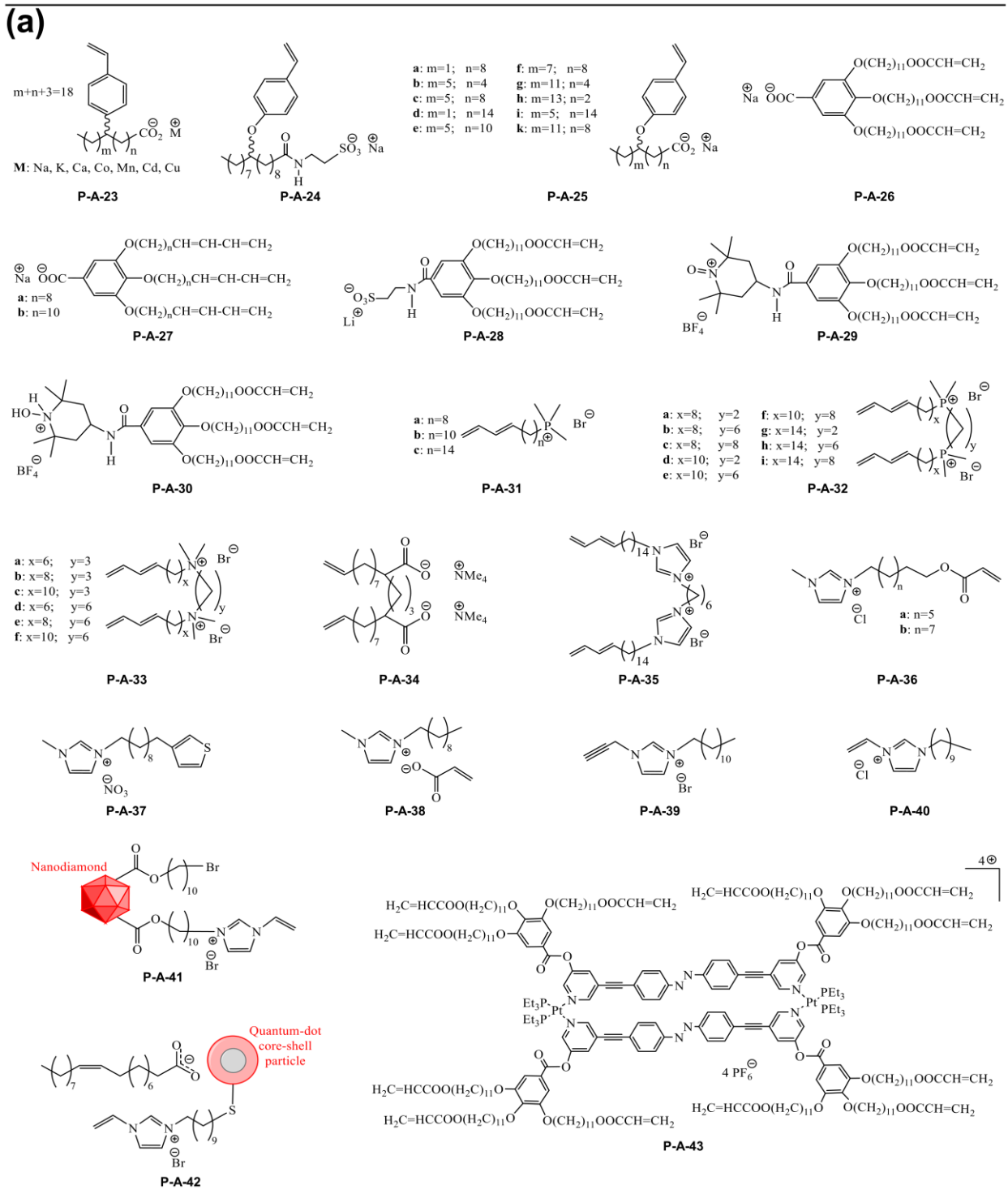

Fig. 4. Chemical structure of (a) polymerizable ionic, (b) polymerizable non-ionic and (c) non-polymerizable amphiphiles used for LLC templating.

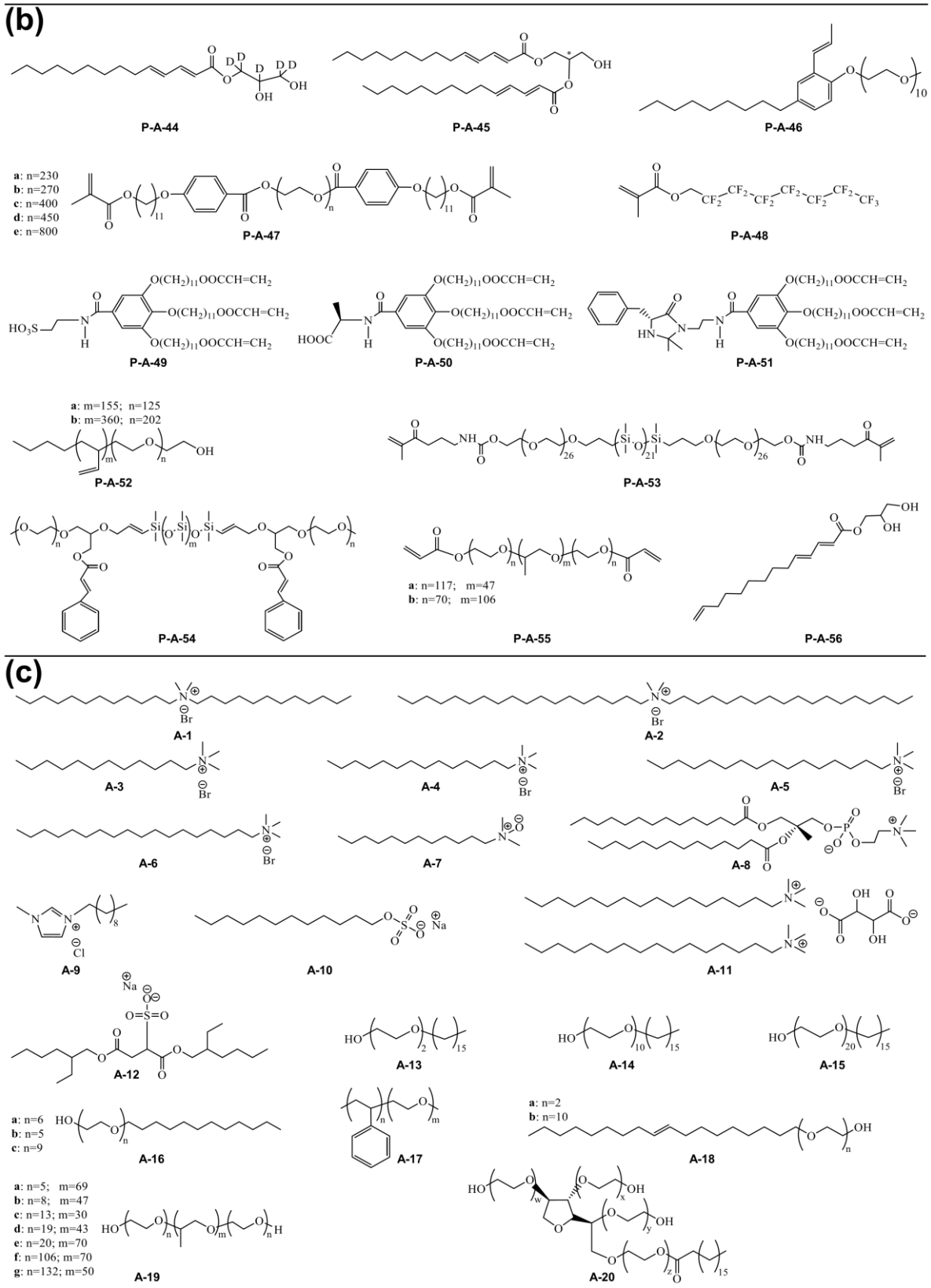

Fig. 4. Chemical structure of (a) polymerizable ionic, (b) polymerizable non-ionic and (c) non-polymerizable amphiphiles used for LLC templating.

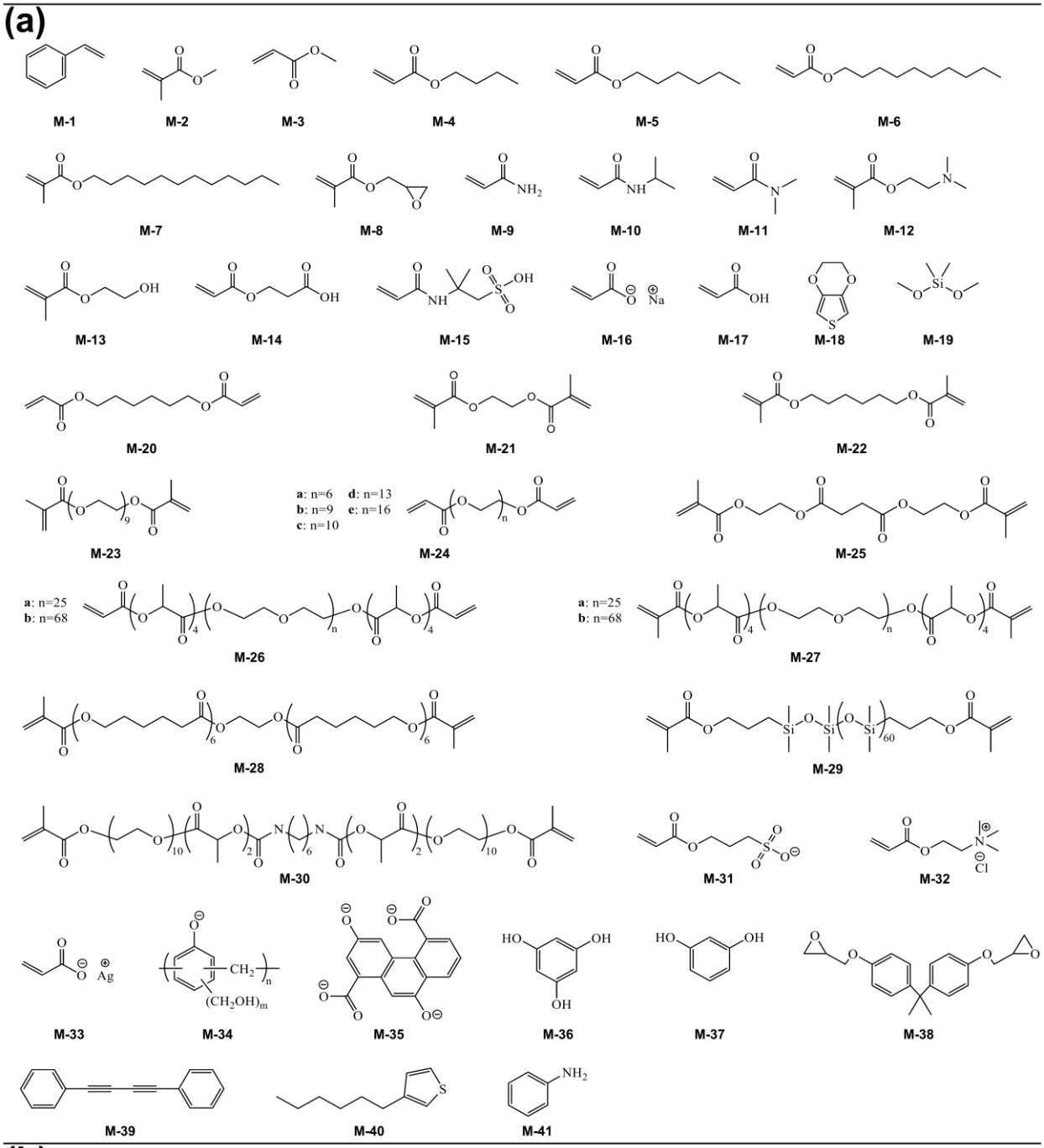

Fig. 5. Chemical structure of (a) (co)monomers and (b) cross-linkers used for LLC templating.

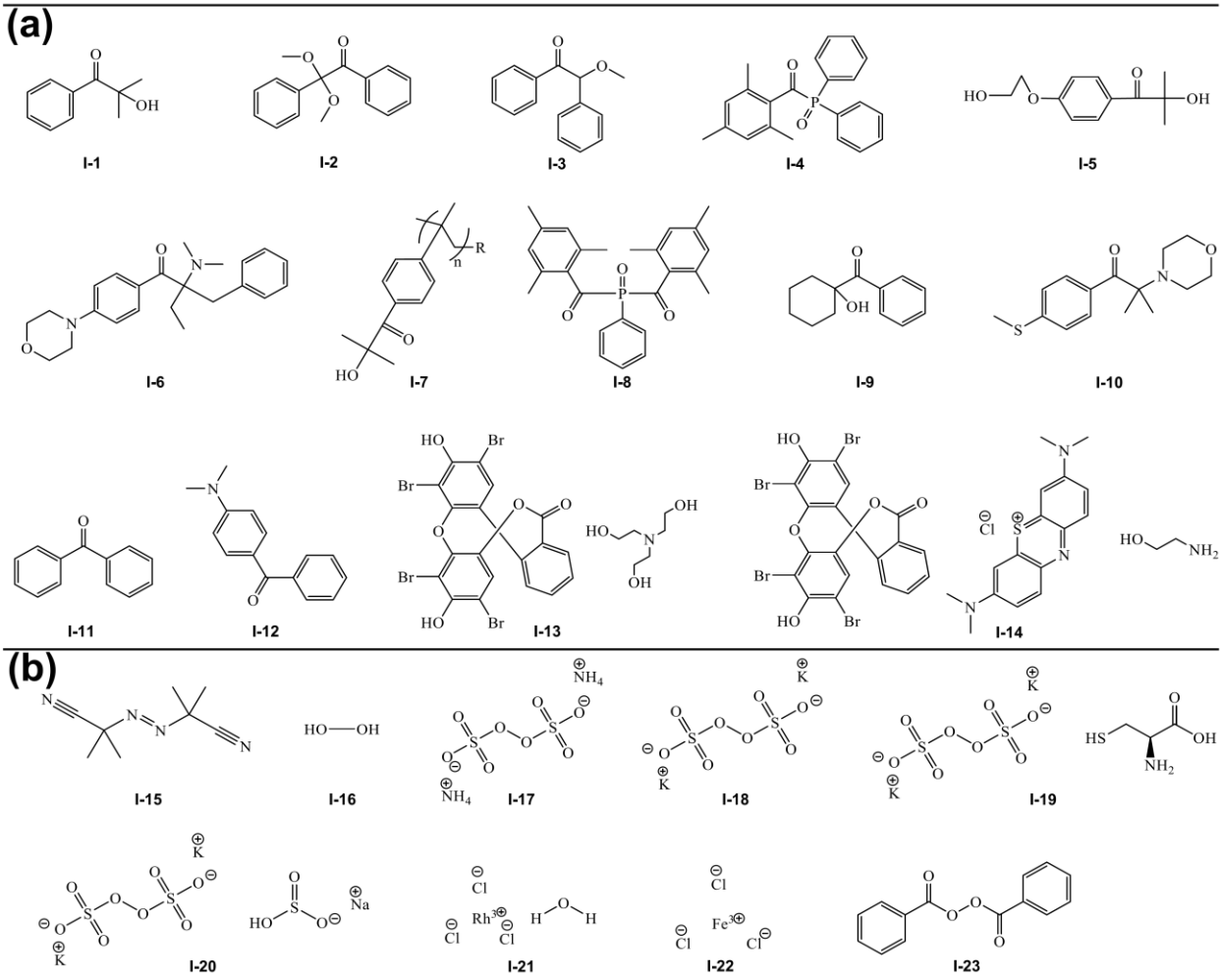

Fig. 6. Chemical structure of the polymerization initiators used for LLC templating: (a) photoinitiators and (b) other (i.e. thermal and ionic) commonly used initiator.

2. Characteristics of LLC structures

As shown in Fig. 1, a variety of LLC nanostructured phases can be obtained from LLC templating processes. Hence, methods for distinguishing different phases/structures are central to verifying a successful templating. X-ray crystallographic studies are the primary tool of choice for LLC structure characterization. In this section, we discuss key geometric characteristics of different LLC structures, which can be revealed via X-ray crystallographic studies. The characteristic period for commonly studied LLC mesophases (~2-5 nm) is amenable to study by X-ray scattering. Both small-angle X_ray scattering (SAXS) and conventional X-ray diffraction (XRD) are used for this purpose, though the latter is typically better suited for elucidating structures at even smaller length scales. A summary of LLC structural characteristics is presented in Table 1.

Table 1. Characteristics of LLC structures used is LLC templating.

LLC structure	CPLM	X-ray Bragg Peak Ratios	Lattice parameter
Hexagonal	Fan-like texture	1:√3:2:√7:3:√12:√13…	$a = \frac{2}{\sqrt{3}} d$, $d = \frac{2\pi}{q_{10}}$
Lamellar	Oily-streak texture	1:2:3:4:5:6…	$d = \frac{2\pi}{q_1}$
Bicontinuous cubic	Not birefringent	*Im3m*: √2:√4:√6:√8:√10… *Pn3m*: √2:√3:√4:√6:√8:√9… *Ia3d*: √6:√8:√14:√16:√18:√20…	$1/a$ = Slope of $1/d_{hkl}$ vs $(h^2 + k^2 + l^2)^{1/2}$
Discontinuous cubic	Not birefringent	*BCC*: 1:√2:√4:√6:√8:√10… *FCC*: 1:√3:√4:√8:√11:√12…	$1/a$ = Slope of $1/d_{hkl}$ vs $(h^2 + k^2 + l^2)^{1/2}$
Frank-Kasper phases	Not birefringent	A15:1:√2:√4:√5:√6:√8:√10:√12… C15:1:√3:√8:√11:√12:√16:√19…	$1/a$ = Slope of $1/d_{hkl}$ vs $(h^2 + k^2 + l^2)^{1/2}$

2.1. Hexagonal (H_α)

The hexagonal columnar structure is one of the most studied phases in LLC templating. H_α consists of closely packed cylindrical micelles arranged in a hexagonal lattice. Depending on the curvature, the hydrophilic head of the surfactant is located on the external or internal surface of the micelles to be in contact with water in H_1 or H_2 structure, respectively. As shown in Fig. 7, there are multiple parameters of interest in the hexagonal phase structure: d is the distance between the planes passing by two adjacent rows of cylinders or d-spacing, a is the center to center distance of two adjacent cylinders or lattice parameter, R_m is the radius of micelle, R_c is the radius of confined phase in micelle, D_m is the intermicellar distance, and $R_{h,max}$ is the radius of the largest circle trapped between the micelles.[56] Bragg peaks with relative positions at the ratios of 1:√3:2:√7:3:√12:√13… (corresponding to the d_{10}, d_{11}, d_{20}, d_{21}, d_{30}, … diffraction planes) are the characteristic signature of the hexagonal structure in X-ray measurements (see Fig. 2b).[17] The d is calculated from Eq. (2) by using the position of the first Bragg peak from SAXS measurement, q_{10}. The lattice parameter can be calculated from Eq. (3) based on the obtained value of d.[17]

$$d = \frac{2\pi}{q_{10}} \tag{2}$$

$$a = \frac{2}{\sqrt{3}} d \tag{3}$$

To calculate R_c, the following equation is used. In this equation, ϕ is the volume fraction of the dispersed phase (i.e., the phase confined in the cylindrical micelles).[17]

$$R_c = a\left(\frac{\sqrt{3}}{2\pi}\phi\right)^{1/2} \tag{4}$$

The radius of micelle R_m is calculated using Eq. (5). Here, ϕ_t is the volume fraction of the confined phase plus the volume fraction of the surfactant.

$$R_m = a\left(\frac{\sqrt{3}}{2\pi}\phi_t\right)^{1/2} \tag{5}$$

The intermicellar distance for H_2 phase D_m, is obtained using Eq. (6). Moreover, the size of the nanoconfinement cavity between micelles can be estimated from the radius of the biggest circle trapped between the micelles $R_{h,max}$. Eq. (7) and (8) can be used for this estimation.

$$D_m = a - 2R_m \tag{6}$$

$$R_{h,\max} = \sqrt{\frac{A_h}{\pi}} \tag{7}$$

$$A_h = a^2\frac{\sqrt{3}}{4} - \pi\frac{(R_m)^2}{2} \tag{8}$$

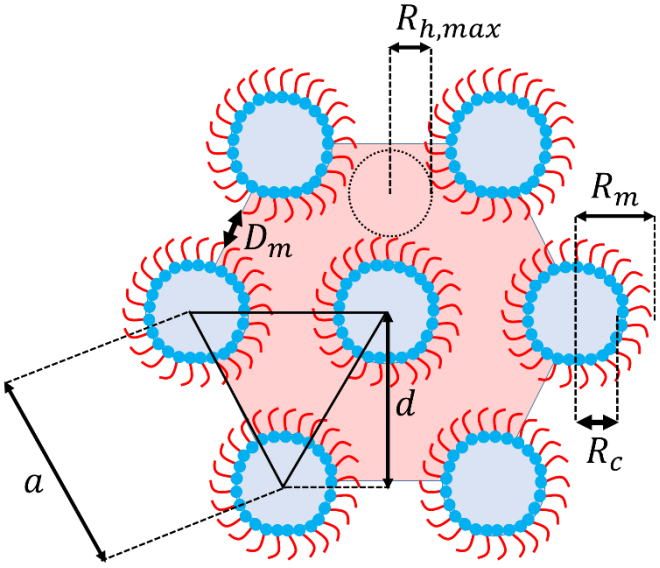

Fig. 7. Typical schematic of H_2 structure with d-spacing (d), lattice parameter (a), radius of micelle (R_m), radius of confined phase in micelle (R_c), intermicellar distance (D_m), and radius of the biggest circle trapped between the micelles ($R_{h,max}$). In this case, ϕ is the volume fraction of the polar phase.

In the broader mesophase literature, other columnar mesophases have been studied which exhibit non-circular cross-sections and/or non-hexagonal packing of the columns. These LLC phases are sometimes termed 'ribbon' phases, and include lattices of rectangularly or obliquely packed mesogen columns.[59] However, they have generally not been studied in the polyLLC context. There

are studies of rectangular columnar phases for thermotropic LCs,[60] but for lyotropic LCs hexagonal columns are the predominantly observed and studied columnar mesophase.

2.2. Lamellar (L_α)

The lamellar phase is formed under zero mean curvature. The hydrophilic heads of the amphiphile molecules assemble toward the water, while lipophilic tails remain away from water. As shown in Fig. 8, L_α has various characteristic dimensions; d is the repeating distance of bilayers or lattice parameter, δ_1 is the thickness of the apolar domain, δ_2 is the thickness of the polar domain, D_1 is the intermicellar distance in apolar phase, D_2 is the intermicellar distance in polar domain, and $R_{1,max}$ and $R_{2,max}$ are the radii of the largest circles trapped between the micelles in apolar and polar domains, respectively.[56] As shown in Fig. 2b,The lamellar phase structure shows a sequence of Bragg peaks in integer ratios of 1:2:3:4:5:6…[17] (corresponding to the d_{001}, d_{002}, d_{003}, d_{004}, d_{005}, d_{006}, … diffraction planes) in X-ray crystallographic studies. The position of the first Bragg peak in SAXS measurement (q_1) is used to calculate d, δ_1 and δ_2 via the following equations, respectively. In these equations, ϕ_1 and ϕ_2 are the volume fraction of the apolar and polar domains, respectively. In other words, ϕ_1 is the volume fraction of oil phase plus surfactant hydrophobic moiety, whereas ϕ_2 is the volume fraction of aqueous phase plus the surfactant hydrophilic segment.

$$d = \frac{2\pi}{q_1} \tag{9}$$

$$\delta_1 = d\phi_1 \tag{10}$$

$$\delta_2 = d\phi_2 \tag{11}$$

To calculate D_1 and D_2, Eq. (12) and (13) can be used. The average intermicellar distance in lamellar structure D_L is obtained via Eq. (14). In these equations, ϕ' and ϕ'' are the volume fraction of the phases confined in the apolar and polar domains, respectively

$$D_1 = d\phi' \tag{12}$$

$$D_1 = d\phi'' \tag{13}$$

$$\frac{1}{D_L^3} = \frac{1}{D_1^3} + \frac{1}{D_2^3} \tag{14}$$

$R_{1,max}$ and $R_{2,max}$ are obtained using Eq. (15) and (16).

$$R_{1,\max} = \frac{D_1}{2} \tag{15}$$

$$R_{2,\max} = \frac{D_2}{2} \tag{16}$$

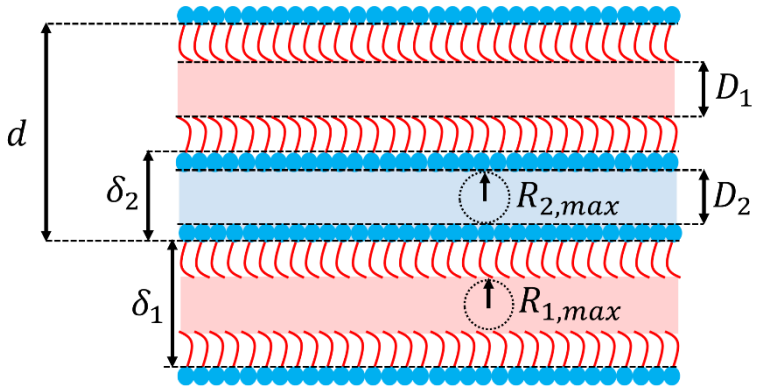

Fig. 8. Typical schematic of L_α structure showing lattice parameter d, δ_1 is the thickness of the apolar domain, δ_2 is the thickness of the polar domain, D_1 is the intermicellar distance in apolar phase, D_2 is the intermicellar distance in polar domain, and $R_{1,max}$ and $R_{2,max}$ are the radii of the biggest circles trapped between the micelles in apolar and polar domains, respectively.

2.3. Bicontinuous cubic (Q_α)

Bicontinuous cubic phases are some of the more interesting but uncommon LLC structures which have been studied for LLC templating. These structures, which are usually obtained by using precisely designed amphiphiles in typically very narrow amphiphile/water weight ratio ranges, consist of continuous but non-intersecting nanochannels separated by a curved bicontinuous layer. Depending on the mean curvature, the bicontinuous bilayer can be hydrophobic tail or polar head (see Fig. 1).[16] Interconnected pores make these structures perfect candidates for a variety of applications, particularly molecular separations because the pores/channels do not require structural alignment. X-ray crystallographic studies typically encounter Q_α structures of three main types, namely the primitive lattice (*Im3m*, Q_{229}), the double-diamond lattice (*Pn3m*, Q_{224}) and the gyroid lattice (*Ia3d*, Q_{230}), as schematically shown in Fig. 1.[9,16,18] The important dimensional parameters of the primitive type are presented schematically in Fig. 9. $2l$ represents the thickness of the apolar domain (including the surfactant tail), $2t_{polar}$ is the polar domain thickness (including the surfactant headgroup), and a is the lattice parameter.[9] In X-ray crystallographic studies, the peak ratios for *Im3m*, *Pn3m* and *Ia3d* are √2:√4:√6:√8:√10… (corresponding to the d_{110}, d_{200}, d_{211}, d_{220}, d_{310}, … diffraction planes),[61] √2:√3:√4:√6:√8:√9… (corresponding to the d_{110}, d_{111}, d_{200}, d_{211}, d_{220}, d_{221} (or d_{300}), … diffraction planes),[61] and √6:√8:√14:√16:√18:√20… (corresponding to the d_{211}, d_{220}, d_{321}, d_{400}, d_{411} (or d_{330}), d_{420}, … diffraction planes),[61] respectively.[9,16] Typical SAXS profiles for different Q_α structures are shown in Fig. 2b. Calculation of these parameters for Q_α structure from X-ray studies is not as simple as for H_α and L_α. To calculate the lattice parameter a, the reciprocal spacings, $1/d_{hkl}$, of the peaks in the X-ray measurement are plotted versus the sum of the Miller indices, $(h^2 + k^2 + l^2)^{1/2}$.[17] The $1/a$ is equal to the slope of the line passing through the data points.

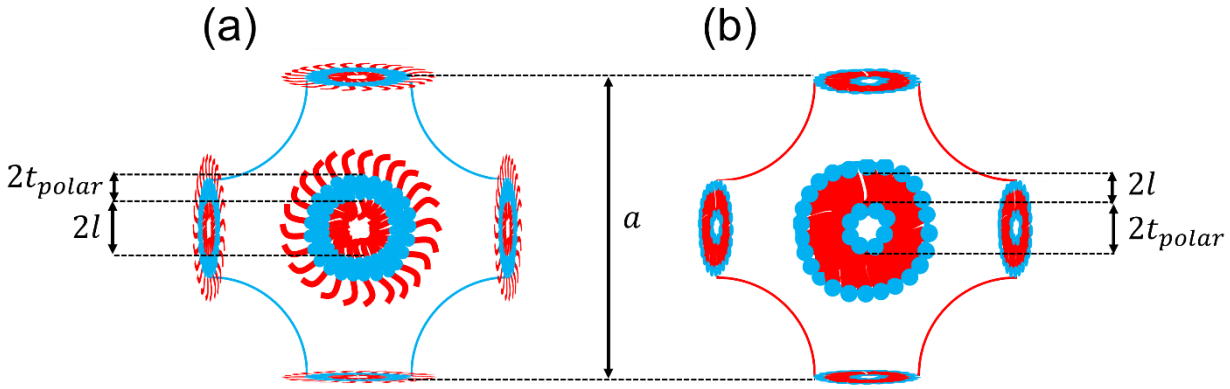

Fig. 9. Typical schematic of (a) normal and (b) reverse primitive Q_α structure with lattice parameter (a) and the thickness of the polar ($2t_{polar}$) and apolar domains ($2l$).

2.4. Discontinuous cubic (I_α)

The discontinuous cubic phases, which are also called micellar cubic, consist of micelles arranged in a cubic lattice. There are two types of cubic lattices for this structure, body-centered cubic (*BCC*) and face-centered cubic (*FCC*), as presented in Fig. 1. In the X-ray measurements, the characteristic peak ratio for BCC and FCC phases are 1:√2:√4:√6:√8:√10… (corresponding to the d_{100}, d_{110}, d_{200}, d_{211}, d_{220}, d_{310},… diffraction planes)[62] and 1:√3:√4:√8:√11:√12… (corresponding to the d_{100}, d_{111}, d_{200}, d_{220}, d_{311}, d_{222},… diffraction planes),[62] respectively (see Fig. 2b).[9] To calculate the lattice parameter (see Fig. 10), a procedure similar to the one for bicontinuous cubic structures is used.[62] Polar domain size α_1 and apolar domain size α_2 of *BCC* lattice can be estimated via Eq. (17) and Eq. (18), respectively.[63] In these equations, R_c is the radius of the spherical micelles and ϕ, which is obtained by Eq. (19), is the volume fraction of continuous domain.

$$\alpha_1 = 2R_c \tag{17}$$

$$\alpha_2 = 2a\left(\frac{3\phi}{8\pi}\right)^{\frac{1}{3}} \tag{18}$$

$$\phi = 1 - 2\frac{\frac{4}{3}\pi R_c^{\,3}}{a^3} \tag{19}$$

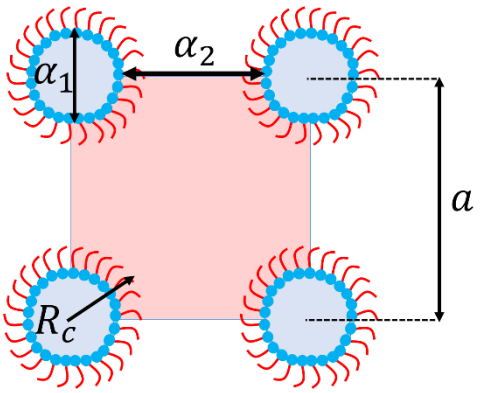

Fig. 10. Typical schematic of inverse *BCC* discontinuous cubic structure with lattice parameter (a), radius of spherical micelles (R_c), polar domain size (α_1) and apolar domain size (α_2).

2.5. Other LLC structures

So far, we have discussed the LLC structures which are commonly observed in different LLC formulations. However, quasi-crystal structures, such as Frank-Kasper (F-K) phases, are also reported for lyotropic systems.[20,21,23,64] F-K phases, which exhibit tetrahedrally close-packed structures, were discovered for metal alloys more than 50 years ago.[65,66] Since then, more than twenty different types of F-K phases have been experimentally observed in metal alloys. Amongst such variety, A15, Laves, σ, μ, M, P, R, and Z phases are the most common ones.[67] In the case of LLCs, formation of A15,[20,23,64] Laves (e.g., C14 and C15)[21] and σ[23,64] phases have been reported in the literature. The LLC with A15 structure contains 8 quasispherical micelles per unit cell with two different types of coordination environments.[20,23,64] The C15 Laves phase includes eight quasispherical micelles located at the positions of a cubic diamond lattice and tetrahedral groupings of smaller micelles fill the remaining tetrahedral interstitial sites.[21] In the case of C14 Laves phase, the micelles are located on the sites of the hexagonal diamond structure.[21] The lyotropic σ mesophase consists of a primitive tetragonal unit cell with 30 quasispherical micelles which belong to five different symmetry-equivalent classes.[23,64] The common F-K phase reported for LLCs are schematically shown in Fig. 11. As with other mesophases, X-ray analysis is used to characterize these structures. Accordingly, as presented in Fig. 2b, the characteristic peak ratio of 1:√2:√4:√5:√6:√8:√10:√12… (corresponding to the d_{100}, d_{110}, d_{200}, d_{210}, d_{211}, d_{220}, d_{310}, d_{222},… diffraction planes) and 1:√3:√8:√11:√12:√16:√19… (corresponding to the d_{100}, d_{111}, d_{220}, d_{311}, d_{222}, d_{400}, d_{331}, … diffraction planes) is observed for A15[20,23,64] and C15[21] Laves phases, respectively. In the case of C14 Laves[21] and σ[23,64] phases, Bragg peaks corresponding to the d_{100}, d_{002}, d_{101}, d_{102}, d_{110}, d_{103}, d_{200}, d_{112}, d_{201}, d_{004},… and the d_{310}, d_{221}, d_{301}, d_{320}, d_{311}, d_{002}, d_{400}, d_{112} or d_{321}, d_{410}, d_{330},…diffraction planes have been reported, respectively. Although these LLC phases have not yet been applied in LLC templating, they seem to have excellent potential in fabrication of nanostructured species with unique properties (see the discussion in section 3.4).

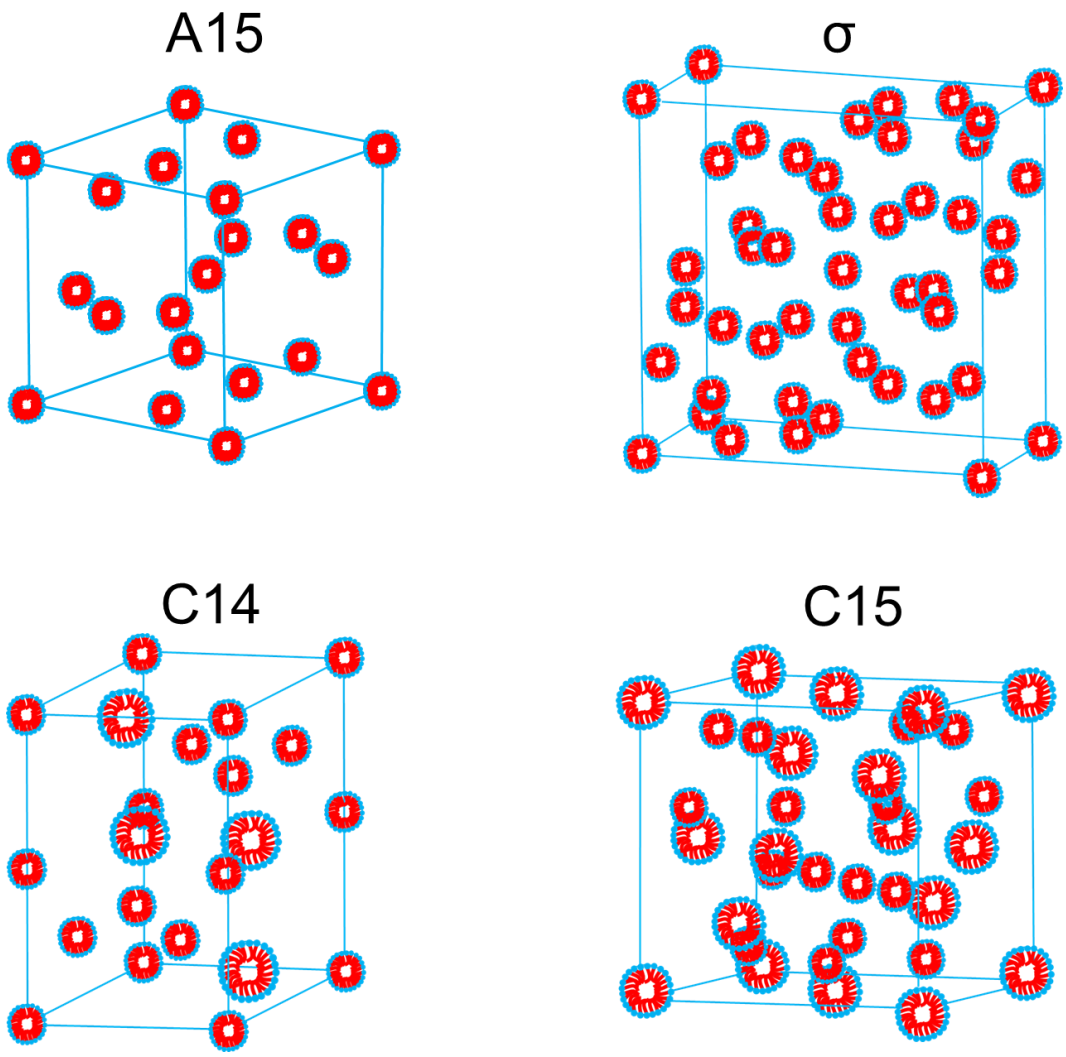

Fig. 11. Typical schematics of different F-K phases observed for LLCs including A15, C14 and C15 Laves, and σ phases.

For the sake of completeness, it should be mentioned that there are other occasionally observed LLC structures which are variously described as 'intermediate', 'transition' or 'irregular' mesophases. One such mesophase is the L_3 'sponge' phase, which has an overall lamellar structural motif, but the spacing of solvent domains is irregular. This polydispersity in feature spacing manifests itself as a broad primary peak in L_3 X-ray diffractograms.[68,69] Another example are the 'ribbon' phases, which are transition/intermediate structures typically observed between hexagonal and lamellar phases.[70] As the focus of this review, and of polyLLC focused research efforts in general, is to obtain regular and well-ordered nanofeatures, these miscellaneous mesophases are understudied in polyLLC literature, likely because they lack any immediately apparent utility because of their non-uniform order and/or transitory nature.

3. Synergistic LLC templating

Since the first works on synergistic LLC templating in 1960s,[53] there have been several successful LLC templating efforts. Early studies suffered from the inability to retain the parent LLC structures after polymerization and/or rather low extents of polymerization/conversion.[57,71–76]

These issues were partly resolved by the introduction of novel reactive amphiphiles, employing highly efficient polymerization initiation systems, and developing new LLC formulations.[7,26] However, the major concern was still to expand the available variety of LLC nanostructures accessible for a successful templating. The performance of different polyLLCs in desired applications is highly dependent on the structures. For instance, in molecular separation applications (e.g., water filtration), permeability, selectivity, and fouling resistance have to be optimized simultaneously.[4] While Q_2 structures offer such opportunity, they are not easily accessible. Moreover, due to the high tortuosity of this structure, cleaning the nanochannels blocked by foulants is highly challenging. On the other hand, H_2 and L_α phases, while easily achievable LLC structures, need further processing steps (e.g., pore/channel alignment by magnetic field) to decrease the tortuosity, thus optimizing the aforementioned membrane characteristics.[30] Similar examples concerning the differences among LLC structures and obtained polyLLCs provide the motivation to classify the following discussion based on the LLC nanostructures.

3.1. Hexagonal (H_α)

A summary of reports in the current literature on synergistic templating of H_α structures is listed in Table 2. As shown in the table, the lattice parameter reported for this structure typically ranges from ~ 3 to ~ 11 nm. The lattice parameter is controlled by the geometric characteristics of the employed reactive amphiphile such as the molecular size and shape, ionic charge, the position of the polymerizable group, and so forth. As an example, P-A-13 which has a 3-head/3-tail structure, results in a larger lattice parameter compared to P-A-12 and P-A-14 with 1-head/3-tail and 3-head/2-tail structures, respectively.[77] P-A-26 is another example for which the *d*-spacing decreases when the hydrophilic head contains trivalent lanthanide salts instead of sodium ion.[78] In addition to the lattice parameter, the accessibility of H_α is also determined by the type of the surfactant. For instance, to form LLC from the mixture of P-A-29 and P-A-30 in water, addition of P-A-50 is crucial.[79] Moreover, specific compositions of amphiphiles in mixture are required to obtain the intended structure. Change in the lattice parameter after polymerization is another important result in most of the studied cases. If the structure is retained, dimensional changes due to the formation of the polymer network[41,56] and formation of a hexagonal structure with different *d*-spacing are believed to be the main reasons for changes in the lattice parameter.

Enhanced thermal stability,[58,61,73,80–88] swelling behavior,[58,76,86–90] and mechanical properties[81,87,90,91] of polyLLC are the common outcomes of a successful synergistic templating process. However, as listed in Table 2, there are some reports on the enhanced properties of polyLLCs in particular applications such as molecular separation membrane,[30,92–94] catalysis,[49,79,95] and light emitting materials.[50,78] As described by Osuji and co-workers, synergistic LLC templating by polymerization of H_1 structure has outstanding potential as membranes in water purification application because such polyLLC membranes offer low tortuosity without requiring any structural alignment. According to their results,[30] it is possible to fabricate a membrane with an excellent permeability coupled with proper selectivity and biofouling resistance by polymerizing H_1 template created from self-assembly of P-A-6 in water.

Using one oil- and one water-soluble cross-linker simultaneously in the mesophase formulation is one promising technique for creating an interconnected network among nanocylinders and therefore fabricating a mechanically robust membrane.

Gin and co-workers have focused on the preparation of molecular separation membranes (e.g., for water purification and gas separation) based on synergistic LLC templating with H_2 structure.[92–94] Although they have obtained promising results demonstrating the higher efficiency of the polyLLC specimens over non-LLC ones, there are still some modifications required (e.g., alignment of the nanochannels) due to the performance mismatch between permeability and selectivity metrics. In addition to the membrane applications, polyLLCs from synergistic H_2 templating have been used as catalyst support in reactions, such as alcohol oxidation[79] and esterification.[95] The reported results show that polyLLC-based catalysts exhibit an improved selectivity and activity comparable to the industrially used catalysts.[49,79,95] In another application, a H_2 template has been used to fabricate a nanocomposite containing poly(*p*-phenylenevinylene) (PPV) inside the nanochannels, resulting in a durable material with higher light emission capabilities compared to pure PPV.[50,78]

3.2. Lamellar (L_α)

As summarized in Table 2, several studies have used L_α structures in synergistic templating. Depending on the amphiphile(s) and LLC formulation, lattice parameters in the range of ~ 3 to ~ 12 nm have been obtained. In addition, in most of the cases, L_α is obtained at relatively high surfactant concentrations (~ > 70 wt%).[51,73,81,96–102] Similar to the hexagonal structure, changes in the lattice dimension are typically observed after polymerization, attributed to the formation of a polymer network as well as the production of L_α structures with different *d*-spacings. Another notable point here is the formation of a unique structure called hexagonal perforated lamellar (HPL) which is a hybrid lamellar-hexagonal structure made from sheets that have in-plane aqueous perforations arranged on a hexagonal lattice. HPL is formed when structural changes from L_α to Q_α takes place during LLC formation or after the polymerization. HPL has been commonly observed in LLCs based on amphiphilic imidazolium-based ionic liquids.[103] HPL is considered to be a necessary kinetic pathway for the existence of Q_α phase.[104]

As mentioned in the Introduction section, improving the thermal, mechanical, and physical properties of nanostructured polymers are the primary goals of polymerization of LLC phases. Therefore, the majority of the reported works on synergistic templating of the L_α phase have focused on proving this concept in addition to studying the polymerization kinetics, which will be discussed in a later section.[58,61,73,80,81,86,87,101,103,105,106] As an example, Firestone et al. have performed several studies to cure L_α and HPL structures made by reactive amphiphilic imidazolium-based ionic liquids to produce a robust ion gels without sacrificing the conductivity of the parent LLC phases.[86,87,103,105]

3.3. Bicontinuous cubic (Q_α)

LLCs with Q_α structures having lattice parameters of ~ 5 to ~ 13.5 nm have been used in synergistic templating efforts (see Table 2). The accessibility of Q_α phase before polymerization is the most important challenge in templating process. Due to the relative scarcity of Q_α phases, researchers have generally focused their efforts in synthesizing new reactive amphiphiles and formulations design and optimizations.[107] For instance, the formation of Q_α phases is less challenging in binary phases rather than in ternary ones.[107] On the other hand, the shape of the amphiphilic monomer (e.g., the volume of the lipophilic tail, the 'effective' area of the hydrophilic head, and the extended lipophilic chain length) dictates the type of the LLC structure. As an example, monomers with small hydrophilic head and a broad flattened hydrophobic tail (tapered shape) tend to form H_2 structure, whereas amphiphilic monomers with cylindrical shape tend to form lamellar phase.[83] O'Brian and co-workers were pioneers in designing reactive surfactants that form Q_2 structure.[58,82,108–111] The Gin group have added a considerable body of knowledge on synergistic templating of Q_α structures. Among other contributions, they have shown that Gemini-structured reactive amphiphiles which have low critical micelle concentration (CMC) are reliable species for obtaining Q_1 structures.[32,33,52,112–121]

Efforts by the Gin group are not limited to design and synthesis of new monomers for LLC templating in bicontinuous cubic structures, but also include investigations of the efficiency of the polymerized LLCs in different applications. In one trial, they have shown that polymerized Q_2 structure of P-A-28/Li salt solution of propylene carbonate shows a conductivity similar to the liquid-like electrolytes while maintaining high flexibility even at temperatures as low as -35 °C.[116] In another series of works, they have used Q_1 phases obtained from P-A-32 to fabricate membranes with different applications. As breathable barrier materials for chemical agent protection, the produced butyl rubber (BR) incorporated membranes (LLC/BR composite) with Q_1 structure show improved water vapor permeability/selectivity over LLC/BR composite membranes with H_2 structure.[115] On the other hand, the water filtration performance of the membranes fabricated with the Q_1 LLC lies in between that of conventional nanofiltration (NF) and reverse osmosis (RO) membranes.[33,119] They have also shown the possibility to modify/reduce the pore size of the final product by atomic layer deposition (ALD) and therefore to increase the efficiency of light gas separations.[117] In another effort, Gin and co-workers decreased the production cost of Q_1-based water filtration membranes by using P-A-33 instead of P-A-32 while maintaining the same efficiency.[118] To further examine the performance of this structure, the team has used a mixture of P-A-35 in glycerol to obtain Q_1-based membranes having a thin active layer (< 0.1 micrometer) as a thin film composite (TFC). The generated membranes show a water flux comparable to the industrially used NF and RO membranes, salt rejection in between of them, and higher fouling resistance and flux recovery.[32,114,120,121] Furthermore, the fabricated membranes exhibit an improved water/chemical agent molar vapor selectivity over Q_1 LLC/BR membranes created by P-A-32 while requiring lower production costs.[112] Modification of ion sorption and pore transport properties via polymerization of an ionic monomer inside the membrane pores has also been explored to modify the performance of the Q_1-based membranes.[113] Finally, they have reported a higher dehydration and resistivity of the Q_1-based anion exchange membrane (AEM) in dilute $FeCl_3$ solutions compared to amorphous AEMs thanks to closer spacing of ion exchange sites.[52]

3.4. Discontinuous cubic

Discontinuous cubic phases have mainly been used in synergistic templating to study the polymerization kinetics in LLCs,[98,122] which will be discussed later. However, Lopez-Barron et al. have used a P-A-55 directed FCC type discontinuous cubic structure to fabricate a cross-linked ion gel with lattice parameter spanning from 15 to 30 nm. Partially deuterated ionic liquid (ethylammonium nitrate) has been used instead of water to fabricate the LLC. By controlling the LLC composition, they have been able to fabricate ion gels having highly viscoelastic or elastomeric behavior with excellent mechanical properties, conductivity, and mechanoelectrical responses.[46,48] They have also shown that the produced ultrastretchable iono-elastomers can be used as a motion sensor as well as a temperature sensor with sufficient sensitivity and accuracy. Impressive mechanical properties of such discontinuous cubic structures, in which discrete micelles (spheres) are cross-linked, can indicate opportunities in other technical fields (e.g., membrane application) which require robust materials.[47] The mentioned properties can possibly be further improved if the F-K phases are employed in the synergistic templating instead of common discontinues cubic structures.

Table 2. Summary of the reported results for synergistic LLC templating.

** Calculated d-spacing for the primary reflection in the SAXS profile; Dis. Cube: Discontinuous Cube; BR: Butadiene rubber; TDS: Total dissolved solid; DOC: Dissolved organic carbon; FW: Flow back water; PDA: Polydopamine; CEES: 2-Chloroethyl ethyl sulfide; DMMP: Dimethyl methylphosphonate; DOP: Dioctyl phthalate; ChO: Chemical oxidation; HPL: Hexagonal perforated lamellar; PPV: Poly(p-phenylenevinylene); ADL: Atomic layer deposition*

Amphiphile	Cross-linker	Initiation system	Reaction temperature [°C]	Amphiphile concentration [wt%]	Structure before polymerization	Structure after polymerization	Lattice parameter before reaction [nm]	Lattice parameter after reaction [nm]	Application characteristics of the product	Polymerization kinetics	Remarks	Ref.
P-A-1	-	I-15 or UV	RT - 60	48 - 83 (H_1) 83 - 92 (Q_1) > 94 (L_α)	H_1, Q_1, L_α	Retention of the structures	4 (H_1), 7.21 (Q_1), 3.02 (L_α)	4.08 (H_1), 7.57 (Q_1), 2.95 (L_α)	20 °C higher thermal stability of the cured LLC	Conversion of ~ 30%	-	73
P-A-2	-	I-15 or UV	RT - 60	>75	L_α	-	2.5 - 2.97	-	-	Polymerization was not successful	-	73
P-A-3	-	I-15 or UV	60	50 - 60 (L_1) 63 - 80 (H_1)	L_1, H_1	Retention of the structures	3.57 (H_1)	3.57 (H_1)	No difference in thermal stability after templating	Conversion of ~ 45%	-	75
P-A-4	-	γ-ray radiation	RT	58 - 65	H_1	Retention of the structures	3.98	-	Swelling with polar and nonpolar solvents	Higher reaction rate than non-LLC sample but lower conversions than P-A-5 (conversion of ~ 60%)	Reactive group in the tail resulted in an incomplete reaction	76
	-	I-2 or I-5	RT	60 - 79 (H_1) > 82 (L_α)	H_1, L_α	Complete structure lose with I-5 and limited retention of H_1 with I-2	4.157 (H_1), 3.05 (L_α)	-	-	Polymerization rate: L_α < H_1 < non-LLC Higher polymerization rate with I-2 Lower reaction rate compared to P-A-5	To prepare H_1 and L_α, 10-29 and 32-40 wt% A-3 was used, respectively with respect to the total surfactant content	96
P-A-5	-	γ-ray radiation	RT	50 - 60 (L_1) 60 - 83 (H_1) 83 - 90 (Q_1)	L_1, H_1, Q_1	Retention of the structures	3.56 (H_1), 7.3 ± 0.7 (Q_1)	3.83 (H_1)	Higher toluene uptake for H_1 over Q_1 Higher water uptake for Q_1 over H_1	Polymerization rate: non-LLC < Q_1 < L_1 < H_1 Almost complete conversion for LLC samples	The order of the structures were changed by swelling	76
	-	I-5	RT - 55	60 - 80 (H_1) 80 - 90 (Q_1) > 90 (L_α)	H_1, Q_1, L_α	Retention of the structures	3.71 (H_1), 3.03 (Q_1)*	3.71 (H_1), 3.3 (Q_1)*	-	Polymerization rate: H_1 < Q_1 < Q_1 + L_α < L_α	-	97
	-	I-5	RT	50 (Dis. Cube) 60 - 78 (H_1) > 90 (L_α)	Dis. Cube, H_1, L_α	H_1 changed to L_α L_α is retained	3.55 (H_1)	3.7 (H_1)	-	Polymerization rate: Dis. Cube = Dis. Cube/H_1 < H_1 < L_α	H_1 structure was highly prone to phase transition	98
	-	I-2 or I-5	RT	60 - 79 (H_1) 79 - 82 (Q_1) > 82 (L_α)	H_1, Q_1, L_α	structure retention in higher reaction rates	3.84 (H_1), 3.2 (Q_1)*, 3.07 (L_α)	3.88 (H_1)	-	Polymerization rate: non-LLC < H_1 = Q_1 < L_α Higher polymerization rate with I-2	To prepare H_1, Q_1 and L_α, 10-29, 29-32 and 32-40 wt A-3 was used, respectively with respect to the total surfactant content	96
P-A-6	-	I-5	RT	50 (Dis. Cube) 60 - 78 (H_1) > 90 (L_α)	Dis. Cube, H_1, L_α	H_1 changed to L_α L_α is retained	4.32 (H_1)	4.18 (H_1)	-	Polymerization rate: Dis. Cube < Dis. Cube/H_1 < H_1 < L_α	The polymerization rate of P-A-6 was lower than P-A-5	98
	C-6	I-5	RT	70	H_1	H_1 is retained when more than 5.9% C-6 is used	4.32 - 4.1 (in 0 - 8.34% of C-6)	-	Higher water uptake when H_1 structure is retained	Polymerization rate was the highest when transition from H_1 to L_α happened (C-6 content of less than 3.5%)	Higher water uptakes at higher cross-linker contents was in contrary with the behavior of the non-LLC samples	89
	C-8 / C-9-b	I-3	RT	55-80	H_1	Retention of the structure	4.16	4.16	Thickness-normalized water permeability of ~10 liters m^{-2} $hour^{-1}$ bar^{-1} µm The molecular weight cut off and size cut off for the charged solutes were ~350 Da and 1 nm Antifouling properties toward biofouling and antimicrobial properties due to the presence of quaternary ammonium groups	-	Using the oil- and water-soluble cross-linkers resulted in excellent mechanical properties and prevented phase transition Alignment was not required	30
P-A-7	-	I-5	RT	50 (Dis. Cube) 60 - 78 (H_1)	Dis. Cube, H_1	H_1 changes to L_α	4.8 (H_1)	4.64 (H_1)	-	Polymerization rate: Dis. Cube < Dis. Cube/H_1 < H_1	-	98
P-A-8	-	I-15 or UV	RT - 60	40 - 57 (L_1) 70 - 73 (H_2) 80.7 (Q_1)	L_1	-	-	-	-	More than 95% conversion in 15 min with I-15	P-A-8 formed H_1, Q_1 and L_α, but polymerization was not successful for these structures	123
P-A-9	This reactive surfactant has been used for transcriptive templating. Please see Table 3/M-9 section.											
P-A-10 or P-A-11	C-3	I-2	RT	-	-	-	-	-	Water contents of around 40% can be tolerated with the transparent polymers	-	The presence of methacrylate at the hydrophilic head group and low cross-linker content resulted in phase transition	124
P-A-12	C-3	I-2	RT	81	H_2	Retention of H_2 at 10 wt% C-3	6.53	7.1	-	-	The structure cannot be retained at 30 wt% C-3	77
P-A-13	C-3	I-2	RT	28 (Dis. Cube) 54 (H_2)	Dis. Cube, H_2	Disordered structure at 30 and 12 wt% C-3 for H_2 and Dis. Cube, respectively	8.65 (H_2)	9.62 (H_2)	-	Incomplete conversion due to the chains mobility restriction in cross-linked network	-	

Table 2. Summary of the reported results for synergistic LLC templating (continue).

Amphiphile	Cross-linker	Initiation system	Reaction temperature [°C]	Amphiphile concentration [wt%]	Structure before polymerization	Structure after polymerization	Lattice parameter before reaction [nm]	Lattice parameter after reaction [nm]	Application characteristics of the product	Polymerization kinetics	Remarks	Ref.
P-A-14	C-3	I-2	RT	54	H_1	Structure Retention at 30 wt% C-3	7.61	7.82	-	-	-	77
P-A-15	-	I-17	60	47 - 59	H_1	Disordered structure at high temperature	4.192 (H_1)	2.883 (L_α)	-	-	After polymerization, L_α was seen when the temperature was decreased to 20 °C	57,71
	-	γ-ray radiation	30 - 60	40 - 60	H_1	Probable change to L_α	-	-	-	Conversion of ~ 20 - 40% The highest polymerization rate happened in LLC structure	-	72
	-	I-15 or UV	RT - 60	< 38 (L_1) 42 - 55 (H_1)	L_1, H_1	Retention of the structures	4.5 (H_1)	3.7 (H_1)	-	Conversion of less than 30% Conversion in non-LLC phase was ~ 80%	-	74
P-A-16	-	γ-ray radiation	0 - 70	-	-	-	-	-	-	Conversion of less than 30%	This mixture can form L_α at temperatures more than 100 °C	72
P-A-17	C-1	I-3	RT	80	L_α	Retention of the structure	3.56	3.62	Insolubility in water and organic solvents even without cross-linker	Almost complete conversion	-	106
P-A-18	C-1	I-3	RT	20 (Q_1) 80 (L_α)	Q_1, L_α	L_α was retained but Q_1 changed to L_α	2.58 (L_α), 10.47 - 11.59 (Q_1)*	2.93 (L_α), 3.33-3.45 (Q_1)*	Insolubility in water and organic solvents even without cross-linker	Almost complete conversion	Q_1 changed to L_α with or without using C-1	106
P-A-19 / P-A-20	-	I-20	60 - 65	2.5 - 50	H_2, L_α, Q_2	Retention of H_2	5.5 (L_α), 6.5 (H_2)	6.75 (H_2)	Improved thermal stability Not soluble in organic solvents	Conversion of more than 80%	H_2 and L_α were seen at temperatures higher and lower than 60 °C, respectively Q_2 structure was obtained via low concentrations of P-A-19/P-A-20 in water (25 - 100 mg/ml)	58
P-A-21	-	I-16 or I-19	60	50	H_2	Retention of the structure	7.26	7.06	Improved thermal stability	Conversion of more than 90%	The presence of H_2 + Q_2 phase was detected for the LLC before polymerization when the temperature was less than 40 °C	82
P-A-22	This reactive surfactant has been used for transcriptive templating. Please see Table 3/M-4 section.											
P-A-23	C-1	I-1	RT	87	H_2, L_α	Retention of the structures	3.2 - 4.24 (H_2), 3.82 (L_α)	3.24 - 4.12 (H_2), 3.82 (L_α)	Precipitation of CdS particles inside the cadmium containing pores by exposure to H_2S	Almost complete conversion	L_α was obtained when the metal ion was potassium *d*-spacing depends on the type of metal ion incorporated in the structure of P-A-23 This structure can also be used for in-situ synthesis of ~ 2 wt% silica in the pores	51,100
P-A-24	C-1	I-1	RT	86	H_2	Retention of the structure	4.71	4.35	The formed catalyst afforded condensation products with consistent syn/anti diastereoselectivity ratios of ~ 2/1 in Mukaiyama aldol and Mannich reactions in water	-	The structure underwent a slight distortion due to Sc(III) ion exchange	49
P-A-25	-	I-1	RT	82	H_2	Retention of the structure	2.87 - 5.33	2.92 - 5.35	Higher thermal stability	Conversion of ~ 80%	High water content can change H_2 to L_α	83
P-A-26	-	I-1	RT	80	H_2	Retention of the structure	4.04	3.98	Higher light emission of the nanocomposite compared to pure PPV Longer stability of PPV in polymerized LLC due to the isolation from oxygen	Almost complete conversion	PPV was in-situ formed as a filler in the pores of H_2 structure	50
	-	I-1	RT	85	H_2	Retention of the structure	3.62 - 4.3	3.49 - 4.13	When PPV was incorporated in trivalent Eu containing polymerized LLC, a new intense emission band appeared compared to sodium ion	Almost complete conversion	Same metal ion charge resulted in same *d*-spacings Trivalent lanthanide salts showed lower spacings	78
	-	I-1	RT	88	H_2	Retention of the structure	4.25	4.18	-	-	Xylene solution of initiator was used in LLC preparation	84
	-	I-1	RT	80	H_2	Retention of the structure	4.04	3.98	Water flux of 0.3 ± 0.1 L m^{-2} h^{-1} at 50 psi The pore size of 1.2 nm based on the molecular weight cut off	Conversion of less than 30% in air Almost complete conversion in nitrogen	To prepare the membrane, a solution of LLC in methanol was used for roll-casting	93

Table 2. Summary of the reported results for synergistic LLC templating (continue).

Amphiphile	Cross-linker	Initiation system	Reaction temperature [°C]	Amphiphile concentration [wt%]	Structure before polymerization	Structure after polymerization	Lattice parameter before reaction [nm]	Lattice parameter after reaction [nm]	Application characteristics of the product	Polymerization kinetics	Remarks	Ref.
P-A-26	-	I-1	RT	25 - 73.5	H_2	Retention of the structure	4.22 (at 13.8 wt% BR)	4.1	The prepared membrane of polymerized LLC/BR composite resulted in water vapor flux of 438 g m^{-2} day Additional BR phase vulcanization step was used to improve CEES rejection	Conversion of ~ 79%	Blending with 25 wt% BR increased *d*-spacing to 3.95 H_2 structure was achieved when up to 75 wt% BR was used BR solution in *n*-hexane was used for blending	92
	-	I-1	RT	80	H_2	Retention of the structure	-	4.03	The membrane of the polymerized LLC significantly influenced the solubility of CO_2 and retarded the diffusion for all gases	Almost complete conversion	To prepare the membrane, a solution of LLC in ethyl acetate was used for casting	94
	-	I-4	RT	88.5	H_2	Retention of the structure	-	-	-	-	Magnetic field was used to successfully align the nano-channels before polymerization 8 wt% of M-4 was also used as the oil phase in LLC	125
P-A-27	-	I-1	RT	86	H_2	Retention of the structure	3.84 (P-A-27a) 4.14 (P-A-27b)	3.77 (P-A-27a) 3.98 (P-A-27b)	Higher thermal stability	-	*n*-Dodecane initiator solution was used in LLC preparation	84
P-A-28	-	I-1	RT	84	Q_2	Retention of the structure	8.87	8.29	The polymerized LLC showed a conductivity similar to the liquid-like electrolytes while maintaining high flexibility even at temperatures as low as -35 °C	Conversion of ~ 85 - 95%	Li salt solution of the liquid electrolyte, propylene carbonate (PC) was used instead of water to prepare LLC Crude P-A-28 containing 0.87 wt% (LiCl + NaCl) free salt contaminants with 15 wt% PC showed L_α structure	116
P-A-29 / P-A-30	-	UV	RT	95	H_2	Retention of the structure	4.91	4.85	The polyLLC-based catalyst showed higher activity compared to industrially available TEMPO-based catalysts Lower catalyst activity toward alcohols with bigger molecules The catalyst can be reused without major loss of activity	Almost complete conversion	19 wt% of amphiphile was a mixture of P-A-29 and P-A-30 The remaining 76 wt% was P-A-50 The polymerized LLC film was powdered and sieved for 75 – 150 µm particle sizes for catalysis experiments	79
P-A-31	C-1	I-2	RT	50 - 75 (H_1) 75 - 85 (Q_2) 85 - 95 (L_α)	H_1	Retention of the structure	4.57	4.5	Higher thermal stability for the sample containing C-1	Conversion of ~ 90%	It was possible to retain the structure without using a cross-linker The results are for P-A-31b	85
P-A-32	-	I-2	≥ RT	45 - 85 (H_1) 80 - 90 (Q_1) 50 - 98 (L_α)	H_1, Q_1, L_α	Retention of the structures	3.44 - 4.91 (H_1) 2.92 - 4.41 (L_α) 7.92 (Q_1)	3.39 - 4.88 (H_1) 3.03 - 4.53 (L_α) 7.67 (Q_1)	Excellent thermal stability in air	Conversion of ~ 23 - 71%	The same conversion range was achieved without initiator LLC formulation and structure characteristics depend on x and y	61
	-	I-1	65	80	Q_1	Retention of the structure	-	7.23	Thickness-normalized water permeability of ~ 0.089 liters m^{-2} $hour^{-1}$ bar^{-1} µm Full water flux recovery (> 95%) and less than 15% water flux loss after contact with salty water Membrane pore size of 0.75 nm based on rejection tests	Conversion of more than 90%	P-A-32e was used in this study	33
	-	I-1	70	73.9	Q_1	Retention of the structure	8.86 (at 8.2 wt% BR)	8.52	Higher water vapor permeability compared to the membrane with H_2 structure prepared via P-A-26 while maintaining proper CEES rejection	Conversion of more than 95%	P-A-32e was used in this study BR solution in n-hexane was used for blending Broader Q_1 range in phase diagram in the presence of BR (44.7 - 76.4 wt% P-A-32e)	115
	-	I-1	65	80	Q_1	Retention of the structure	-	8.73 before ALD ~ 8.52 after 5 cycles ALD ~ 6.21 after 10 cycles ALD	After 10 cycles of ALD, the gas selectivity of hydrogen/nitrogen increased from 12 to 65 while gas permeability decreased ~ 40%	Conversion of more than 90%	P-A-32e was used in this study ALD of alumina was carried out to modify/reduce the pore size	117
	-	I-1	65	80	Q_1	Retention of the structure	-	-	Water filtration performance in between that of conventional NF and RO membranes Low water flux due to high thickness Higher resistance against chlorine degradation	-	P-A-32e was used in this study	119
P-A-33	-	I-1	60	84.2	Q_1	Retention of the structure	4.95 - 6.73	7.35 - 9.46	The prepared membrane showed water flux and permeability comparable to the membrane prepared by P-A-32	Conversion of more than 95%	Only P-A-33c and P-A-33f can produce Q_1 structure P-A-33 is cheaper than P-A-32 to be produced	118
P-A-34	This reactive surfactant has been used for transcriptive templating. Please see Table 3/M-22 section.											

Table 2. Summary of the reported results for synergistic LLC templating (continue).

Amphiphile	Cross-linker	Initiation system	Reaction temperature [°C]	Amphiphile concentration [wt%]	Structure before polymerization	Structure after polymerization	Lattice parameter before reaction [nm]	Lattice parameter after reaction [nm]	Application characteristics of the product	Polymerization kinetics	Remarks	Ref.
P-A-35	-	I-1	70	79.7	Q_I	Retention of the structure	8.71	9.34	Thickness-normalized water permeability of ~ 0.066 liters m^{-2} $hour^{-1}$ bar^{-1} µm Water flux was comparable to the industrially used NF and RO membranes Salt rejection was between NF and RO Partial ion exchange can result in a reversible change in water flux Unique selectivity toward TDS and DOC under different FW pH Higher fouling resistance and flux recovery compared to industrially used membranes	Conversion of more than 90%	Glycerol was used instead of water for the formation of LLC To prepare the membrane, a solution of LLC in methanol was used for roll-casting Ion exchange did not affect *d*-spacing	32,114,120,121
	-	I-1	70	79.4	Q_I	Retention of the structure	-	4.03 *	Higher water/CEES and water/DMMP molar vapor selectivity compared to previously reported LLC based membranes	Almost complete conversion	Glycerol was used instead of water for the formation of LLC The prepared membrane was cheaper than the BR/LLC system in same application The membrane did not have appropriate selectivity toward water over CEES without addition of a PDA layer on the surface of the membrane	112
	-	I-1	52.5	79.4	Q_I	Retention of the structure	-	-	Eternal presence of anionic polymer inside the pores resulted in significant changes in ion sorption and pore transport properties	Almost complete conversion	Glycerol was used instead of water for the formation of LLC The internal surface of the pores was modified by polymerization of M-31 inside the pores	113
	-	I-1	52.5	79.4	Q_I	Retention of the structure	-	10.57	Higher dehydration and resistivity of Q_I AEM in dilute $FeCl_3$ solutions compared to amorphous AEMs thanks to closer spacing of ion exchange sites	Almost complete conversion	Glycerol was used instead of water for the formation of LLC The prepared membrane was used as anion exchange membrane (AEM)	52
P-A-36a	-	UV	RT	78 ± 3	No structure	Formation of L_α	-	2.8	Proper thermal stability and high swelling capacity via water and polar hydrogen-bonding solvents	Conversion of more than 98% Thermal polymerization resulted in a limited conversion	Reversible swellability of the polymer and insolubility in organic solvents were signs of cross-linked network Both thermal and photopolymerization were carried out without initiator	86,87
P-A-36b	-	UV and I-1	RT	60 - 70 (H_2)	H_2	Formation of Q_α at low water contents Retention of H_2	3.23 (H_2)	3.78 (H_2) 4.3 - 7.97 (Q_α)	Enhanced mechanical properties and insolubility in a variety of solvents were the key characteristics of the obtained compatible IPN	-	Mechanically robust gel was obtained through production of IPN via swelling the polymerized LLC by M-33 and then photopolymerization initiated by I-1 The structure changed to L_α after formation of the IPN (lattice parameter of 3.3 nm)	87,90
P-A-37	-	ChO	RT	> 85	H_2	Disordered structure	3.41	-	-	-	Anion-exchange to a divalent anion (sulfate and sulfite) and difficulty of controlling the regio-regularity during the polymerization of thiophene were the reason of losing the structure after polymerization	126
P-A-38	C-10b	I-1	RT	87.9	H_2	Formation of HPL structure	3.12	-	Relatively low T_g, high thermal stability, and high resistance toward swelling by in organic solvents and water were the important features of the product	Conversion of 93 ± 4%	It was not possible to produce a durable, self-supporting materials without C-10 or by using I-18	88
P-A-39	-	I-21	90 ± 5	50 ± 5	HPL	HPL changed to a hybrid of H_2 and L_α	3.74 *	3.38 *	Enhanced conductivity of the thin film via LLC templating	Conversion of 40 - 60%	The polymer showed L_α structure when it was applied on a glass substrate as a thin film	103
P-A-40	C-10b	I-13 and UV	RT	~ 15.25	H_2	H_2 changed to HPL structure H_2 was retained by post-UV curing of 3D-printed sample	4.6	3.92 (for the retained Hα)	Proper structure stability toward swelling and de-swelling by ethanol	Incomplete conversion for the 3D-printed sample 1 hr exposure to UV was used to complete the reaction	Disruption of the structure was observed at C-10 contents of higher and lower than 20 w%	91
P-A-40 / P-A-41	-	UV	RT	~ 80	No structure	Formation of H_2	-	3.2	Enhanced thermal stability due to the presence of covalently bound nanodiamond	Complete conversion	A mixture of 17 wt% DMSO and 3 wt% water was used as the solvent	80

Table 2. Summary of the reported results for synergistic LLC templating (continue).

Amphiphile	Cross-linker	Initiation system	Reaction temperature [°C]	Amphiphile concentration [wt%]	Structure before polymerization	Structure after polymerization	Lattice parameter before reaction [nm]	Lattice parameter after reaction [nm]	Application characteristics of the product	Polymerization kinetics	Remarks	Ref.
P-A-40 / P-A-42	-	UV	RT	70 ± 2	H_2	H_2 changed to HPL structure	3.29	-	Minor structure variations via limited swelling with water	Complete conversion	Pairs of quantum-dot core-shell particles were confined within the center of mesoscale cylinders 10 wt% of the total amphiphile was P-A-42	127
P-A-43	-	I-15	60	50	H_2	Loss of some long-range order	6.14	5.1	The cross-linked network showed photo-responsive behavior	Conversion of 40 - 50%	P-A-43 showed thermotropic LC with columnar hexagonal structure that can be swollen by diglyme to form LLC Photopolymerization resulted in loss of structure due to isomer changes before cross-linking	128
P-A-44 / P-A-45	-	I-16	45	25	Q_2	Retention of the structure	12.3	13.5	The polymerized LLC was soluble in organic solvents due to incomplete cross-linking but it showed higher thermal stability compared to non-polymerized LLC	-	The ratio of P-A-44/P-A-45 in LLC was 9/1	108
P-A-46	This reactive surfactant has been used for transcriptive templating. Please see Table 3/M-4 section.											
P-A-47	This reactive surfactant has been used for transcriptive templating. Please see Table 3/M-7 section.											
P-A-48	-	I-5	RT	10 - 50	Dis. Cube, L_α	Higher reaction rate results in structure retention	-	-	-	L_α had the highest polymerization rate	The LLC structure was altered with changing pH at a fixed amphiphile content	122
P-A-49	-	I-1	RT	93	H_2	Retention of the structure	4.81	4.56	Similar activity and 10 times higher selectivity compared to industrially available catalysts for esterification reaction	Conversion of more than 90%	The ratio of P-A-49/P-A-50 in LLC was 5/1 to have pure H_2 phase P-A-49 contained strong acid properties and P-A-50 directed the LLC assembly via amide H-bonding	129
P-A-50	This reactive surfactant was discussed in P-A-29/P-A-30 and P-A-49 sections											
P-A-51	-	I-1	RT	90 (solution in an acid)	H_2	Retention of the structure	4.7 - 5.7	4.83 - 5.67	No enhancement of enantio- or diastereo-selectivity by polymerized LLC	Conversion of more than 90%	LLC structure depends on the nature of the acid used for LLC formation	130
P-A-52	-	γ-ray radiation	RT	a: 25 - 57 (H_1) > 66 (L_α) b: 45 - 75 (H_1) > 85 (L_α)	H_1, L_α	Retention of the structures	5.1 (H_1)	4.83	The gel morphology was stable against temperature changes, extraction, drying, and reswelling with polar or nonpolar solvents	Complete conversion	H_1 structure was used as a template for mesoporous silica synthesis and the structure was retained without cross-linking	101
P-A-53	-	I-1	RT	55 - 65 (H_1) 75 - 80 (L_α)	H_1, L_α	Retention of the structures	6.01 - 6.59 (H_1) 5.46 - 5.54 (L_α)	6.14 - 6.72 (H_1) 5.61 - 5.68 (L_α)	Enhanced mechanical and thermal stability of the polymerized LLC when P-A-53 is used	-	P-A-53 cannot form LLC, but it can in combination with A-18b	81
P-A-54	-	UV	RT	50 (H_1) 73 (L_α)	H_1, L_α	Retention of the structures	10.95 (H_1) 8.34 (L_α)	10.17 (H_1) 8.03 (L_α)	The polymerized structure was destroyed when swelled by an organic solvent, but after drying and swelling with water, the original structure was retained	Almost complete conversion	The direct UV-initiated polymerization happened due to the photosensitive cinnamoyl moieties	102
P-A-55a / A-7 / A-8	C-10b	I-1	RT	~ 26.5	L_α	Retention of the structure	12.2	11.7	Enhanced mechanical properties and preserving the structure after swelling even by organic solvents were the main characteristics of the obtained hydrogel	-	The presence of the self-assembled lipid bilayer was crucial for formation of L_α The weight ratio of P-A-55a/A-7/A-8 was 60/5/35	105
P-A-55	C-10b	I-1	RT	22.8	L_α + L_1	Packed hard sphere structure	19.5	26.5	-	Complete conversion	P-A-55a was used in this study	105
	-	I-3 or I-9	RT	5 - 24	Dis. Cube with FCC lattice	Retention of the structure	~ 15 - 30 (depending on the surfactant content and temperature)	~ 15 - 30 (depending on the surfactant content and temperature)	Having highly viscoelastic or elastomeric behavior with excellent mechanical properties, conductivity, and mechanoelectrical response through controlling the composition of the LLC was the key feature of the product The produced iono-elastomer can be used as a motion sensor as well as temperature sensor with sufficient sensitivity and accuracy	-	P-A-55b was used in these studies Partially deuterated ionic liquid ethylammonium nitrate was used instead of water to prepare the ion gel	46–48
P-A-56	C-1	I-12 or I-20	RT	25	Q_2	Retention of the structure	-	-	-	Conversion of 95%	The LLC was used to prepare and polymerize nanoparticles with Q_2 structure (stabilized cubosomes)	110

4. Transcriptive LLC templating

Although synergistic templating is in many cases sufficient for obtaining polymerized LLCs with a variety of nanostructures for different applications, the tedious in-lab synthesis of many reactive amphiphiles can be a drawback. While some recent works have used commercially available formulation additives in conjuction with surfactants obtained from one-pot synthesis,[30] the synthesis of many reactive amphiphiles can be more involved (e.g. Gemini surfactants for cubic bicontinuous mesophases). This issue is also an obstacle in rapid industrial adoption of polyLLCs. Therefore, there have been several efforts to use a combination of commercially available surfactants and monomers instead. In this approach, a non-polymerizable surfactant is usually used to direct the LLC formation followed by the polymerization of the monomer. At the end of this process, which is called transcriptive templating, a polymer having the structure of the parent LLC is formed. Both ternary mixtures of water/hydrophobic monomer/surfactant and binary mixtures of hydrophilic monomer + water/surfactant are common in this templating approach. Despite the advantages obtained from easy sourcing of commercially available materials, preserving the structure of LLC template during polymerization is more challenging in transcriptive templating compared to synergistic templating. Because the formed polymer is not chemically bond to the surfactant, polymerization-induced phase separation/inversion becomes highly probable, reducing the chances of successful transcriptive templating. This issue has been addressed by addition of cross-linkers in the mesophase formulation, using reactive (co)surfactants, and employing block copolymer (BCP) surfactants. The first two approaches are centered around the formation of a kinetically trapped cross-linked network and the last one makes phase-separation/inversion process kinetically slow, enhancing the retention of the structure.[31] Transcriptive templating is very flexible since different monomers can be polymerized with the same surfactant system without the need for synthesis of new chemicals. Moreover, copolymerization can also be used in the process to add chemical functionality to the final product.[131] As such, a wide variety of surfactants, (co)monomers, and cross-linkers have been used in transcriptive LLC templating, as shown in Fig. 4 and Fig. 5. A summary of the reported results for each monomer is presented in Table 3. Similar to synergistic templating, we will discuss the results of transcriptive templating for each type of LLC structure separately in the following sections.

4.1. Hexagonal (H_α)

Transcriptive templating of a variety of monomers has been reported for the hexagonal phase structure. Based on the employed surfactants and LLC formulations, lattice parameters of ~ 2.7 to ~ 14 nm have been obtained for the templated products, a range which is quite similar to that obtained for synergistic templating with H_α. As stated previously, the retention of structure in transcriptive templating is a major concern, especially after removal of the template. While most of the studies have used the three approaches mentioned above, Zhang et al. have also tried an additional step to preserve the H_1 structure directed by A-3 or A-14 surfactants after polymerization of M-24c and removal of the template.[132] They have reported that when the drying step is carried out under zero surface tension (by replacing water with CO_2) it is possible

to retain the structure.[132] In another effort, they were able to retain the parent structure using a regular drying method via reinforcing the polymerized LLC by an in-situ formed silica network.[133] They have also shown that the required silica content for the structure retention can be reduced from 50 to 10 wt% with respect to the total monomer content if low surface tension solvents (e.g., mixture of hexane and ethanol) are used for the template extraction.[134] It is noteworthy to point out that the silica present in the polymerized domains of the obtained composite material not only participates in the structure preservation, but also imparts relatively higher thermal stability[134] and enhanced hydrophilicity to the final product.[133]

There have been several efforts to utilize transcriptive templating of H_α structures in different applications. For instance, Guymon and co-workers have used this approach to prepare hydrogels that possess a proper balance of water uptake, swelling/de-swelling rate, and mechanical properties without compromising other properties such as stimuli-responsiveness and biodegradability.[35–45] They have also used transcriptive templating for compatibilization of immiscible monomers. To do so, hydrophilic M-24c and hydrophobic M-20 are mixed with the aqueous solution of A-14, resulting in the formation of an LLC with H_1 structure. The polymerization of these two monomers in the LLC template results in a semi-interpenetrating polymer network (IPN) structure having excellent polymer compatibility.[135]

Templating with H_2 structure has also been applied for the fabrication of water filtration membranes. In one such effort, Osuji and co-workers magnetically aligned the nanochannels of a H_2 phase before polymerization to decrease the tortuosity of the produced membrane. Although they were able to successfully retain the aligned structure after polymerization, the study did not extend to filtration membrane fabrication.[136] Qavi et al. have successfully utilized LLC templating of H_2 structures to fabricate ultrafiltration (UF) membranes that show excellent permeability as well as higher fouling resistance over commercially available UF membranes.[31] Successful production of antimicrobial UF membranes has also been reported by polymerization of M-32 in the same LLC structure.[137]

Fabrication of ordered mesoporous carbon (OMC) material is another application of transcriptive templating of H_1 structures. Polycondensation and cross-linking of monomers such as M-34, M-35, M-36 and M-37 results in a nanostructured thermoset polymer such as phenol-formaldehyde. Subsequently, calcination and carbonization of the polymerized LLC at high temperature (e.g., above 600 °C) is carried out to obtain OMC species.[19,55,138–141] In the reported results, OMC materials obtained via this technique show extremely high thermal stability,[19,141] excellent mechanical properties,[19,55] enhanced electrochemical performance,[140] and promising CO_2 capture properties.[55]

4.2. Lamellar (L_α)

The Lamellar phases are easily accessible structures in most LLC formulations (especially in ternary systems). Several studies performed on transcriptive templating of L_α structure have reported lattice parameters between ~ 2.8 to ~ 10.5 nm. In most such studies, the focus has been on the investigation of fundamental/mechanistic underpinnings of retention of the L_α

structure during templating as well as the polymerization kinetics in nanoconfinement. However, there are also studies which primarily focus on the templated products in particular application scenarios. As an illustration, Qavi et al. fabricated UF membranes with transcriptive templating of M-4 in lamellar structure directed by A-19c. According to the obtained results, L_α-based membranes not only show higher permeability and fouling resistance over commercially available UF membranes, but also exhibited slightly higher water flux compared to H_2-based membranes described earlier.[31] Antimicrobial membranes with lamellar structure have also been successfully fabricated.[137] In a recent trial, Bandegi et al. have produced a robust ion gel with decent ion conductivity by LLC templating in the presence of 1-ethyl-3-methylimidazolium tetrafluoroborate ionic liquid.[142] In other demonstrations of important applications of transcriptive templating in the lamellar phase, Guymon's team performed compatibilization of immiscible monomers[143] and synthesis of hydrogels which have a good balance of water uptake, swelling/de-swelling rate, and mechanical properties without changing the chemistry or sacrificing the general biocompatibility of the biopolymers.[45,89,144]

4.3. Bicontinuous cubic (Q_α)

The Q_α phases have been studied less than H_α and L_α for transcriptive templating due to the limited accessibility of bicontinuous cubic phase in LLC systems and difficulties in structure retention after polymerization. As shown in Table 3, lattice parameters of ~ 6 to ~ 23.5 nm have been reported so far for the Q_α structures used for the templating. In addition to the fundamental studies on the transcriptive templating process with this structure,[54,145–148] a handful of works have also investigated the applicability of the final product. For instance, Guymon's group has been able to produce a hydrogel with an improved water uptake and de-swelling rate while keeping the mechanical properties intact by taking the advantages of structural interconnectivity in Q_I phase created by a mixture of A-13 and M-10.[149] They have also used bicontinuous cubic structure directed by A-15 to polymerize M-9 and produce a hydrogel with a faster swelling rate, higher swelling capacity, and higher compressive modulus over non-LLC product.[43] In another trial, they have employed P-A-34, a Gemini surfactant, to make Q_I phase easily accessible. Although the retention of the structure after the template removal was not possible, they observed an enhanced swelling of the polyLLC in water and 2-propanol.[22] Generation of a Q_I structured OMC material with excellent thermal stability and mechanical properties is another notable application of transcriptive templating via bicontinuous cubic mesophase.[19]

4.4. Discontinuous cubic

The discontinuous cubic phases are the least studied structure for transcriptive templating. Almost all of the studies on these mesophases, which have been conducted by Guymon and co-workers, have focused on revealing the differences among LLC structures in terms of polymerization kinetics[35,36,38,39,42,43,99,150,151]. However, the observed higher water uptake in prepared hydrogels with micellar cubic structure over ones with H_I structure[39], as well as the

impressive properties of the ion gels obtained from synergistic templating within discontinuous cubic structure[46–48] indicate that there may be plenty of opportunities in transcriptive templating of such structures to fabricate materials with exceptional properties.

Table 3. Summary of the reported results for transcriptive LLC templating.

** Calculated d-spacing for the primary reflection in the SAXS profile; SWNT: Single-walled carbon nanotube; EP: Electropolymerization; PC: Polycondensation; TEOS: Tetraethoxysilane; EISA: Evaporative induced self-assembly*

Monomer	Amphiphile	Cross-linker	Initiation system	Reaction temperature [°C]	Amphiphile / oil (monomer) w/w	Structure before polymerization	Structure after polymerization	Lattice parameter before reaction [nm]	Lattice parameter after reaction [nm]	Application characteristics of the product	Polymerization kinetics	Remarks	Ref.
M-1	A-1	C-1	I-15	85	44.9 / 7	Q_α	-	-	-	-	-	Uniform microporous materials of arbitrary size and shape was produced	145
	A-1	-	I-15 / UV	RT	42.66-64.32 / 7.23-19.81	Q_α	Retention of the structure	6.01 - 10.017	Remained almost unchanged	-	Conversion of less than 100%	C-1 was also used as monomer instead of M-1 to increase the cross-linking density Q_α structure was obtained in surfactant/oil ratio of 30.43 / 4.99 for C-1	54
	A-2	-	I-15	70	19.4 - 37.5 / 3.2 - 6.2	Q_α	Q_α changed to L_α	9.4 - 18.8	8.4 - 14.2	-	-	Phase separation was observed between polymer and the template	146
	A-17	-	-	-	50 / 33 (H_1) 63 / 16 (L_α)	H_1, L_α	H_1 changed to L_α Disordered L_α	-	-	-	-	-	152
	A-19f	C-1	I-15	70	45 - 65 / 10 - 30	-	H_α or L_α having some disordered domains	-	-	High mechanical properties while maintaining proper ion conductivity was the main feature of the product	Conversion of ~ 90%	1-Ethyl-3-methylimidazolium tetrafluoroborate ionic liquid was used instead of water to prepare the LLC Polymerization of M-1 was used to enhance the mechanical properties of the ion gel	142
M-2	A-1	-	I-15	RT	55 / 10	Q_α	Retention of the structure	-	11.8	-	-	-	145
M-3	A-3	-	I-2	RT	35 / 25 (L_1) 40 / 25 (Q_1) 45 / 25 (H_1) 65 / 25 (L_α)	L_1, H_1, Q_1, L_α	Retention of H_1	4.28 (H_1)	4.31 (H_2)	-	Polymerization rate: L_1 <<< Q_1 < H_1 < L_α	Relative water solubility of M-3 resulted in polymerization in the polar domains of the self-assembled molecules and therefore encapsulation of the surfactant aggregates	153
	A-3	-	I-2	RT	30 / 10 (L_1) 50 / 10 (H_1) 70 / 10 (Q_1) 75 / 10 (L_α)	L_1, H_1, Q_1, L_α	-	-	-	-	Polymerization rate: L_1 <<< H_1 < Q_1 < L_α	Higher reaction rate resulted in higher MW of the produced polymer	99
M-4	P-A-22 / P-A-46	C-7	I-18	RT	63.2 / 19	H_2	Retention of the structure	5.37	5.5	It is expected that the prepared membrane has high permeability as well as proper selectivity due to the low-tortuosity of the aligned nanostructure	-	To be able to preserve the structure, 6.3 wt% cyclohexane was added to the mixture as a non-reactive oil phase Nano-channels alignment was carried out via 5 - 6 T magnetic field before polymerization The reactive amphiphiles were commercially available	136
	A-19	C-8	I-9 / I-15	RT - 70	55 - 60 / 25 - 30 (H_2) 50 - 60 / 10 - 15 (L_α)	H_2, L_α	Retention of the structures	10.2 - 10.4 (H_2) 7.4 - 8.5 (L_α)	10.4 - 10.7 (H_2) 7.8 - 9.2 (L_α)	The fabricated membrane showed excellent permeability as well as higher fouling resistance over a commercially used UF membrane	-	A-19c was used	31
	A-19	C-8	I-15	60 - 70	40 - 55 / 25 (H_2) 57 - 60 / 25 (L_α)	H_2, L_α	Retention of the structures	6.6 - 7.4 (H_2) 6 - 10 (L_α)	7.32 - 7.41 (H_2) 6 - 10.18 (L_α)	-	Polymerization rate: L_α < H_2 <<< non-LLC	A-19a, A-19c, and A-19d were used The formulation of LLC and LLC characteristics depend on m and n in the amphiphile structure	56
	A-19	C-8	I-15, I-17 or I-23	55 - 75	50 / 15 (L_α) 55 / 30 (H_2)	H_2, L_α	Retention of the structures	6.4 (L_α) 5.75 (H_2)	4.98 - 51 (L_α) 6.25 – 6.47 (H_2)	Mechanical properties of polyLLCs improved when I-17 was used	Polymerization rate: L_α < H_2 I-17 resulted in faster polymerization rate in both LLC structures	A-19c was used	154
M-5	A-3	-	I-2	RT	50 / 25 (H_1)	H_1	Disordered structure	-	-	-	-	-	153
	A-3	-	I-2	RT	30 / 10 (L_1) 50 / 10 (H_1) 80 / 10 (L_α)	L_1, H_1, L_α	Disordered structure for H_1	4.92 (H_1)	4.46 (H_1)	-	Polymerization rate: L_α < H_1 < L_1 < L_1/H_1	Higher reaction rate resulted in higher MW of the produced polymer Phase separation was seen for LLC and polymer for H_1 structure	99
M-6	A-3	-	I-2/I-5	RT	35 / 10 (L_1) 40 / 10 (Dis. Cube) 55 / 10 (H_1) > 60 / 10 (L_α)	L_1, Dis. Cube, H_1, L_α	-	-	-	-	Polymerization rate: L_α < H_1 < Dis. Cube <L_1	-	42
	A-3	-	I-2	RT	40 / 25 (Q_1) 50 / 25 (H_1) 60 / 25 (L_α)	H_1, Q_1, L_α	Disordered structure of H_1	5.52 (H_1)	4.25	-	Polymerization rate: L_α <H_1 < Q_1	M-6 tends to be present at nonpolar domains, so the formed polymer framework was weak, resulting in structure disruption	153

Table 3. Summary of the reported results for transcriptive LLC templating (continue).

Monomer	Amphiphile	Cross-linker	Initiation system	Reaction temperature [°C]	Amphiphile / oil (monomer) w/w	Structure before polymerization	Structure after polymerization	Lattice parameter before reaction [nm]	Lattice parameter after reaction [nm]	Application characteristics of the product	Polymerization kinetics	Remarks	Ref.
M-6	A-3	-	I-2	RT	30 / 10 (L_1) 40 / 10 (Dis. Cube) 55 / 10 (H_1) 75 / 10 (L_α)	L_1, Dis. Cube, H_1, L_α	-	-	-	-	Polymerization rate: $L_1 < L_\alpha$ < Dis. Cube < H_1	The MW of the produced polymer increased from micellar to H_1 and then decreased in L_α structure	99
M-7	P-A-47 / A-16b	C-5	-	35	21.6 / 20	L_α	Retention of the structure	-	7.2	Anisotropic increase of the dimensions through swelling with water	Conversion of more than 95%	3.8 wt% P-A-47 was used in this study The structure was retained even after removal of the template 2 T magnetic field was used for the alignment of the structure before polymerization MW of P-A-47 did not affect *d*-spacing	155
M-8	A-15 or A-20	C-8	I-18	55	7 -9 / 20 -37 for A-15 30 / 7.6 for A-20	-	-	-	-	-	Complete conversion	M-8 was copolymerized with M-17 with 1:1 ratio The produced copolymer showed continuous gel structures of high connectivity, where the gel is composed of polymer strings, resembling the morphology of a marine sponge The type of surfactant had only a marginal influence on the final gel structure	131
M-9	A-1 or A-16a	C-2	I-16 / UV	RT - 55	24.3 / 10 for A-1 69.7 / 6.05 for A-16a	Q_α	Retention of the structure	-	9.3 for A-16a	-	-	Decane was also used in preparation of LLC with A-1	145,147
	A-10 or A-12	C-2	I-14	RT	47.7 / 10 for A-10 50 / 10 for A-12	H_1 with A-10 Q_α and L_α with A-12	Retention of the structures	4.53 (H_1) 3.81 (L_α)	4.69 (H_1) 3.69 (L_α)	-	Conversion of ~ 95% for H_1 and L_α Conversion of ~ 75% for Q_α	Q_α was obtained from ternary system of water/A-12/decanol	148
	A-5 or A-11	C-2	I-18	60	43 - 48 / 26	H_1	H_1 changed to L_α with A-11	-	-	Enhanced mechanical stability of water-swollen gels	-	The structures can be destroyed with the removal of the template The prepared gels can be chemically functionalized by incorporation of M-17, M-15, M-12, M-14 and M-13/M-21	152,156
	A-14	C-2	I-18	55	6 -28 / 23 - 30	-	-	-	-	The prepared gel showed a reduction of the moduli by only 10 - 40%	Complete conversion	Continuous gel structures of high mechanical strength was obtained due to the presence of a structure having connected spherical gel particles of ~ 500 nm diameter	131
	A-15	C-2	I-5 or I-15	RT - 60	30 / 25 (L_1) 40 - 60 / 25 (Q_2) 70 / 25 (L_2)	L_1, Q_2, L_2	Retention of Q_2	6.1 (Q_2) *	Remained almost unchanged	Faster swelling rate, higher swelling capacity and higher compressive modulus of the structured gel compared to non-LLC one	Polymerization rate: non-LLC <<< $L_1 = L_2 < Q_2$	Monomer concentration had a minor effect on the polymerization rate Q_2 changed to L_α when I-15 was used to carry out the reaction at 60 °C	35,36,43,157
	A-14	C-2	I-5, I-6 or I-15	RT - 80	40 / 25 (Dis. Cube) 50 - 60 / 25 (H_1) 70 / 25 (L_2)	Dis. Cube, H_1, L_2	Retention of the structures when I-5 was used Disruption of the structures when I-15 was used for thermal polymerization	-	-	Anisotropic increase of the dimensions through swelling with water in the case of the LLCs polymerized via I-15 and I-5 at high temperatures Higher water uptake for the polymerized Dis. Cube structure compared to H_1	Polymerization rate with I-5: non-LLC <<< L_2 < Dis. Cube < H_1 Polymerization rate with I-6: non-LLC <<< Dis. Cube ≤ H_1 ≤ L_2 Photoinitiation resulted in much faster polymerization rate compared to thermal initiation	Higher temperature resulted in lower reaction rate by changing structure to micellar Slow reaction rate was the reason of structure lose after polymerization by I-15	35,36,38,39
	A-5 / P-A-9	C-2	I-2	RT	50 / 20	H_1	Retention of the structure was not possible with A-5 Addition of 10-15 wt% P-A-9 resulted in the structure retention	4.53 - 4.68	5.58 - 6.04	Higher water swelling rate was seen for the hydrogel having H_1 structure The water uptake decreased with an increase in hydrophobic P-A-9 content The hydrogel with H_1 structure showed improved release properties Higher compressive modulus was seen in dehydrated state for the polymerized LLC compared to non-LLC sample	The polymerization rate increased with an increase in the content of P-A-9 due to the structure retention	-	40
M-10	A-14	C-2	I-18	55	10 - 24 / 24 - 30	-	-	-	-	The moduli of the formed gels strongly depend on the frequency and the gels have a low absolute strength	Complete conversion	A “cauliflower” morphology was obtained	131

Table 3. Summary of the reported results for transcriptive LLC templating (continue).

Monomer	Amphiphile	Cross-linker	Initiation system	Reaction temperature [°C]	Amphiphile / oil (monomer) w/w	Structure before polymerization	Structure after polymerization	Lattice parameter before reaction [nm]	Lattice parameter after reaction [nm]	Application characteristics of the product	Polymerization kinetics	Remarks	Ref.
M-10	A-13	C-2	I-2	RT	50 / 20	Q_I	Retention of the structure	-	-	400% more water uptake in the temperatures less than 33 °C, similar compressive modulus despite of higher water uptake and higher de-swelling rate of templated hydrogel compared to non-LLC sample	-	-	149
	A-13	C-2	I-1	RT	50 / 40	H_I	Retention of the structure (especially at high M-29 contents)	7.18 - 7.65	7.04 - 7.18	Relatively lower water uptake, intact thermoresponsive behavior, high de-swelling rate and appropriate mechanical properties when M-29 was incorporated in LLC	Limited effect of M-29 concentration on the conversion	M-29 was incorporated in the LLC (6.7 - 50 wt% with respect to the total monomer content) to improve the mechanical properties of the produced hydrogel without compromising other properties	41
	A-13	C-2	I-2	RT	40 / 20	Q_I	Retention of Q_I at low M-16 contents Q_I changed to H_I at 4 wt% M-16 content	-	8.24 (H_I)	Dramatic increase in water uptake, shifting the thermoresponsive behavior to higher temperatures and lower de-swelling rate by incorporation of M-16 in the LLC structure	-	M-16 was incorporated in the structure of the LLC (up to 4 wt% with respect to the total monomer content) to improve water uptake while preserving other properties	37
M-11	A-14 or A-20	C-2	I-18	55	24 / 24 for A-14 28 / 14 for A-20	-	-	-	-	The prepared gel showed a reduction of the moduli by only 10 - 40%, a weak frequency dependence and low mechanical loss	Complete conversion	Continuous gel structures of high mechanical strength was obtained due to the presence of a structure having connected spherical gel particles of ~ 500 nm diameter	131
M-12	This monomer was discussed in M-9 section												
M-13	A-14 or A-20	C-8	I-18	55	24 / 24 for A-14 28 / 14 for A-20	-	-	-	-	The prepared gels had a low absolute modulus and a very high mechanical loss	Complete conversion	The obtained gel showed a morphology consisting of porous sheets	131
	A-3	C-9	I-2 / I-5	RT	40 - 45 / 20 (Dis. Cube) 50 - 55 / 20 (H_I) 60 - 65 / 20 (L_α)	Dis. Cube, H_I, L_α	Disordered H_I and L_α	4.2 (H_I) 2.96 (L_α)	4.4 (H_I) 3.22 (L_α)	Lower water uptake, slower swelling rate and lower compressive modulus compared to non-LLC sample	Polymerization rate: non-LLC < H_I = Dis. Cube < L_α	Lower effective cross-linking density seemed to be the reason of weak hydrogel properties	42,43
	A-3	C-9	I-4	RT	47.5 / 19	H_I	Retention of the structure	3.7	3.81	-	-	The hydrophobic tails of the surfactant adsorbed to the hydrophobic SWNTs, resulting in the confinement of the nanoparticles inside the pores of H_I structure 5 T magnetic field was used to align the structure before polymerization	29
M-14	This monomer was discussed in M-9 section												
M-15	This monomer was discussed in M-9 section												
M-16	This monomer was discussed in M-10 section												
M-17	This monomer was discussed in M-8 and M-9 sections												
M-18	A-18b	-	EP	-	35 - 60 / 0.25 M	H_I	Retention of the structure even after removal of the template	6.65	-	Higher conductivity, and anisotropic absorption and conductivity of the templated film compared to the non-templated sample	-	LLC templating eliminated the need for post-polymerization methods (e.g., stretching and rubbing) to align the conductive film layer	158,159
	A-5	-	I-22	RT	Up to 0.3 M monomer was used	H_I	Limited retention of the structure	-	40 (thickness of spindle like nanostructures)	Good thermal stability (up to 200 ℃) of the obtained nanostructures Higher electrical conductivity of the produced nanostructures compared to non-templated products	-	Pentanol was used as a cosurfactant Solution of M-18 in toluene was used as the oil phase	160
M-19	A-18	C-4	PC	-	50 - 70 / ~8	H_I, L_α	Formation of rod and sheet particles from H_I and L_α, respectively after about 5 days	6.37 (H_I)	6.62 (H_I) after 5 days	The particles were thermally stable while the polymerized LLCs were not	-	LLC structures were preserved after reaction. However, the structure of produced polymer changed from polyLLC to polymeric particles after ~ 5 days Slow condensation and cross-linking kinetics, gradual build-up of molecular weight, and the nonlinear architecture of the polysiloxane molecules seemed to be the reason of the particles formation	161
M-20	A-3	-	I-2, I-5, I-6 or I-8	RT	40 / 10 (Dis. Cube) 50 - 60 / 10 (H_I) 70 - 80 / 10 (L_α)	Dis. Cube, H_I, L_α	Retention of H_I	2.69 - 3.9 (H_I) 3.17 (L_α)	-	-	Polymerization rate with I-2: $L_\alpha \leq H_I <$ Dis. Cube Polymerization rate with I-5: $L_\alpha < H_I <$ Dis. Cube Polymerization rate with I-6: $H_I < L_\alpha <$ Dis. Cube Polymerization rate with I-8: $L_\alpha = H_I <$ Dis. Cube	MW of the produced polymer depends on the extinction efficiency of the initiator, monomer segregation, and LLC-dependent initiation efficiency	38,42,150,151,162

Table 3. Summary of the reported results for transcriptive LLC templating (continue).

Monomer	Amphiphile	Cross-linker	Initiation system	Reaction temperature [°C]	Amphiphile / oil (monomer) w/w	Structure before polymerization	Structure after polymerization	Lattice parameter before reaction [nm]	Lattice parameter after reaction [nm]	Application characteristics of the product	Polymerization kinetics	Remarks	Ref.
M-20	A-19b	-	I-10	RT	18 / 10 (L_1) 40 / 10 H_1) 58 / 10 (Q_1) 78 / 10 (H_2) 82 / 10 (L_2)	L_1, H_1, Q_1, H_2, L_2	Retention of H_1 and H_2	7.27 (H_1) 10.22 (H_2)	7.33 (H_1) 9.95 (H_2)	Higher thermal stability of the templated sample in H_2 structure compared to H_1	Polymerization rate: $L_2 = H_2 < H_1 < Q_1 < L_1$	-	44
	A-14	-	I-5	RT	40 / 40	H_1	Retention of the structure	-	-	The water uptake decreased, and compressible modulus and Tg increased linearly with an increase in M-20 content approving the compatibility of two polymers via LLC templating	-	This study showed that it is possible to blend two immiscible polymers via LLC templating 25 - 100 wt% M-24c was used with respect to the total monomer content along with M-20	135
	A-14	-	I-2	RT	30 - 40 / 20 (H_1) 50 - 60 / 20 (L_α)	H_1, L_α	Disordered L_α	6.16 (L_α)	-	-	Polymerization rate: non-LLC < L_α < H_1	-	151
M-21	This monomer was discussed in M-9 section												
M-22	P-A-34	-	I-2	RT	29 / 25 (H_1) 59 / 14 (Q_1) 64 / 25 (L_α)	H_1, Q_1, L_α	Retention of Q_1 H_1 and L_α changed to Q_1	4.7 (H_1) 8.3 (Q_1) 2.8 (L_α)	6.5 - 6.8 (Q_1)	Higher 2-propanol swelling capacity of the sample which retained Q_1 structure compared to others Water-swollen polymerized LLCs showed lower compressive modulus over less hydrated non-LLC one Enhanced swelling in water and 2-propanol even after losing the structure due to the surfactant removal	Almost complete conversion	P-A-34 can accommodate up to 37% monomer to form LLC The polymerized LLC that retained Q_1 structure had uniform structure Retention of the structure after surfactant removal was not possible	22
M-23	A-3	-	I-2, I-5, I-6, I-7 or I-8	RT	40 / 20 (Dis. Cube) 50 - 60 / 20 (H_1) 65 - 70 / 20 (L_α)	Dis. Cube, H_1, L_α	Retention of H_1 and L_α	-	-	-	Polymerization rate with I-2, I-5, I-7 and I-8: Dis. Cube < H_1 < L_α Polymerization rate with I-6: Dis. Cube ≤ H_1 << L_α	-	38,42,150,162
	A-3	-	I-5	RT	50 / 10 - 30	H_1	Retention of the structure with some structural changes at high M-23 contents	3.96 (10 wt% M-23) 3.6 (30 wt% M-23)	4 (10 wt% M-23) 3.82 (30 wt% M-23)	-	-	At 30% M-23 rod-like morphology was seen in SEM images	163
M-24	A-3	-	I-1	RT	36.7 / 35.6	H_1	Retention of the structure after surfactant removal under certain conditions	3.87	3.82	-	-	The retention of the structure was not possible after removal of the surfactant and drying under vacuum or via air drying When drying was carried out by CO_2, it was possible to retain the structure thanks to maintaining zero surface tension M-24c was used in this work	132
	A-3	-	I-1	RT	36.7 / 35.6	H_1	Retention of the structure	3.6 (0% TEOS) 3.68 (10% TEOS) 3.98 (30% TEOS) 4.61(50% TEOS)	3.9 (0% TEOS) 3.6 (10% TEOS) 3.46 (30% TEOS) 3.41 (50% TEOS)	Enhanced hydrophilicity of the product by incorporation of a silica network	-	A polymerized LLC reinforced by an in-situ formed silica network (via condensation of 0 - 50 wt% TEOS with respect to the total monomer content) was produced The presence of silica network resulted in the retention of the structure even after the surfactant removal and drying under vacuum M-24c was used in this work	133
	A-14	-	I-1	RT	40 / 35	H_1	Retention of the structure	8.37 (0% TEOS) 8.88 (10% TEOS) 9.04 (30% TEOS) 9.39 (50% TEOS)	8.7 (0% TEOS) 8.35 (10% TEOS) 8.02 (30% TEOS) 7.5 (50% TEOS)	Relatively enhanced thermal stability of the product having silica network	-	A polymerized LLC reinforced by an in-situ formed silica network (via condensation of 0 - 50 wt% TEOS with respect to the total monomer content) was produced A mixture of hexane and ethanol was used as the low surface tension solvent to first extract the surfactant and then dry the samples Drying via the low surface tension solvent mixture, reduced the content of the silica which is required for the retention of the structure M-24c was used in this work	134
	A-19b	-	I-5	RT	20 / 10 (L_1) 44 / 10 H_1) 58 / 10 (Q_1) 81 / 10 (L_2)	L_1, H_1, Q_1, L_2	Retention of H_1	7.33 (H_1)	7.27 (H_1)	Enhanced thermal stability and compressive modulus of the templated gel	Polymerization rate: $L_1 < H_1 < L_2 < Q_1$	M-24b was used in this study	44
	This monomer was also discussed in M-20 section												

Table 3. Summary of the reported results for transcriptive LLC templating (continue).

Monomer	Amphiphile	Cross-linker	Initiation system	Reaction temperature [°C]	Amphiphile / oil (monomer) w/w	Structure before polymerization	Structure after polymerization	Lattice parameter before reaction [nm]	Lattice parameter after reaction [nm]	Application characteristics of the product	Polymerization kinetics	Remarks	Ref.
M-24	A-14	-	I-9	RT	3 - 33 / 40 (L_I + Dis. Cube) 33 - 38 / 40 (H_I) 38 - 42 / 40 (Q_I) 42 - 60 / 40 (L_α)	L_I + Dis. Cube, H_I, Q_I, L_α	Retention of the structures	-	-	Enhanced water uptake, rate of swelling and rate of diffusion through the obtained hydrogel with a change in structure from L_I to lamellar	-	M-24c was used in this study	164
	A-14	-	I-2	RT	40 - 50 / 20 (H_I) 60 - 70 / 20 (L_α)	H_I, L_α	Disordered H_I	6.27 (H_I)	7.6 (H_I)	-	Polymerization rate: non-LLC < H_I (50% A-14) <L_α (70%) < L_α (60%) < H_I (40%)	M-24a was used in this study	151
	A-3	-	I-5	RT	30 / 20 (L_I) 50 - 60 / 20 (H_I) 70 / 20 (L_α)	L_I, H_I, L_α	Retention of H_I structure for M-24a Loss of order of H_I for M-24e	For M-24a: 3.72 (H_I) For M-24e: 3.6 (H_I)	For M-24a: 3.7 (H_I) For M-24e: 3.8	-	Polymerization rate: L_α < H_I < L_I Higher reaction rate at L_I was more pronounced in the case of M-24e Polymerization rate for M-24a was higher than M-24e in H_I structure	M-24a, d and e were used in this study The results for M-24d was similar to M-24e	163
	A-9	-	I-1	RT	83.3 / 9.34	Q_α	Formation of hexagonal perforated lamellar (HPL) structure	-	-	Relatively low Tg, high thermal stability, and high resistance toward swelling in organic solvents and water were the important features of the product	-	M-24b was used in this study Due to the absence of a dense cross-linked network, almost 80% of ionic liquid amphiphile washed off with ethanol	88
M-25	A-14	-	I-9	RT	45 / 40	L_α	Retention of the structure after surfactant removal	-	-	Linear decrease of water uptake and linear increase of compressive modulus and Tg with an increase in M-25 content approved the compatibility of two polymers via LLC templating The rate of degradation decreased with incorporation of higher M-25 contents	-	The immiscible polymers of hydrophilic M-27a and hydrophobic M-25 was blended through LLC templating 0 - 100 wt% M-25 was used with respect to the total monomer content M-25 showed higher cross-linking density than M-28	143
M-26	A-14	-	I-9	RT	40 / 40	L_α	Retention of the structure after surfactant removal	-	-	-	Almost complete conversion The polymerization rate in LLC was faster than non-LLC phase	-	144
M-27	A-14	-	I-9	RT	40 / 40	L_α	Retention of the structure after surfactant removal	6.3	6.35	Higher water uptake, permeability and degradation rate over non-LLC sample without changing the chemistry or general biocompatibility of the biopolymer	-	-	144
	This monomer was also discussed in M-25 and M-28 sections												
	A-14	-	I-9	RT	35 / 40	L_α	Retention of the structure after surfactant removal	-	-	Higher water uptake, rate of swelling and rate of degradation while having lower compressive modulus compared to non-LLC sample	The polymerization rate in LLC was faster than non-LLC phase	-	45
M-28	A-14	-	I-9	RT	45 / 40	L_α	Retention of the structure after surfactant removal	-	-	The water uptake decreased linearly with an increase in M-28 content approving the compatibility of two polymers via LLC templating The rate of degradation decreased with incorporation of higher M-28 contents	-	The immiscible polymers of hydrophilic M-27a and hydrophobic M-28 formed interpenetrating polymer network through LLC templating 0 - 75 wt% M-28 was used in respect to the total monomer content	143
M-29	This monomer was discussed in M-10 section												
M-30	A-14	-	I-9	RT	Specific contents of A-14 and 40 wt% M-30	H_I, L_α	-	-	-	Enhanced water uptake of the gel obtained from the parent LLC with H_I structure while maintaining high compressive modulus	-	The obtained gel from H_I LLC structure seemed to be a perfect candidate for tissue engineering scaffolds	45
M-31	This monomer was discussed in synergistic templating/P-A-35 section												
M-32	A-19c	C-8, C-10a or C-11	I-18	≥ 5	50 / 17.5 (H_2) 50 / 25 (L_α)	H_2 in the presence of oil phase L_α without oil phase	Retention of the structures	9.3 (H_2) 6.9 - 7.4 (L_α)	9.5 (H_2) 7.3 - 7.5 (L_α)	No bacterial colony growth on the surface of the prepared membrane	-	A mixture of M-4 and C-8 was also used as oil phase to enhance the mechanical properties of the polymerized LLC	137
M-33	This monomer was discussed in synergistic templating/P-A-36b section												

Table 3. Summary of the reported results for transcriptive LLC templating (continue).

Monomer	Amphiphile	Cross-linker	Initiation system	Reaction temperature [°C]	Amphiphile / oil (monomer) w/w	Structure before polymerization	Structure after polymerization	Lattice parameter before reaction [nm]	Lattice parameter after reaction [nm]	Application characteristics of the product	Polymerization kinetics	Remarks	Ref.
M-34	A-4, A-5 or A-6	-	-	60 - 70	1 / 1 - 6 molar ratio	H_1, L_α	Disordered structure at high M-34 contents	-	2.9 for A-4 * 3.5 for A-5 * 3.7 for A-6 *	No porous carbon was obtained via LLC templating due to improper thermal stability of the structure	-	A base or acid was used to catalyze the condensation reaction	24
	A-19	-	-	100	1 / 0.5 - 2.5	H_1, Q_1, L_α	Retention of the structures	-	9.8 - 14 (H_1) 12.6 - 23.5 (Q_1) 10.5 (L_α)	Ultrahigh thermal stability up to 1400 °C, mechanical stability up to 500 Mpa and proper high reverse electronic capacity was observed for the obtained mesoporous carbon material	-	A-19e, A-19f, and A-19g were used in this study The LLC precursor was prepared in ethanol followed by EISA to fabricate the structures L_α was not stable under surfactant removal and calcination steps A-19g was only able to produce Q_α The LLC structure and its characteristics were mainly depend on amphiphile/monomer ratio and n/m ratio in A-19	19
M-35	A-5	-	-	RT - 100	2.1 / 1.2	H_1	Limited structure retention	-	3.7 - 4.2 *	-	-	Ordered mesoporous carbon material was not obtained after removal of the template	165
M-36	A-19f	C-12	-	RT - 100	1 / 1	H_1	Retention of the structure	-	-	-	Polymerization of M-36 was much faster than M-34	The LLC precursor was prepared in a mixture of ethanol and water Highly ordered H_1 structure was achieved by controlled solvent evaporation or a shear force	138
	A-19f	C-13	I-11	RT	2 / 1	H_1	Retention of the structure	-	9.9 - 11.8	-	Polymerization was faster in the presence of I-11 compared to the sample without initiator	EISA was carried out under mild conditions while maintaining high polymerization rate by the aid of light Highly organized H_1 structure was obtained at high contents of I-11	139
	A-19f	C-13	-	75	2 / 1	H_1	Retention of the structure	-	9.5 - 12	The product of bio-based material showed better electrochemical performance due to the presence of a more suitable/accessible porous structure	-	It was possible to replace half of M-36 with lignin, as a less toxic and bio-derived monomer, and have the same ordered mesoporous carbon material No order was observed without M-36	140
	A-19f	C-12 / C-14	-	RT - 75	2 / 1	H_1	Retention of the structure	-	-	The product had a robust organic framework while maintaining a promising CO_2 capture property	-	The significant structural shrinkage during the curing and template removal was addressed by hypercross-linking the organic matrix via Friedel–Crafts alkylation reaction and C-14	55
M-37	A-19f	C-12	-	RT - 120	1 / 1	H_1	Retention of the structure	-	12.24	The obtained highly ordered carbon material showed extremely high thermal stability and could be graphitized at 2400 - 2600°C	Highly acidic reaction conditions promoted the polymerization rate	-	141
M-38	A-19e	C-15	-	60-100	10 - 80 / 80 - 20 (L_1) 30 - 50 / 0 - 30 (L_α) 70 - 90 / 0 - 25 (H_1)	L_1, L_α, H_1	Order-order and order-disorder changes were observed	9 - 22 *	12.4 – 19 *	-	Near complete monomer conversion	C-15 also acts as structure directing agent instead of water The structural changes continue even after completion of the polymerization	166
M-39	A-10	-	I-3 and γ-ray radiation	RT	Up to 20 wt% monomer was used	H_1	Retention of the structure when γ-ray radiation is used	7.5 *	18.4 *	Conductivity of 10^{-1} S/cm was obtained for the obtained nanofibers which was higher than the reported values in the literature	-	1-Pentanol was used as cosurfactant Micron-sized spherical particles were obtained by photo-polymerization Nanofibers were obtained by γ-ray radiation Solution of M-39 in cyclohexane was used as the oil phase	167
M-40	A-5	-	I-22	RT	Up to 0.1 M monomer can be used	H_1	Retention of the structure	27 (diameter of the oil domain)	30 (diameter of the obtained nanowires)	The optical band gap (estimated from the absorption edge, at 550 nm) of 2.25 eV was observed for the templated product Strong absorption in the visible region was observed	-	n-Pentanol was used as cosurfactant Solution of M-40 in toluene was used as the oil phase	168
M-41	A-10	-	I-17	0	Up to 20 vol% monomer was used	H_1	Limited retention of the structure under slow agitation of the mixture	-	100 – 200 (diameter of nanorods)	-	-	1-Pentanol was used as cosurfactant Nanospheres were produced under vortex mixing Nanorods were obtained under slow agitation of the mixture Solution of M-41 in cyclohexane was used as the oil phase	169

5. Kinetics of polymerization in LLC templates

Studying the polymerization kinetics in nanoconfinements of LLC templates is an attractive research ground not only due to the dramatic changes of the polymerization reaction rates in LLC templates, but also due to the important role of kinetics in ensuring structure retentionduring polymerization. As a rule of thumb, for both synergistic and transcriptive templating approaches, the faster the polymerization rate, the higher the probability of structure retention. When the reaction rate is high, the kinetically trapped cross-linked network forms rapidly, decreasing the chances of phase separation/inversion. This is why photopolymerization, which can often be completed in a few minutes, has been the first choice in most of the studies. The self-assembly of amphiphiles is temperature dependent.[73–75,123] In addition, the polymerization reaction is exothermic. Therefore, the change in temperature during non-isothermal reactions due to the heat of reaction may induce mesophase transition.[56] However, rapid formation of cross-linked polymer network can inhibit such phase separation/inversion.

Polymerization kinetics in different LLC structures have mainly been studied by Guymon and co-workers. They have shown that reactive sites segregation (e.g., double bond) and diffusion limitations are the main factors that determine the differences in the radical reaction rate among different mesophases.[26] The effect of the mentioned parameters will be discussed for the two types of LLC templating approaches separately in the following sections.

5.1. Synergistic LLC templating

In synergistic templating, the location of polymerizable group on the reactive amphiphile and the length of lipophilic chain are the main parameters that control the polymerization kinetics (see Fig. 12).[26] The impact of polymerizable group placement on the kinetics has been demonstrated by comparing the reaction rates between P-A-4 and P-A-5 in which the reactive groups are located on the lipophilic tail and hydrophilic head, respectively. Based on the reported results, the polymerization rate for P-A-4 increases when the LLC structure changes from lamellar to micellar cubic, whereas an opposite trend is seen for P-A-5. With a change in the structure from micellar cubic to lamellar, the proximity of the double bonds decreases for P-A-4, resulting in fewer propagation reactions and therefore a lower polymerization rate.[96–98] It is worth noting that the effect of the initiation system cannot be neglected in this comparison since applying γ-ray radiation on a similar templating formulation with P-A-5 results in a slightly different trend compared to photoinitiation method (see Table 2).[76] To evaluate the effect of lipophilic chain length on the reaction rate, one can compare P-A-5, P-A-6, and P-A-7 in synergistic templating. Under the same conditions (e.g., surfactant content), the reaction becomes slower with an increase in the chain length. The formation of LLC structures that offer lower local double bond concentration (e.g., micellar cubic) is the reason why slower polymerization rates are observed when lengthy surfactants are used.[89,98]

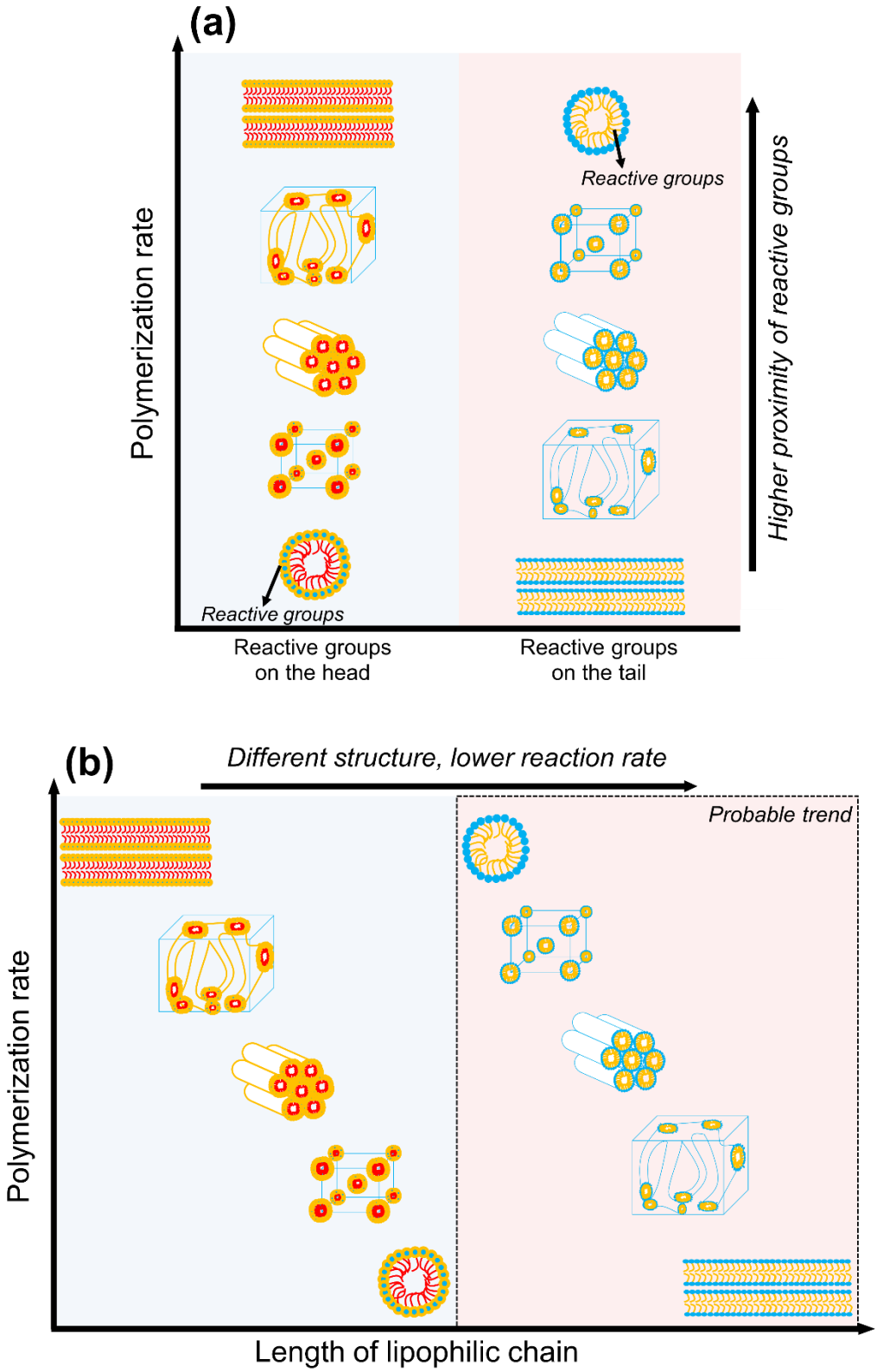

Fig. 12. The relative effect of (a) polymerizable group placement on the reactive amphiphile and (b) the lipophilic chain length on the polymerization rate in synergistic templating. Different structures are obtained with an increase in the length of lipophilic chain, resulting in lower reaction rate. Higher proximity of the reactive groups enables higher reaction rates.[26]

5.2. Transcriptive LLC templating

Studies on transcriptive templating have shown that monomer and initiator polarity are the key parameters controlling the polymerization kinetics, as schematically demonstrated in Fig. 13. Hydrophilic monomers tend to be present at the interface of water/surfactant. Such arrangements inhibit termination reactions by limiting the mobility and diffusion of the propagating polymer chains. In addition, when the LLC structure changes from micellar to lamellar, the local concentration of monomer increases in the continuous polar domain, resulting in higher radical propagation rates. When the limited mobility of the propagating chains and higher local concentration of the monomer exist simultaneously, a dramatic increase in polymerization rate is observed.[26] Hydrophilic monomers such as M-9,[35,36,38–40,43,157] M-13,[42,43] and M-23[38,42,150,162] have experimentally shown this behavior (see Table 3).

Hydrophobic monomers show the opposite behavior i.e. the polymerization rate decreases with a change in LLC structure from micellar to lamellar. The concentration of surfactant increases with a change in LLC structure from micellar to lamellar, resulting in an augment of the apolar domains' volume fraction. The local monomer concentration diminishes at higher apolar domain sizes which results in a lowering of polymerization rates.[26] Monomers such as M-4,[56] M-5,[99] M-6,[42,99,153] and M-20[38,42,44,150,151,162] are some of the hydrophobic species exhibiting lowered polymerization rates at high surfactant content, as shown in Table 3. A slightly different trend is seen for some of the monomers presented in Table 3. This is believed to be due to phase separation, which alters the local concentration, segregation, and diffusional behavior of the monomers. It is worth mentioning that M-3 exhibits unique behavior among hydrophobic monomers. As shown in Table 3, this monomer shows higher reaction rates when the LLC structure changes from micellar to lamellar, a behavior similar to the hydrophilic species. This observation is attributed to the partial water solubility of this monomer, which results in polymerization in the polar domains of the self-assembled molecules.[99,153] In addition to the monomer partitioning and mobility of the propagating chains, the effect of nanoconfinement on the polymerization rates cannot be underestimated. Qavi and co-workers have shown that the probability of termination steps increases when the reaction is carried out in nanoconfinement, with smaller domain sizes of polymerizing phase resulting in slower polymerization rates.[56]

The effect of the photoinitiator polarity on the reaction rate is another parameter that has been examined in the templating of M-20 and M-23 by Guymon and co-workers. [38,150,162] Generally, the initiation efficiency of the initiator is a measure of this effect. Higher initiator efficiency leads to higher polymerization rates. The obtained results show that the efficiency of hydrophilic initiators (e.g., I-5) decreases as the structure changes from micellar to lamellar. The volume fraction of polar domains diminishes for this change in the structure, resulting in higher proximity of the molecules of the water-soluble initiator. When the free radicals are formed, radical recombination due to the cage effect occurs, usually producing nonreactive components which in turn result in lower initiator efficiency. On the other hand, hydrophobic initiators (e.g., I-6) are partitioned in the opposite way, resulting in lower probability of cage effects and thus higher initiation efficiency.[26]

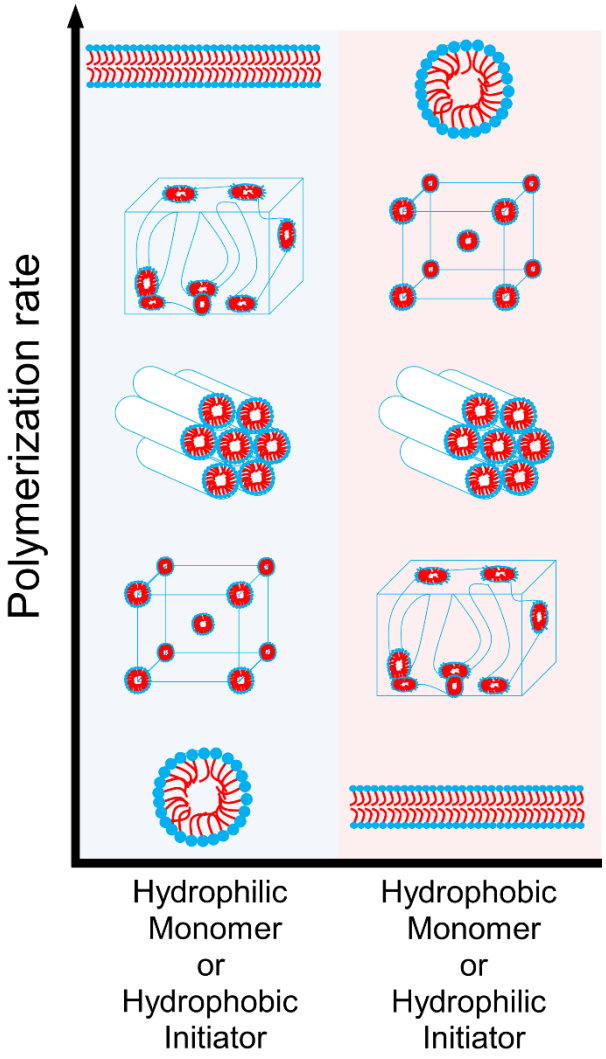

Fig. 13. The relative effect of monomer and initiator polarity on the polymerization rate in transcriptive templating.[26]

6. Synergistic versus transcriptive LLC templating: a summary

So far, we have discussed the two types of LLC templating approaches in detail. As a summary of our discussion in previous sections, Table 4 lists the differences and advantages/disadvantages of the mentioned techniques.

Table 4. The differences and advantages/disadvantages of synergistic and transcriptive LLC templating methods in summary.

	Synergistic	Transcriptive
Differences	Reactive surfactant(s) is the polymerizable species	Reactive monomer(s) is the polymerizable species
Advantages	Chemically bonding the surfactant to the structure, and thus, a higher chance of structural retention	The commercial availability of the employed components (e.g., monomers and surfactants)
Disadvantages	Unavailability of commercial reactive surfactants, and thus, requiring multi-step synthesis methods to prepare surfactants	Physically bonding the surfactant to the structure and thus lower chance of structural retention

7. Advanced functional materials: opportunities, challenges and outlook

LLC templating is an efficient "bottom-up" approach to fabricate nanostructured polymers that can be applicable in a wide variety of applications, as shown in Fig. 14. The membranes developed from the polyLLCs show enhanced permeability, selectivity, and fouling resistance compared to the current industry standard.[30–34] For instance, NF membranes having a thickness of 100 nm with effective pore sizes in the 1 nm range, MWCO ~ 300 Da, and permeability of ~ 20 L m^{-2} h^{-1} bar^{-1} have been fabricated via polyLLC technology.[30,170] These membranes have better performance than the commercially available NF membranes like Dow FILMTEC NF90-400 which have typical permeabilities in the range of 10 to 15 L m^{-2} h^{-1} bar^{-1}. The mentioned polyLLC membranes have also an intrinsic degree of biofouling resistance thanks to the presence of water-facing quaternary ammonium groups available in the structure of the employed reactive surfactant (P-A-6). As another example, fabrication of UF polyLLC membranes with a molecular weight cut-off of about 1500 Da and a permeability of ~ 85 L m^{-2} h^{-1} bar^{-1} (twice that of commercially control membrane, GE PT8040F30) has been reported.[31] In another effort, NF membranes with Q_1 structure have been fabricated, which outperform the commercial NF90 (Dow Filmtec) membrane in the treatment of hydraulic fracturing produced water. These PolyLLC membranes show a thickness-normalized flux of ~ 2.9 L µm m^{-2} h^{-1} (about 8 times of the commercial membrane) with much higher stability against fouling compared to NF90.[114] Additionally, the Q_1 membranes are able to recover up to 22% dissolved organic carbon while rejecting 75% of the salt which is a unique selectivity feature of these advanced materials over commercial opponents.[32] PolyLLC membranes have also proven advantages in breathable barrier materials for chemical agent protection. Dense polymers such as cross-linked BR, which are the common components used in such application, can cause heat and fatigue for the wearer as they are impermeable to water vapor. However, a proper water vapor permeability (~ 500 g m^{-2} day^{-1}) can be achieved without compromising the selectivity when BR incorporated polyLLC membranes are employed.[112]

The hydrogels prepared thorough the templating processes offer a proper balance of water uptake, swelling/de-swelling rate, and mechanical properties without compromising other key characteristics such as biocompatibility, biodegradability, and stimuli-responsiveness.[35–45] As an example, transcriptive templating has been used to fabricate nanostructured biodegradable hydrogel made of M-26 monomer, exhibiting 80% increase in network swelling and around 230% increase in diffusivity compared to the corresponding non-LLC polymer without changing the biocompatibility of the material. [144] Polyacrylamide hydrogels have been synthesized in LLC templates with ~ 10% higher water uptake and almost two times faster swelling rate than non-LLC analogous with no change in compressive modulus.[43] In another effort,[37] LLC templated poly(N-isopropylacrylamide) (PNIPAM) hydrogels have been prepared, which not only show twice the equilibrium swelling of analogous non-LLC counterparts but also exhibit 5 times greater dynamic range between the swollen and deswollen state. In other words, the nanostructured hydrogels possess faster deswelling rates at temperatures above the lowest critical solution temperature for PNIPAM. These important properties have further been improved via the incorporation of about 2 wt% M-16 in the polyLLC structure. [37]

The templating process can also result in conductive components with excellent mechanical properties compared to non-LLC materials.[46–48] The work done by Lopez-Barron et al. [46,48] is one of the best examples in this field. They have created FCC lattice by combining P-A-55 and a partially deuterated ionic liquid (ethylammonium nitrate) to fabricate a cross-linked ion gel having a highly elastomeric behavior with excellent mechanical properties, conductivity, and mechanoelectrical responses. The produced highly stretchable iono-elastomers (exhibiting a maximum elongation of 340%) are accurately and reliably sensitive to small motion as they show a linear strain-resistance response. Additionally, they have a large temperature-dependent conductivity (3.24 %/°C @ 30 °C) which is more than twice that of the most sensitive reported materials.[47] Therefore, they have been employed as thermo-mechanical sensors to capture the simultaneous/real-time strain and temperature of the human body during anaerobic exercise. This tough nanostructured material can resist external damages such as rubbing, pinching, and directional cutting while maintaining its functionality over 1000 cycles. Thus, it can potentially be used in sports training, prosthetic, personable healthcare, and robotics applications.[47]

It has also been shown that the nanostructured catalytic components obtained from mesophase templating exhibit unique catalytic activity/selectivity over commercially used catalysts.[28,49] For example, Gin et al. have shown that a polyLLC of P-A-23 with H_2 structure can be used as an effective heterogeneous base catalyst for the Knoevenagel condensation of ethyl cyanoacetate with benzaldehyde in refluxing THF while maintaining faster reaction compared to basic versions of zeolite-Y and MCM-41 mesoporous sieves.[28] In another study, heterogeneous polyLLC-based catalyst with the application in aerobic oxidation of alcohols has shown higher activity (~ 93% versus ~ 72% benzyl alcohol conversion) and selectivity (~ 4.2 versus ~ 1.9 benzyl alcohol/ 3,5-bis(*tert*-butyldiphenylsilyloxy)benzyl alcohol) over the industrially available TEMPO-based catalysts (e.g., Silicat® brand).[79]

The distinctive light emitting behavior of LLC templated products is another advantage of such materials over non-LLC ones.[50,51] PPV-incorporated polyLLCs with H_2 structure are the best

example in this application. Photoluminescence quantum efficiency of about 80% has been reported for such nanostructured materials, which is much higher than 5 - 27% yields reported for the pure PPV. Additionally, the stability of PPV against oxidation can be improved by chain isolation/protection inside the polyLLC pores.[50] Polarized photoluminescence behavior can also be obtained by shear-aligning the PPV containing H_2 phase.[28] Moreover, metal-based luminescence can be introduced into this system by using transition-metal and lanthanide cations as the counterions.[78]

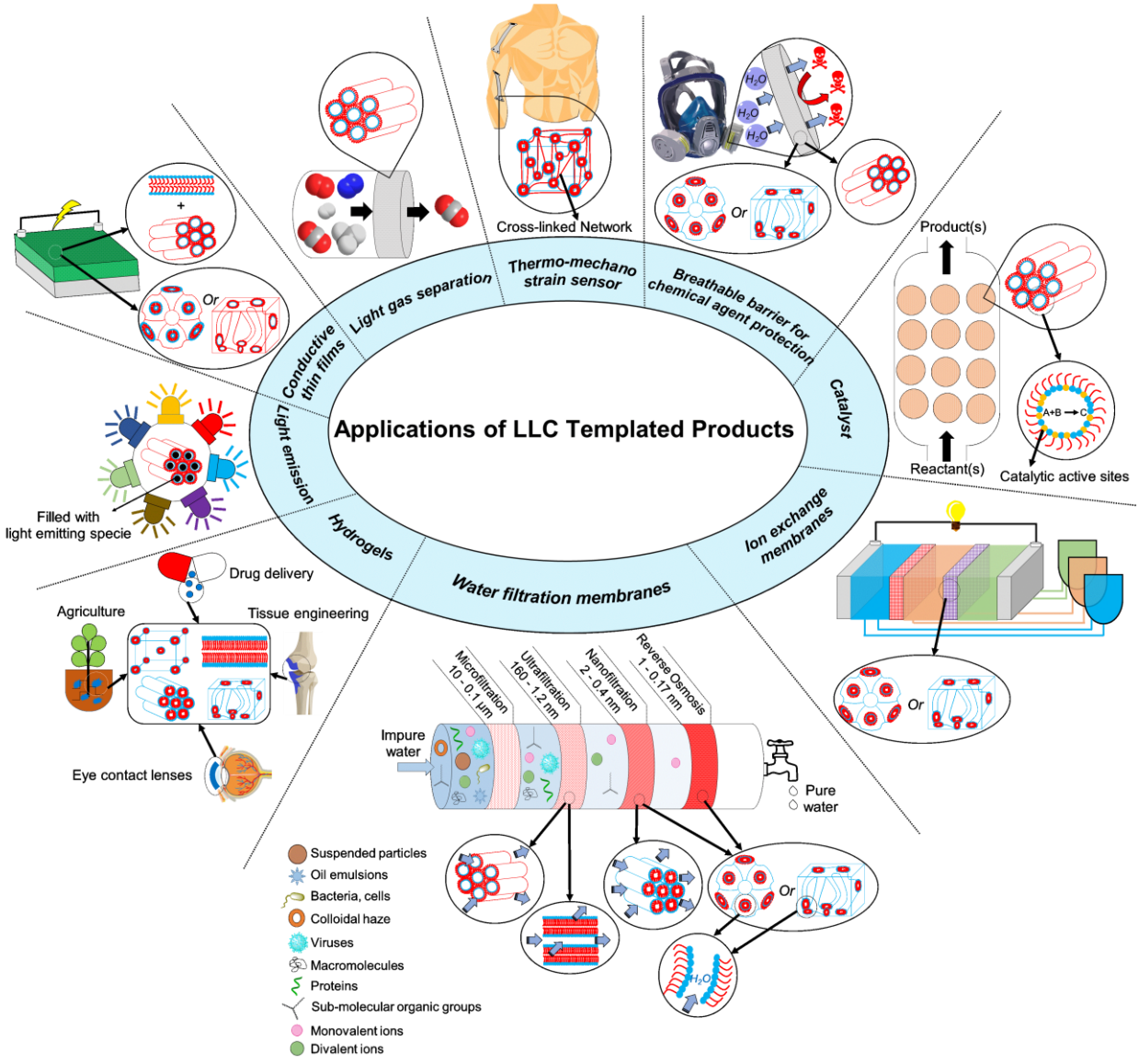

Fig. 14. Potential applications of LLC templated products

Although there have been plenty of studies on the advancement of LLC templating, some challenges still exist in the field. Scalability of the templating process is perhaps the most challenging hurdle to making polyLLCs fabrication applicable on larger scales. Synergistic templating requires reactive surfactants which are currently not commercially available and are usually synthesized through relatively complicated and expensive chemistries. This issue has

been addressed by Gin's groups to a limited extent through the introduction of polymerizable species synthesized via cheaper raw materials (e.g., P-A-33).[118] The alternative approach is transcriptive templating, although it requires a large amount of non-reactive components (i.e., surfactant) which are not chemically integrated in the polymerized phase.

For membrane applications, H_2 and L_α phases that are easily accessible suffer from improper alignment of the nanochannels and need additional pre-polymerization steps (e.g., magnetic alignment),[29] which are complicated and/or costly. On the other hand, no alignment is required for Q_α structure, but stable polyLLC structures are not easily achieved via commercially available amphiphiles. This challenge can be resolved to a large extent by using easily accessible H_1 structures which do not need any alignment, as recently shown by Osuji and co-workers, using a synergistic templating approach.[30] The accessibility of the H_1 mesophase makes it a feasible structure for developing a broad range of membranes tailored for different uses, including ion transport, and organic solvent nanofiltration. Recent work by the same group[170] has demonstrated a solution-based process for rapid fabrication of ~100 - 200 nm thick membrane selective layers over large areas using H_1 mesophases. The permeability and rejection characteristics are on par with several commercial NF membranes, with effective pore sizes in the 1 nm range, MWCO ~ 300 Da and permeabilities ~ 2 L m^{-2} h^{-1} bar^{-1} μm. At thicknesses of 100 nm, this corresponds to a permeance of ~ 20 L m^{-2} h^{-1} bar^{-1}.

In the general liquid crystal literature, there are a plethora of studies on the influence of surface conditions to aid the anchoring/alignment of liquid crystalline molecules or phases. In commercial display devices based on nematic phases, surface modification by lecithin surfactant coatings or microgrooves[171] is used to order the nematic phases. For thermotropic mesophases, Osuji et al., among others, have demonstrated the uniform homeotropic alignment of hexagonal cylindrical pores by confined annealing of the pre-polymerization phase between compatible substrates such as glass and PDMS.[172] There are also examples in literature utilizing surface anchoring techniques to align lyotropic chromonic liquid crystal phases.[173] It stands to reason that surface anchoring-based alignment techniques can be utilized to resolve the alignment issues for H_2 and L_α LLC structures. Foudazi et. al. have also shown that it is possible to induce the alignment in LLCs simply via applying large amplitude oscillatory shear, although further studies are still required.[174] Additionally, the thicknesses of the polyLLC derived active layer in water filtration membranes have to be further decreased via industrially scalable approaches to acquire higher water fluxes necessary for economic feasibility. Gin and co-workers have introduced techniques to produce TFC-based membranes to address this issue,[32,114,120,121] but there is much room for further work in this area.

The typical molecular weight range of the amphiphiles (< 2 kDa) discussed in this review necessarily limits the feature sizes of their lyotropic mesophases to the sub-10-nm, and more typically the sub-5-nm regime. Recent advances in block-copolymer self-assembly have enabled BCP systems which exhibit self-assembled features in the 5 - 10 nm range, thereby providing a continuous spectrum of options for fabrication of self-assembled materials with features in the 1 - 5 nm range templated by polyLLC, and features larger than 5 nm enabled by BCP micro-phase segregation. However, there are at least two approaches based on lyotropic liquid-crystalline materials to obtain features sizes near- and beyond-10 nm.

The first of these approaches relies on so-called 'giant surfactants' or 'shape amphiphiles', which are higher molecular weight analogues of small-molecules amphiphiles. As summarized by Yue et al,[175] giant surfactant analogous can be synthesized to mirror their lower-MW polyLLC counterparts in terms of architecture i.e. single-headgroup single-tail, single-headgroup multiple tail, bolaform architecture, gemini architecture and beyond. Typically, the headgroup consists of a large 'cage' like structure, sometimes termed a molecular nanoparticle (MNP). MNP headgroups in giant surfactant literature[176] are most often fullerene or functionalized polyhedral oligomeric silsesquioxane (POSS) derivatives, although globular proteins[177] can also be incorporated as the hydrophilic head-groups . The most commonly studied tails in the literature are polystyrene tails. Work by Yu et al[178] has demonstrated that with appropriately designed chemical structures, POSS-PS giant surfactants can display most of the phases (micellar, lamellar, hexagonal, cubic) found in LLCs with 2 or 3 times larger periodicities i.e. 7 - 20 nm. Given the longer tail lengths and larger headgroup radii of giant surfactants compared to typical surfactants, the former provide many more atomic sites for targeted/localized synthetic modifications to increase functionality for advanced applications such as protein/biomolecular sensing platforms, although with the trade-off of increased synthetic and purification complexity. In principle, the additional functional sites afforded by the larger molecular size could be utilized to incorporate unsaturated bonds/cross-linking sites in giant surfactant molecules. In one case,[179] a methacrylate cross-linker based on the giant surfactant headgroup (M-POSS) was utilized for phase preservation in a small-molecule amphiphile mesophase. However, in general, there is very little work focusing on synergistic or transcriptive templating for giant surfactant mesophases at this time.

A second approach relies upon swelling of lyotropic bicontinuous cubic mesophases unit cell sizes by addition of charged lipids. Angelov et al[180] reported a 50% swelling in unit cell dimensions of a Diamond-type cubic bicontinuous phase consisting of an aqueous Monoolein cubic phase swelled with a small amount of octyl-glucoside, resulting in a lattice parameter of 15.3 nm. Work by the Brooks group has shown that increasing the formulation complexity of similar swollen mesophases of ternary lipid mixtures and beyond can yield even larger unit cell sizes and provide additional handles for controlling the unit cell spacing. Barriga and Tyler et al[181] have shown that addition of cholesterol and charged lipids to monoolein-water bicontinuous phase swell the primitive cubic unit cell spacing from ~ 10 nm to nearly 50 nm, while also enabling pressure and temperature sensitivity in the phase to tune the unit cell parameter. In a follow up work,[182] they further elucidate the importance of the electrostatic stability imparted to the swelled cubic bicontinuous phase by the added anionic lipid in the ternary mixture. This additional stability allows the mesophase to surpass the theoretically expected limit[183] of ~ 30 nm lattice parameter due to the effect of thermal oscillations. Recent work from Leal's group has demonstrated even larger lattice cell parameters. In glycerol monooleate based mesophases,[184] doped with charged lipids and PEG-lipids, a gyroid phase with unit cell parameter 64.4 nm was obtained, corresponding to an estimated water channel diameter of 38 nm. Further work[185] on this composition identified the role of the PEG-lipid composition as a reliable handle to switch the mesophase between diamond, gyroid and primitive cubic bicontinuous morphology. The larger water channels of the swollen lipidic mesophases reduce much of their suitability for selective separations such as filtration, but in

turn enable their use in emerging biotechnology applications such as platforms for protein crystallization processes.[186]

Most of the existing literature on the aforementioned two approaches focuses on the chemical synthesis or formulation stability of the larger lattice parameter lyotropic mesophases. Neither approach has been extensively studied for phase and feature preservation after polymerization, thus presenting opportunities for future researchers to combine synergistic or transcriptive templating approaches to preserve large unit cell self-assembled mesophases of giant surfactants or swelled LLC phases.

The optimization of transcriptive templating recipes seems necessary to decrease the required concentration of surfactant and thus to improve the thermal and mechanical properties of the final products. Using specific types of amphiphiles which have very low CMCs (such as sodium alkoxy sulfate reported by Chen et al.[187]) might be helpful in resolving this issue. Furthermore, the high porosity of polymerized LLCs after extraction/drying of non-reactive component(s) results in poor mechanical properties. Although the random alignment of the nanostructures overshadows this effect to some extent, incorporation of nanoparticles (e.g., carbon nanotubes) in LLC structures might be a proper approach to overcome this challenge if the structure retention is not affected by the presence of nanoparticles.[80] Nanoparticles may induce heterogeneity in the structure or direct the self-assembly toward formation of a different LLC structure.

In addition to the discussed challenges, there are still some relatively unexplored application-oriented opportunities available in the field. For instance, production of stimuli-responsive (e.g., thermoresponsive and pH-responsive) membranes through LLC templating needs further attention. To the best of our knowledge, except for the reported works on LLC templated thermo-responsive hydrogels (hydrophilic polymers),[37,41] there is only one report exploring the possibility of having dynamic pore sizes in hydrophobic polymers by synergistic templating of a stimuli-responsive amphiphile (P-A-43).[128] As discussed earlier, syntheses of such reactive species are highly challenging; therefore, transcriptive templating of commercially available monomers that result in stimuli-responsive polymers is a potentially new direction in this field. According to the literature, stimuli-responsive membranes that possess inherent pore size tuneability exhibit higher water flux recovery and variable permeability/selectivity.[5,188] Application of LLC templating in the production of ion gels is another fertile research ground. The combination of BCPs and ionic liquids is the common approach to fabricate ion gels.[189–195] While this method works perfectly, in some cases, to preserve the conductivity of the obtained polymer electrolyte, a relatively high amount of ionic liquid is required which results in deterioration of the mechanical properties over time. To address this issue, a limited number of reports have used LLC templating to fabricate robust ion gels having proper conductivity.[46–48,142] Nevertheless, expanding the available formulations and using different structures are still required to improve the mechanical properties beyond those offered by the current polymer electrolytes.

LLC templating through electrochemical templating, which has already been explored for inorganic species (e.g., Pt), is another unexplored research area for organic compounds. Based

on the available reports in the literature, this approach is simple, has low cost, and requires mild conditions. Moreover, the obtained products show enhanced properties like enhanced catalytic activity and stability.[196] Fabrication of polyLLC membranes with controlled thicknesses is a potential application of electrochemical templating.

There has been a great deal of interest toward commercialization of energy conversion devices in fuel cells and solar cells.[197] Therefore, it can be a great opportunity to employ polyLLCs with different nanostructures to improve the efficiency of such materials and thus facilitate the commercialization process. PolyLLCs and LLC templating methods offer several advantages over the materials and methods currently used in this field. For instance, microemulsion-templated products usually do not have anisotropic structure as L_α , H_1 and H_2 LLCs do.[197] Moreover, LLC templating is much more straightforward than multi-step gas bubble templating approach employed to create porous structures.[198] Additionally, templating with soft LLCs is simpler and safer than employing hard templates which not only is a complex technique, but also is not safe as harmful chemicals are used for the template removal.[199]

Successful production of inorganic nanostructures (e.g., Pt, Pd and bimetallic) in LLC templates has already been documented. According to the experimental results, the obtained nanomaterials exhibit remarkable electrocatalytic activity, high conductivity and chemical stability, and low cost of production.[197] Nevertheless, there are still limited works on LLC templating of organic species. In one work, Hulvat et al. used M-18 in normal hexagonal structure to fabricate nanostructured conductive materials. The obtained products have shown higher conductivity compared to the non-templated formulation.[158,159] Similar increase in conductivity has been reported for the products obtained from LLC templating of M-18 by Ghosh et al.[160] In another effort, M-39 has been polymerized in H_1 structure, resulting in nanofibers with a conductivity higher than the values reported in the literature for same polymer.[167] M-40 has been used in LLC templating to fabricate nanostructured semiconductors with the optical band gap of 2.25 eV and strong absorption in the visible region, applicable in electronic devices or solar light harvesting applications.[168] Furthermore, there are some works in the literature showing that the properties of LLC-templated conductive polymers can be further enhanced by incorporation of inorganic nanoparticles in the LLC structure.[197] These appealing results confirm the potential of polyLLCs in this field.

Another area of opportunity lies in the use of polymerized LLCs to control the synthesis and organization of inorganic nanomaterials. The use of LLCs to template synthesis of nanostructured inorganic materials is well-known and is the basis for the production of mesoporous molecular sieves such as SBA-15[200] and MCM-41[201]. These siliceous materials are valued as catalyst supports[201,202]. The opportunity exists for templated synthesis of inorganic materials in the aqueous channels of polymerized LLCs. A simple route for example is the formation of nanoparticles by reduction of precursor species (e.g. metal ions). The resulting nanomaterial-containing nanostructured polymer membranes are of potential utility as catalytic membranes. Early work by Gin et al.,[203] highlighted this potential with the formation of Pd nanoparticles in polymerized hexagonal mesophases derived from a wedge-shaped amphiphile. The concept of nanostructured catalytic polymer membranes is a compelling one. In some cases, rather than relying on the synthesis of a second phase material,

the chemistry of the polar headgroup itself can be used, as demonstrated by Gin et al., for Lewis[49] and Bronsted[95] acid catalysis. In total however, well-controlled nanomaterial synthesis in polymerized LLCs can be challenging due to the difficulties in controlling the polymerization, as identified in this review.

Acknowledgements

YS and RF would like to thank the support by the National Science Foundation (NSF) under grant no. 1840871. OI and CO acknowledge NSF support under DMR-1945966 and CBET-1703494

References

1 D. Chimene, D. L. Alge and A. K. Gaharwar, *Adv. Mater.*, 2015, **27**, 7261–7284.

2 N. M. Bardhan, *J. Mater. Res.*, 2017, **32**, 107–127.

3 F. Iskandar, *Adv. Powder Technol.*, 2009, **20**, 283–292.

4 J. R. Werber, C. O. Osuji and M. Elimelech, *Nat. Rev. Mater.*, 2016, **1**, 16018.

5 D. Wandera, S. R. Wickramasinghe and S. M. Husson, *J. Memb. Sci.*, 2010, **357**, 6–35.

6 Q. Zhang, E. Uchaker, S. L. Candelaria and G. Cao, *Chem. Soc. Rev.*, 2013, **42**, 3127–3171.

7 D. L. Gin, X. Lu, P. R. Nemade, C. S. Pecinovsky, Y. Xu and M. Zhou, *Adv. Funct. Mater.*, 2006, **16**, 865–878.

8 H. Hu, M. Gopinadhan and C. O. Osuji, *Soft Matter*, 2014, **10**, 3867.

9 S. T. Hyde, in *Handbook of Applied Surface and Colloid Chemistry*, 2001, pp. 299–332.

10 T. Tachibana, T. Mori and K. Hori, *Bull. Chem. Soc. Jpn.*, 1980, **53**, 1714–1719.

11 R. Atkin, S. M. C. Bobillier and G. G. Warr, *J. Phys. Chem. B*, 2010, **114**, 1350–1360.

12 L. A. Robertson, M. R. Schenkel, B. R. Wiesenauer and D. L. Gin, *Chem. Commun.*, 2013, **49**, 9407–9409.

13 R. Nagarajan, *Langmuir*, 2002, **18**, 31–38.

14 V. Lutz-Bueno, S. Isabettini, F. Walker, S. Kuster, M. Liebi and P. Fischer, *Phys. Chem. Chem. Phys.*, 2017, **19**, 21869–21877.

15 Y. C. Lee, T. F. Taraschi and N. Janes, *Biophys. J.*, 1993, **65**, 1429–1432.

16 Y. Huang and S. Gui, *RSC Adv.*, 2018, **8**, 6978–6987.

17 S. S. Soni, G. Brotons, M. Bellour, T. Narayanan and A. Gibaud, *J. Phys. Chem. B*, 2006, **110**, 15157–15165.

18 R. Rajabalaya, M. N. Musa, N. Kifli and S. R. David, *Drug Des. Devel. Ther.*, 2017, **Volume11**, 393–406.

19 Y. Meng, D. Gu, F. Zhang, Y. Shi, L. Cheng, D. Feng, Z. Wu, Z. Chen, Y. Wan, A. Stein and D. Zhao, *Chem. Mater.*, 2006, **18**, 4447–4464.

20 A. Jayaraman, D. Y. Zhang, B. L. Dewing and M. K. Mahanthappa, *ACS Cent. Sci.*, 2019, **5**, 619–628.

21 C. M. Baez-Cotto and M. K. Mahanthappa, *ACS Nano*, 2018, **12**, 3226–3234.

22 J. Jennings, B. Green, T. J. Mann, C. A. Guymon and M. K. Mahanthappa, *Chem. Mater.*, 2018, **30**, 185–196.

23 A. Jayaraman and M. K. Mahanthappa, *Langmuir*, 2018, **34**, 2290–2301.

24 I. Moriguchi, A. Ozono, K. Mikuriya, Y. Teraoka, S. Kagawa and M. Kodama, *Chem. Lett.*, 1999, 1171–1172.

25 H.-P. Hentze, C. C. Co, C. A. McKelvey and E. W. Kaler, in *Topics in Current Chemistry*, 2003, pp. 197–223.

26 K. S. Worthington, C. Baguenard, B. S. Forney and C. A. Guymon, *J. Polym. Sci. Part B Polym. Phys.*, 2017, **55**, 471–489.

27 C. Wang, D. Chen and X. Jiao, *Sci. Technol. Adv. Mater.*, 2009, **10**, 023001.

28 D. L. Gin, W. Gu, B. A. Pindzola and W.-J. Zhou, *Acc. Chem. Res.*, 2001, **34**, 973–980.

29 M. S. Mauter, M. Elimelech and C. O. Osuji, *ACS Nano*, 2010, **4**, 6651–6658.

30 X. Feng, Q. Imran, Y. Zhang, L. Sixdenier, X. Lu, G. Kaufman, U. Gabinet, K. Kawabata, M. Elimelech and C. O. Osuji, *Sci. Adv.*, 2019, **5**, eaav9308.

31 S. Qavi, A. P. Lindsay, M. A. Firestone and R. Foudazi, *J. Memb. Sci.*, 2019, **580**, 125–133.

32 S. M. Dischinger, J. Rosenblum, R. D. Noble, D. L. Gin and K. G. Linden, *J. Memb. Sci.*, 2017, **543**, 319–327.

33 M. Zhou, P. R. Nemade, X. Lu, X. Zeng, E. S. Hatakeyama, R. D. Noble and D. L. Gin, *J. Am. Chem. Soc.*, 2007, **129**, 9574–9575.

34 D. L. Gin, J. E. Bara, R. D. Noble and B. J. Elliott, *Macromol. Rapid Commun.*, 2008, **29**, 367–389.

35 C. A. Guymon and C. L. Lester, *ACS Symp. Ser.*, 2003, **847**, 378–388.

36 C. L. Lester, S. M. Smith, W. L. Jarrett and C. Allan Guymon, *Langmuir*, 2003, **19**, 9466–9472.

37 J. R. McLaughlin, N. L. Abbott and C. A. Guymon, *Polymer*, 2018, **142**, 119–126.

38 M. A. DePierro, A. J. Olson and C. A. Guymon, *Polymer*, 2005, **46**, 335–345.

39 M. A. DePierro, K. G. Carpenter and C. A. Guymon, *Chem. Mater.*, 2006, **18**, 5609–5617.

40 B. S. Forney, C. Baguenard and C. A. Guymon, *Chem. Mater.*, 2013, **25**, 2950–2960.

41 B. S. Forney, C. Baguenard and C. Allan Guymon, *Soft Matter*, 2013, **9**, 7458–7467.

42 C. L. Lester, C. D. Colson and C. A. Guymon, *Macromolecules*, 2001, **34**, 4430–4438.

43 C. L. Lester, S. M. Smith, C. D. Colson and C. A. Guymon, *Chem. Mater.*, 2003, **15**, 3376–3384.

44 D. T. McCormick, K. D. Stovall and C. A. Guymon, *Macromolecules*, 2003, **36**, 6549–6558.

45 J. D. Clapper and C. A. Guymon, *Mol. Cryst. Liq. Cryst.*, 2009, **509**, 30/[772]-38/[780].

46 C. R. López-Barrón, R. Chen and N. J. Wagner, *ACS Macro Lett.*, 2016, **5**, 1332–1338.

47 Y. Xie, R. Xie, H. C. Yang, Z. Chen, J. Hou, C. R. López-Barrón, N. J. Wagner and K. Z. Gao, *ACS Appl. Mater. Interfaces*, 2018, **10**, 32435–32443.

48 C. R. López-Barrón, R. Chen, N. J. Wagner and P. J. Beltramo, *Macromolecules*, 2016, **49**, 5179–5189.

49 W. Gu, W. J. Zhou and D. L. Gin, *Chem. Mater.*, 2001, **13**, 1949–1951.

50 R. C. Smith, W. M. Fischer and D. L. Gin, *J. Am. Chem. Soc.*, 1997, **119**, 4092–4093.

51 D. H. Gray, S. Hu, E. Juang and D. L. Gin, *Adv. Mater.*, 1997, **9**, 731–736.

52 M. J. McGrath, N. Patterson, B. C. Manubay, S. H. Hardy, J. J. Malecha, Z. Shi, X. Yue, X. Xing, H. H. Funke, D. L. Gin, P. Liu and R. D. Noble, *Ind. Eng. Chem. Res.*, 2019, **58**, 22250–22259.

53 J. Herz, F. Reiss-Husson, P. Rempp and V. Luzzati, *J. Polym. Sci. Part C Polym. Symp.*, 2007, **4**, 1275–1290.

54 P. Ström and D. M. Anderson, *Langmuir*, 1992, **8**, 691–709.

55 J. Zhang, Z. A. Qiao, S. M. Mahurin, X. Jiang, S. H. Chai, H. Lu, K. Nelson and S. Dai, *Angew. Chemie - Int. Ed.*, 2015, **54**, 4582–4586.

56 S. Qavi, A. Bandegi, M. Firestone and R. Foudazi, *Soft Matter*, 2019, **15**, 8238–8250.

57 S. E. Friberg, R. Thundathil and J. O. Stoffer, *Science (80-.).*, 1979, **205**, 607–608.

58 Y. S. Lee, J. T. Gleeson, J. Z. Yang, T. M. Sisson, D. A. Frankel, D. F. O'Brien, S. L. Keller, E. Aksay and S. M. Gruner, *J. Am. Chem. Soc.*, 1995, **117**, 5573–5578.

59 C.-M. Young, C. L. Chang, Y.-H. Chen, C.-Y. Chen, Y.-F. Chang and H.-L. Chen, *Soft Matter*, 2021, **17**, 397–409.

60 B. Soberats, M. Yoshio, T. Ichikawa, X. Zeng, H. Ohno, G. Ungar and T. Kato, *J. Am. Chem. Soc.*, 2015, **137**, 13212–13215.

61 B. A. Pindzola, J. Jin and D. L. Gin, *J. Am. Chem. Soc.*, 2003, **125**, 2940–2949.

62 S. Qavi, M. A. Firestone and R. Foudazi, *Soft Matter*, 2019, **15**, 5626–5637.

63 M. G. Marquez Garcia, New Mexico State University, 2020.

64 S. A. Kim, K.-J. Jeong, A. Yethiraj and M. K. Mahanthappa, *Proc. Natl. Acad. Sci.*, 2017, **114**, 4072–4077.

65 F. C. Frank and J. S. Kasper, *Acta Crystallogr.*, 1958, **11**, 184–190.

66 F. C. Frank and J. S. Kasper, *Acta Crystallogr.*, 1959, **12**, 483–499.

67 M. Huang, K. Yue, J. Wang, C.-H. Hsu, L. Wang and S. Z. D. Cheng, *Sci. China Chem.*, 2018, **61**, 33–45.

68 D. Roux, C. Coulon and M. E. Cates, *J. Phys. Chem.*, 1992, **96**, 4174–4187.

69 B. Angelov, A. Angelova, R. Mutafchieva, S. Lesieur, U. Vainio, V. M. Garamus, G. V. Jensen and J. S. Pedersen, *Phys. Chem. Chem. Phys.*, 2011, **13**, 3073–3081.

70 B. Kent, C. J. Garvey, D. Cookson and G. Bryant, *Chem. Phys. Lipids*, 2009, **157**, 56–60.

71 R. Thundathil, J. O. Stoffer and S. E. Friberg, *J. Polym. Sci. A1.*, 1980, **18**, 2629–2640.

72 Y. Shibasaki and K. Fukuda, *Colloids and Surfaces*, 1992, **67**, 195–201.

73 K. M. McGrath and C. J. Drummond, *Colloid Polym. Sci.*, 1996, **274**, 316–333.

74 K. M. McGrath, *Colloid Polym. Sci.*, 1996, **274**, 499–512.

75 K. M. McGrath, *Colloid Polym. Sci.*, 1996, **274**, 399–409.

76 D. Pawlowski, A. Haibel and M. Tieke, *Berichte der Bunsengesellschaft/Physical Chem. Chem. Phys.*, 1998, **102**, 1865–1869.

77 M. Li, W. Yang, Z. Chen, J. Qian, C. Wang and S. Fu, *J. Polym. Sci. Part A Polym. Chem.*, 2006, **44**, 5887–5897.

78 H. Deng, D. L. Gin and R. C. Smith, *J. Am. Chem. Soc.*, 1998, **120**, 3522–3523.

79 G. E. Dwulet and D. L. Gin, *Chem. Commun.*, 2018, **54**, 12053–12056.

80 B. S. Ringstrand, S. Seifert, D. W. Podlesak and M. A. Firestone, *Macromol. Rapid Commun.*, 2016, **37**, 1155–1167.

81 S. Peng, P. G. Hartley, T. C. Hughes and Q. Guo, *Soft Matter*, 2015, **11**, 6318–6326.

82 W. Srisiri, T. M. Sisson, D. F. O'Brien, K. M. McGrath, Y. Han and S. M. Gruner, *J. Am. Chem. Soc.*, 1997, **119**, 4866–4873.

83 M. A. Reppy, D. H. Gray, B. A. Pindzola, J. L. Smithers and D. L. Gin, *J. Am. Chem.*

Soc., 2001, **123**, 363–371.

84 B. P. Hoag and D. L. Gin, *Macromolecules*, 2000, **33**, 8549–8558.

85 B. A. Pindzola, B. P. Hoag and D. L. Gin, *J. Am. Chem. Soc.*, 2001, **123**, 4617–4618.

86 D. Batra, D. N. T. Hay and M. A. Firestone, *Chem. Mater.*, 2007, **19**, 4423–4431.

87 D. Batra, S. Seifert and M. A. Firestone, *Macromol. Chem. Phys.*, 2007, **208**, 1416–1427.

88 S. Grubjesic, S. Seifert and M. A. Firestone, *Macromolecules*, 2009, **42**, 5461–5470.

89 L. Sievens-Figueroa and C. A. Guymon, *Chem. Mater.*, 2009, **21**, 1060–1068.

90 G. A. Becht, M. Sofos, S. Seifert and M. A. Firestone, *Macromolecules*, 2011, **44**, 1421–1428.

91 B. G. Ndefru, B. S. Ringstrand, S. I. Y. Diouf, S. Seifert, J. H. Leal, T. A. Semelsberger, T. A. Dreier and M. A. Firestone, *Mol. Syst. Des. Eng.*, 2019, **4**, 580–585.

92 J. Jin, V. Nguyen, W. Gu, X. Lu, B. J. Elliott and D. L. Gin, *Chem. Mater.*, 2005, **17**, 224–226.

93 M. Zhou, T. J. Kidd, R. D. Noble and D. L. Gin, *Adv. Mater.*, 2005, **17**, 1850–1853.

94 J. E. Bara, A. K. Kaminski, R. D. Noble and D. L. Gin, *J. Memb. Sci.*, 2007, **288**, 13–19.

95 Y. Xu, W. Gu and D. L. Gin, *J. Am. Chem. Soc.*, 2004, **126**, 1616–1617.

96 L. Sievens-Figueroa and C. A. Guymon, *Macromolecules*, 2009, **42**, 9243–9250.

97 C. L. Lester and C. A. Guymon, *Polymer*, 2002, **43**, 3707–3715.

98 L. Sievens-Figueroa and C. Allan Guymon, *Polymer*, 2008, **49**, 2260–2267.

99 M. A. DePierro, C. Baguenard and C. Allan Guymon, *J. Polym. Sci. Part A Polym. Chem.*, 2016, **54**, 144–154.

100 D. H. Gray and D. L. Gin, *Chem. Mater.*, 1998, **10**, 1827–1832.

101 H. P. Hentze, E. Krämer, B. Berton, S. Förster, M. Antonietti and M. Dreja, *Macromolecules*, 1999, **32**, 5803–5809.

102 J. Yang and G. Wegner, *Macromolecules*, 1992, **25**, 1791–1795.

103 B. Ringstrand, S. Seifert and M. A. Firestone, *J. Polym. Sci. Part B Polym. Phys.*, 2013, **51**, 1215–1227.

104 M. Imai, K. Sakai, M. Kikuchi, K. Nakaya, A. Saeki and T. Teramoto, *J. Chem. Phys.*, 2005, **122**, 214906.

105 S. Grubjesic, B. Lee, S. Seifert and M. A. Firestone, *Soft Matter*, 2011, **7**, 9695.

106 P. C. Hartmann and R. D. Sanderson, *Macromol. Symp.*, 2005, **225**, 229–237.

107 B. R. Wiesenauer and D. L. Gin, *Polym. J.*, 2012, **44**, 461–468.

108 W. Srisiri, A. Benedicto, D. F. O'Brien, T. P. Trouard, G. Orädd, S. Persson and G. Lindblom, *Langmuir*, 1998, **14**, 1921–1926.

109 A. Mueller and D. F. O'Brien, *Chem. Rev.*, 2002, **102**, 727–757.

110 D. Yang, D. F. O'Brien and S. R. Marder, *J. Am. Chem. Soc.*, 2002, **124**, 13388–13389.

111 D. F. O'Brien, B. Armitage, A. Benedicto, D. E. Bennett, H. G. Lamparski, Y. S. Lee, W. Srisiri and T. M. Sisson, *Acc. Chem. Res.*, 1998, **31**, 861–868.

112 G. E. Dwulet, S. M. Dischinger, M. J. McGrath, A. J. Basalla, J. J. Malecha, R. D. Noble and D. L. Gin, *Ind. Eng. Chem. Res.*, 2019, **58**, 21890–21893.

113 M. J. McGrath, S. H. Hardy, A. J. Basalla, G. E. Dwulet, B. C. Manubay, J. J. Malecha, Z. Shi, H. H. Funke, D. L. Gin and R. D. Noble, *ACS Mater. Lett.*, 2019, **1**, 452–458.

114 S. M. Dischinger, J. Rosenblum, R. D. Noble and D. L. Gin, *J. Memb. Sci.*, 2019, **592**, 117313.

115 X. Lu, V. Nguyen, M. Zhou, X. Zeng, J. Jin, B. J. Elliott and D. L. Gin, *Adv. Mater.*, 2006, **18**, 3294–3298.

116 R. L. Kerr, S. A. Miller, R. K. Shoemaker, B. J. Elliott and D. L. Gin, *J. Am. Chem. Soc.*, 2009, **131**, 15972–15973.

117 X. Liang, X. Lu, M. Yu, A. S. Cavanagh, D. L. Gin and A. W. Weimer, *J. Memb. Sci.*, 2010, **349**, 1–5.

118 E. S. Hatakeyama, B. R. Wiesenauer, C. J. Gabriel, R. D. Noble and D. L. Gin, *Chem. Mater.*, 2010, **22**, 4525–4527.

119 E. S. Hatakeyama, C. J. Gabriel, B. R. Wiesenauer, J. L. Lohr, M. Zhou, R. D. Noble and D. L. Gin, *J. Memb. Sci.*, 2011, **366**, 62–72.

120 B. M. Carter, B. R. Wiesenauer, E. S. Hatakeyama, J. L. Barton, R. D. Noble and D. L. Gin, *Chem. Mater.*, 2012, **24**, 4005–4007.

121 B. M. Carter, B. R. Wiesenauer, R. D. Noble and D. L. Gin, *J. Memb. Sci.*, 2014, **455**, 143–151.

122 C. L. Lester and C. A. Guymon, *Macromolecules*, 2000, **33**, 5448–5454.

123 K. M. McGrath and C. J. Drummond, *Colloid Polym. Sci.*, 1996, **274**, 612–621.

124 M. H. Li, W. L. Yang, J. Qian, C. C. Wang and S. K. Fu, *Des. Monomers Polym.*, 2004, **7**, 505–519.

125 X. Feng, M. E. Tousley, M. G. Cowan, B. R. Wiesenauer, S. Nejati, Y. Choo, R. D. Noble, M. Elimelech, D. L. Gin and C. O. Osuji, *ACS Nano*, 2014, **8**, 11977–11986.

126 C. T. Burns, S. Lee, S. Seifert and M. A. Firestone, *Polym. Adv. Technol.*, 2008, **19**, 1369–1382.

127 P. M. Welch, T. A. Dreier, H. D. Magurudeniya, M. G. Frith, J. Ilavsky, S. Seifert, A. K. Rahman, A. Rahman, A. J. Singh, B. S. Ringstrand, C. J. Hanson, J. A. Hollingsworth and M. A. Firestone, *Macromolecules*, 2020, **53**, 2822–2833.

128 C. S. Pecinovsky, E. S. Hatakeyama and D. L. Gin, *Adv. Mater.*, 2008, **20**, 174–178.

129 W. Zhou, W. Gu, Y. Xu, C. S. Pecinovsky and D. L. Gin, *Langmuir*, 2003, **19**, 6346–6348.

130 C. S. Pecinovsky, G. D. Nicodemus and D. L. Gin, *Chem. Mater.*, 2005, **17**, 4889–4891.

131 M. Antonietti, R. A. Caruso, C. G. Göltner and M. C. Weissenberger, *Macromolecules*, 1999, **32**, 1383–1389.

132 J. Zhang, Z. Xie, A. J. Hill, F. H. She, A. W. Thornton, M. Hoang and L. X. Kong, *Soft Matter*, 2012, **8**, 2087–2094.

133 J. Zhang, Z. Xie, M. Hoang, A. J. Hill, W. Cong, F. H. She, W. Gao and L. X. Kong, *Soft Matter*, 2014, **10**, 5192–5200.

134 J. Zhang, Z. Xie, A. J. Hill, W. Cong, F. H. She, W. Gao, M. Hoang and L. X. Kong, *Polym. Bull.*, 2018, **75**, 581–595.

135 J. D. Clapper and C. A. Guymon, *Adv. Mater.*, 2006, **18**, 1575–1580.

136 M. E. Tousley, X. Feng, M. Elimelech and C. O. Osuji, *ACS Appl. Mater. Interfaces*, 2014, **6**, 19710–19717.

137 S. Qavi, New Mexico State University, 2019.

138 C. Liang and S. Dai, *J. Am. Chem. Soc.*, 2006, **128**, 5316–5317.

139 C. M. Ghimbeu, M. Sopronyi, F. Sima, C. Vaulot, L. Vidal, J. M. Le Meins and L. Delmotte, *RSC Adv.*, 2015, **5**, 2861–2868.

140 S. Herou, M. C. Ribadeneyra, R. Madhu, V. Araullo-Peters, A. Jensen, P. Schlee and M. Titirici, *Green Chem.*, 2019, **21**, 550–559.

141 X. Wang, C. Liang and S. Dai, *Langmuir*, 2008, **24**, 7500–7505.

142 A. Bandegi, J. L. Bañuelos and R. Foudazi, *Soft Matter*, 2020, **16**, 6102–6114.

143 J. D. Clapper and C. A. Guymon, *Macromolecules*, 2007, **40**, 7951–7959.

144 J. D. Clapper, S. L. Iverson and C. A. Guymon, *Biomacromolecules*, 2007, **8**, 2104–2111.

145 D. M. Anderson and P. Ström, ACS Symposium Series, 1989, pp. 204–224.

146 M. Jung, A. L. German and H. R. Fischer, *Colloid Polym. Sci.*, 2001, **279**, 105–113.

147 D. M. Anderson and P. Ström, *Phys. A Stat. Mech. its Appl.*, 1991, **176**, 151–167.

148 R. Laversanne, *Macromolecules*, 1992, **25**, 489–491.

149 B. S. Forney and C. Allan Guymon, *Macromol. Rapid Commun.*, 2011, **32**, 765–769.

150 M. A. DePierro and C. A. Guymon, *Macromolecules*, 2006, **39**, 617–626.

151 B. S. Forney and C. A. Guymon, *Macromolecules*, 2010, **43**, 8502–8510.

152 H. P. Hentze, C. G. Göltner and M. Antonietti, *Berichte der Bunsengesellschaft/Physical Chem. Chem. Phys.*, 1997, **101**, 1699–1702.

153 M. A. DePierro, K. G. Carpenter and C. A. Guymon, *Radtech Tech. Proc.*, 2006.

154 Y. Saadat, K. Kim and R. Foudazi, *Polym. Chem.*, 2021, **12**, 2236–2252.

155 W. Meier, *Macromolecules*, 1998, **31**, 2212–2217.

156 M. Antonietti, C. Göltner and H. P. Hentze, *Langmuir*, 1998, **14**, 2670–2672.

157 C. L. Lester, S. M. Smith and C. A. Guymon, *Macromolecules*, 2001, **34**, 8587–8589.

158 J. F. Hulvat and S. I. Stupp, *Angew. Chemie - Int. Ed.*, 2003, **42**, 778–781.

159 J. F. Hulvat and S. I. Stupp, *Adv. Mater.*, 2004, **16**, 589–592.

160 S. Ghosh, H. Remita, L. Ramos, A. Dazzi, A. Deniset-Besseau, P. Beaunier, F. Goubard, P.-H. Aubert, F. Brisset and S. Remita, *New J. Chem.*, 2014, **38**, 1106–1115.

161 M. N. Wadekar, R. Pasricha, A. B. Gaikwad and G. Kumaraswamy, *Chem. Mater.*, 2005, **17**, 2460–2465.

162 M. A. DePierro, A. J. Olson and C. A. Guymon, *Radtech Tech. Proc.*, 2004.

163 M. A. Depierro and C. A. Guymon, *Macromolecules*, 2014, **47**, 5728–5738.

164 J. D. Clapper and C. Allan Guymon, *Macromolecules*, 2007, **40**, 1101–1107.

165 Z. Li, W. Yan and S. Dai, *Carbon N. Y.*, 2004, **42**, 767–770.

166 D. Y. Liu and D. V. Krogstad, *Macromolecules*, 2021, **54**, 988–994.

167 S. Ghosh, L. Ramos, S. Remita, A. Dazzi, A. Deniset-Besseau, P. Beaunier, F. Goubard, P.-H. Aubert and H. Remita, *New J. Chem.*, 2015, **39**, 8311–8320.

168 D. Floresyona, F. Goubard, P.-H. Aubert, I. Lampre, J. Mathurin, A. Dazzi, S. Ghosh, P. Beaunier, F. Brisset, S. Remita, L. Ramos and H. Remita, *Appl. Catal. B Environ.*, 2017, **209**, 23–32.

169 S. Dutt and P. F. Siril, *J. Appl. Polym. Sci.*, 2014, **131**, 40800.

170 Y. Zhang, R. Dong, U. R. Gabinet, R. Poling-Skutvik, N. K. Kim, C. Lee, O. Q. Imran, X. Feng and C. O. Osuji, *ACS Nano*, 2021, acsnano.1c00722.

171 J. A. Castellano, *Mol. Cryst. Liq. Cryst.*, 1983, **94**, 33–41.

172 X. Feng, S. Nejati, M. G. Cowan, M. E. Tousley, B. R. Wiesenauer, R. D. Noble, M. Elimelech, D. L. Gin and C. O. Osuji, *ACS Nano*, 2016, **10**, 150–158.

173 Y. Guo, H. Shahsavan, Z. S. Davidson and M. Sitti, *ACS Appl. Mater. Interfaces*, 2019, **11**, 36110–36117.

174 S. Qavi and R. Foudazi, *Rheol. Acta*, 2019, **58**, 483–498.

175 K. Yue, C. Liu, K. Guo, K. Wu, X.-H. Dong, H. Liu, M. Huang, C. Wesdemiotis, S. Z. D. Cheng and W.-B. Zhang, *Polym. Chem.*, 2013, **4**, 1056–1067.

176 X. Yu, Y. Li, X.-H. Dong, K. Yue, Z. Lin, X. Feng, M. Huang, W.-B. Zhang and S. Z. D. Cheng, *J. Polym. Sci. Part B Polym. Phys.*, 2014, **52**, 1309–1325.

177 I. C. Reynhout, J. J. L. M. Cornelissen and R. J. M. Nolte, *Acc. Chem. Res.*, 2009, **42**, 681–692.

178 X. Yu, K. Yue, I.-F. Hsieh, Y. Li, X.-H. Dong, C. Liu, Y. Xin, H.-F. Wang, A.-C. Shi, G. R. Newkome, R.-M. Ho, E.-Q. Chen, W.-B. Zhang and S. Z. D. Cheng, *Proc. Natl. Acad. Sci.*, 2013, **110**, 10078–10083.

179 W.-J. Yoon, K. M. Lee, D. R. Evans, M. E. McConney, D.-Y. Kim and K.-U. Jeong, *J. Mater. Chem. C*, 2019, **7**, 8500–8514.

180 B. Angelov, A. Angelova, M. Ollivon, C. Bourgaux and A. Campitelli, *J. Am. Chem. Soc.*, 2003, **125**, 7188–7189.

181 H. M. G. Barriga, A. I. I. Tyler, N. L. C. McCarthy, E. S. Parsons, O. Ces, R. V. Law, J. M. Seddon and N. J. Brooks, *Soft Matter*, 2015, **11**, 600–607.

182 A. I. I. Tyler, H. M. G. Barriga, E. S. Parsons, N. L. C. McCarthy, O. Ces, R. V. Law, J. M. Seddon and N. J. Brooks, *Soft Matter*, 2015, **11**, 3279–3286.

183 R. Bruinsma, *J. Phys. II*, 1992, **2**, 425–451.

184 H. Kim, Z. Song and C. Leal, *Proc. Natl. Acad. Sci.*, 2017, **114**, 10834–10839.

185 S. S. W. Leung and C. Leal, *Soft Matter*, 2019, **15**, 1269–1277.

186 A. Zabara, J. T. Y. Chong, I. Martiel, L. Stark, B. A. Cromer, C. Speziale, C. J. Drummond and R. Mezzenga, *Nat. Commun.*, 2018, **9**, 544.

187 C. Chen, S. Wang, B. P. Grady, J. H. Harwell and B.-J. Shiau, *Langmuir*, 2019, **35**, 12168–12179.

188 J.-Y. Choi, T. Yun and S.-Y. Kwak, *J. Memb. Sci.*, 2018, **554**, 117–124.

189 P. M. Simone and T. P. Lodge, *Macromolecules*, 2008, **41**, 1753–1759.

190 A. Panday, S. Mullin, E. D. Gomez, N. Wanakule, V. L. Chen, A. Hexemer, J. Pople and N. P. Balsara, *Macromolecules*, 2009, **42**, 4632–4637.

191 N. S. Wanakule, A. Panday, S. A. Mullin, E. Gann, A. Hexemer and N. P. Balsara, *Macromolecules*, 2009, **42**, 5642–5651.

192 M. Singh, O. Odusanya, G. M. Wilmes, H. B. Eitouni, E. D. Gomez, A. J. Patel, V. L. Chen, M. J. Park, P. Fragouli, H. Iatrou, N. Hadjichristidis, D. Cookson and N. P. Balsara, *Macromolecules*, 2007, **40**, 4578–4585.

193 M. L. Hoarfrost, M. S. Tyagi, R. A. Segalman and J. A. Reimer, *Macromolecules*, 2012, **45**, 3112–3120.

194 J. M. Virgili, M. L. Hoarfrost and R. A. Segalman, *Macromolecules*, 2010, **43**, 5417–5423.

195 W.-S. Young, W.-F. Kuan and T. H. Epps, *J. Polym. Sci. Part B Polym. Phys.*, 2014, **52**, 1–16.

196 S. Akbar, J. M. Elliott, A. M. Squires and A. Anwar, *J. Nanoparticle Res.*, 2020, **22**, 170.

197 S. Ghosh, L. Ramos and H. Remita, *Nanoscale*, 2018, **10**, 5793–5819.

198 X. Fan, Z. Zhang, G. Li and N. A. Rowson, *Chem. Eng. Sci.*, 2004, **59**, 2639–2645.

199 A. Thomas, F. Goettmann and M. Antonietti, *Chem. Mater.*, 2008, **20**, 738–755.

200 X. Wang, K. S. K. Lin, J. C. C. Chan and S. Cheng, *J. Phys. Chem. B*, 2005, **109**, 1763–1769.

201 X. S. Zhao, G. Q. (Max) Lu and G. J. Millar, *Ind. Eng. Chem. Res.*, 1996, **35**, 2075–2090.

202 F. das C. M. da Silva, M. J. dos S. Costa, L. K. R. da Silva, A. M. Batista and G. E. da Luz, *SN Appl. Sci.*, 2019, **1**, 654.

203 J. H. Ding and D. L. Gin, *Chem. Mater.*, 2000, **12**, 22–24.